ISSN 0912-232X

# PHOTOMEDICINE AND PHOTOBIOLOGY

Vol.46 2025


*The Japanese Society for Photomedicine and Photobiology*

# Photomedicine and Photobiology
# Vol.46

2025



## Chief Editor

Daisuke Tsuruta, M.D.
Dermatology (Osaka)

## Editing Secretaries

Toshiyuki Ozawa, M.D.
Dermatology (Osaka)

## Former Editors

Nobuyuki Mizuno, M.D. Dermatology (1978-1990)
Muneo Ohkido, M.D. Dermatology (1991-1993)
Kunihiko Yoshikawa, M.D. Dermatology (11994-1997)
Masamitsu Ichihashi, M.D. Dermatology (1998-2002)
Itsuro Matsuo, M.D. Dermatology (2003-2004)
Takeshi Horio, M.D. Dermatology (2005-2006)
Katsumi Hanada, M.D. Dermatology (2007-2009)
Fujio Otsuka, M.D. Dermatology (2010-2012)
Chikako Nishigori, M.D. Dermatology (2013-2016)

## Editorial Board

Hiroyuki Okamoto, M.D. (Moriguchi)
Dermatology

Hiroshi Fukumura, Ph.D. (Sendai)
Organic Physical Chemistry

Daisuke Sawamura, M.D. (Hirosaki)
Dermatology

Atsushi Ito, Ph.D. (Hiratsuka)
Energy Resources

Tadamichi Shimizu, M.D. (Toyama)
Dermatology

Akira Kawada, M.D. (Sayama)
Dermatology

Hiroshi Sugiyama, Ph.D. (Kyoto)
Chemical Biology

Shosuke Kawanishi, Ph.D. (Suzuka)
Hygiene

Tadashi Suzuki, Ph.D. (Sagamihara)
Photochemistry

Tetsuro Majima, Ph.D. (Ibaraki)
Molecular Excitation Chemistry

Takeshi Toda, Ph.D. (Suita)
Radiation Biology

Akimichi Morita, M.D. (Nagoya)
Geriatric and Environmental Dermatology

Yoshiki Tokura, M.D. (Hamamatsu)
Dermatology

Shinichi Moriwaki, M.D. (Takatsuki)
Dermatology

Chikako Nishigori, M.D. (Kobe)
Dermatology

Nobuhisa Naoi, M.D. (Miyazaki)
Ophthalmology

Yasuteru Urano, Ph.D. (Tokyo)
Chemical Biology and Molecular Imaging

Masahide Yasuda, Ph.D. (Miyazaki)
Materials Chemistry

Akihiro Ohira, M.D. (Izui)
Ophthalmology



**The Japanese Society for Photomedicine and Photobiology**
**Founded in 1978**

*Office : Depaetment of Dermatology, Osaka Metropolitan University Graduate School of Medicine, 1-4-3 Asahimachi, Abeno-ku, Osaka 545-8585, Japan*

## CONTENTS

## 【Article】

# 液-液相分離したタンパク質のダイナミクスを可視化する顕微分光学的手法

田原進也

東北大学大学院 薬学研究科

***Corresponding author:**
東北大学大学院薬学研究科
〒 980-8578 宮城県仙台市青葉区荒巻字青葉 6-3
TEL: +81 022-795-6856
E-mail: shinya.tahara.c6@tohoku.ac.jp

## ABSTRACT

This review describes microscopy techniques for analyzing liquid-liquid phase separation (LLPS) of proteins. LLPS is a phenomenon in which a homogeneous solution of biomacromolecules separates into two or more distinct liquid phases and causes the formation of liquid droplets containing the solutes at a high concentration. The droplet formation usually promotes the pathological aggregation of the proteins inside, which is recently considered responsible for neurodegenerative diseases including Parkinson's disease and amyotrophic lateral sclerosis (ALS). Recent experimental approaches using microscopy techniques have been revealing the molecular mechanism of LLPS and the following aggregation, essential for the development of therapeutics for these diseases. This review presents the basic knowledge of fluorescence recovery after photobleaching (FRAP), Raman microscopy, and autofluorescence microscopy, all of which provide unique information on the protein dynamics inside the droplets, and how these methods have been contributing to the progress in the LLPS study.

**Key words**: 液 - 液相分離、タンパク質凝集、神経変性疾患、顕微分光法

## 1. 序論

### タンパク質の液 - 液相分離（LLPS）と凝集

液 - 液相分離（LLPS）は、タンパク質などの生体高分子の均一溶液が濃度の異なる二相以上の液相に分離する現象である [1-3]。LLPS は温度や塩濃度などが特定の条件になると起こり、緩衝液中や細胞内で高濃度のタンパク質や核酸を含む「液滴」が形成される（図 1 中央）。液滴の外部はこれらの分子をほとんど含まない希薄溶液となる。LLPS は明確な二次構造を形成しないアミノ酸配列（天然変性領域）を持つ天然変性タンパク質に多く見られる。真核生物では 3 割を超えるタンパク質が天然変性タンパク質であると言われており、LLPS が生体内における普遍的な現象の一つであることが想像される。

LLPS によって形成された液滴は、様々な生理機能を発現する。核小体などといった膜のない細胞小器官は、LLPS によって形成された液滴であると捉えられている。またある種のタンパク質は細胞が置かれている環境･ストレスに応答して液滴を形成することで、シグナル分子や酵素を液滴内に格納し、特定の細胞内反応を停止あるいは促進することができる。例えば細胞に酸化ストレスや浸透圧ストレスがかかると、ストレス顆粒と呼ばれる液滴が形成される [4]。内部には液滴を形成するための足場となる天然変性タンパク質に加え、そ

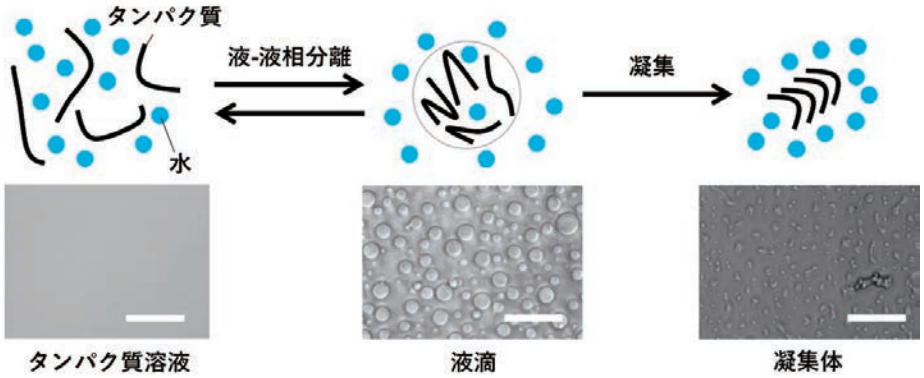


**図 1.** タンパク質の液 - 液相分離（LLPS）と凝集の模式図およびタンパク質溶液、液滴、凝集体の明視野画像（スケールバーは 10 μm）。中央の明視野画像に見られる直径 1-5 μm の円形の構造体が液滴である。右側の明視野画像に見られる直径数 μm 程度のいびつな形状の構造体が凝集体である。タンパク質溶液が LLPS を起こすと、液滴を形成する。この過程は可逆的であり、元の均一溶液の状態に戻ることができる。液滴の状態が長時間続くと、液滴内部のタンパク質が凝集体を形成する。

の他のタンパク質やRNAが含まれている。ストレス顆粒に取り込まれたタンパク質は細胞内の分解機構から保護される。また、RNAが顆粒内に取り込まれることで翻訳が促進または抑制される。以上のようにLLPSは、環境・ストレスに応答した細胞内反応のスイッチング機構を司っている。

LLPSは上記のような重要な生理機能を担うが、神経変性疾患の原因となることも指摘されている[5]。神経変性疾患は神経細胞が脱落することにより引き起こされる疾患群である。神経細胞中の環境変化などによりタンパク質が本来の構造を失い、自己集合することで凝集体が形成される。これらの凝集体が神経細胞に蓄積すると、神経細胞が機能不全や細胞死を起こし、疾患の発症に繋がると考えられている。LLPSによって生成した液滴内部には高濃度のタンパク質が存在するため、タンパク質の凝集が促進されると考えられる（図1）。実際にアルツハイマー病原因タンパク質タウやパーキンソン病原因タンパク質α-シヌクレイン、筋萎縮性側索硬化症（ALS）原因タンパク質TPD-43, Fused in sarcoma（FUS）などがLLPSによって液滴を形成することが明らかになってきた。これらのタンパク質の液滴内部ではオリゴマー化や凝集が促進される知見が得られており、LLPSが神経変性疾患を引き起こす引き金になると考えられている。

液滴内部のタンパク質が時間とともに立体構造を失うと、タンパク質間に相互作用が生じ、オリゴマーや凝集体が形成される。したがって液滴内部のタンパク質は並進運動の変化・立体構造の変化・会合など様々なダイナミクスを起こす。このような液滴内部のタンパク質のダイナミクスを理解することは、神経変性疾患の早期発見や治療法・薬剤の開発への手がかりとなる。しかし従来の生化学的手法による研究だけでは現象論的な議論にとどまることが多く、分子レベルの情報はほとんど得られていない。近年、様々な顕微鏡を用いた研究によって液滴内部の分子を観測する試みがなされており、どのようなダイナミクスで凝集体を形成するのかが明らかになりつつある。本稿ではLLPSにより生成した液滴内のタンパク質の散逸・並進・構造ダイナミクス等を調べるための代表的な顕微分光学的手法について解説する。また、これらの手法によって明らかになった各種神経変性疾患関連タンパク質の液滴の物理化学的性質と凝集ダイナミクスについて議論する。

## 2. LLPSにより生成した液滴内のタンパク質ダイナミクスの観測手法

### 蛍光褪色後回復法（FRAP法）

LLPSの研究では、蛍光標識を用いた手法が多く利用されている。これらの手法では、タンパク質の主鎖末端またはアミノ酸側鎖に蛍光色素を化学的に結合させる。あるいは蛍光タンパク質などとの融合タンパク質を利用する。蛍光標識したタンパク質の溶液がLLPSを起こすと、液滴から強い蛍光が観測される。この蛍光を観測することにより、液滴内部にタンパク質が高濃度で存在することを確認できる。

蛍光褪色後回復法（FRAP法）は、この蛍光を応用し、液滴内の分子の流動性を解析する手法である。前述のとおり、神経変性疾患原因タンパク質がLLPSによって液滴を形成すると、徐々に固体である凝集体へと相転移を起こす。FRAP法はこのような液滴内のタンパク質の相状態（液体・ゲル・固体）の変化に伴う流動性の変化を追跡するために広く用いられている。

FRAP法では蛍光標識したタンパク質の液滴を調製する。液滴内部の1点にレーザー光を照射すると、その点の色素が褪色する。褪色した箇所の蛍光強度は、液滴内部のタンパク質の並進拡散によって徐々に回復し、回復時間は液滴内部の流動性によって変化する。液滴内の流動性が保持されている場合、褪色部位の蛍光強度が速やかに回復する。一方で液滴内においてタンパク質がゲル化や凝集体形成を起こすと、タンパク質の並進拡散が遅くなり、蛍光の回復時間が長くなる。したがって蛍光の回復時間を測定することにより、タンパク質がモノマーやオリゴマーなどの液体状態であるか、ゲルや凝集体を形成しているかといった情報が得られる。

Combsらは FRAP法を用い、アルツハイマー病原因タンパク質であるタウタンパク質のLLPSを研究した[6]。タウタンパク質と緑色蛍光タンパク質（GFP）の融合タンパク質を精製し、細胞内における生体分子の混み合った環境を模倣する高分子ポリエチレングリコール（PEG）を加えたところ、液滴が形成された。GFPの蛍光強度から液滴内部には数百μMのタンパク質が濃縮されていることが示された。LLPS直後には円形の液滴が形成されていたが、24時間経過すると、円形から大きくひずんだ構造体へと変化した。液滴内部の流動性を評価するため、GFPを用いたFRAP測定が行われた。その結果、LLPS直後は液滴が速やかな蛍光強度

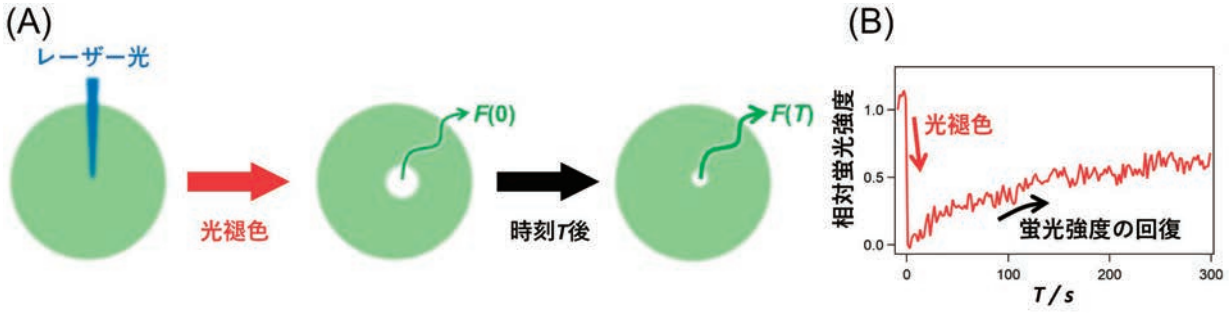


**図2.**（A）タンパク質液滴の蛍光褪色後回復法（FRAP法）の概念図および（B）得られる実験結果の例。蛍光標識したタンパク質を含む液滴を調製し、その一部分に強いレーザー光を照射することで、局所的に褪色を誘起する。その後、褪色箇所の蛍光強度の時間変化を観測する。液滴内分子の流動性が高いほど、速い回復が見られる。

の回復を示したのに対し、インキュベートとともに回復が遅くなった。このことは、液滴内部のタウタンパク質の流動性が低下していることを意味しており、ゲルや凝集体が形成されていることが示唆された。病原性のコンフォメーションに特異的な抗体を利用し、液滴内部には病原性の構造を持つタウタンパク質が時間とともに増加したことが示された。さらに彼らは強い病原性を持つ P301L 変異体やリン酸化修飾を受けたタウタンパク質が液滴内部の流動性を低下させることを示した。以上の結果から、彼らは FRAP 法を用いてタウタンパク質の液滴内部の流動性と病原性の相関を示し、タウタンパク質が液滴内部でコンフォメーション変化を起こし、病原性を獲得するまでのダイナミクスを可視化した。Alberti らは FRAP 法を細胞内のストレス顆粒の解析に応用した。ストレス顆粒が ALS の原因になることが知られているが、その機構は不明であった。彼らはストレス顆粒内部の構成タンパク質に注目した[7]。顆粒を形成する主成分は G3BP1 と呼ばれるタンパク質であるが、その中に天然状態の構造を失った Fused in sarcoma（FUS）や Cu/Zn- スーパーオキシドジスムターゼ（SOD1）などといった ALS 原因タンパク質が含まれていることを明らかにした。これら ALS 原因タンパク質の病原性変異体を細胞に発現させたところ、さらに効率よくストレス顆粒内部に取り込まれることを明らかにした。液滴内部に取り込まれた SOD1 の流動性を調べるため、FRAP 法が用いられた。ストレス顆粒内部の SOD1 の並進運動が徐々に遅くなることが示され、顆粒が徐々に凝集体へと変化したことが示された。ストレス顆粒が SOD1 などの ALS 原因タンパク質をリクルートし、凝集体などといった異常状態に導くことで、疾患を引き起こすことが提案された。

以上のように FRAP 法は、液滴から凝集体への相転移や液滴内のタンパク質の動きを解析するのに極めて有効な手法である。蛍光標識を用いた測定法の長所はその高い感度であり、タンパク質の局在を明瞭に可視化できる。一方で、蛍光標識がタンパク質の物性に影響することが短所として挙げられる。LLPS によって生成した液滴は非常に弱い分子間相互作用によって形成されており、蛍光色素や蛍光タンパク質の付加がこれらの相互作用に影響を与え、液滴の物性を変化させてしまう可能性がある。実際に蛍光タンパク質を付加することにより、液滴の形成されやすさや液滴内部のタンパク質の凝集しやすさが変化することが報告されている[8]。

**ラマン顕微鏡**

ラマン分光法は、分子構造解析手法の一つである。分子に光を照射すると、照射光に対して分子振動のエネルギー分だけ長波長シフトしたラマン散乱光が発生する。ラマン散乱光のスペクトル（ラマンスペクトル）を解析することで、分子振動の振動数の情報が得られるため、分子構造を推定することができる。また、散乱光強度は濃度と相関することから、試料に含まれる分子の濃度定量に用いることもできる。ラマン分光測定を顕微鏡下で行うラマン顕微鏡は、生細胞イメージングなどにも応用されており、細胞内の各部位における構成成分や分子構造の詳細が明らかにされてきた。細胞のイメージングでは従来、蛍光顕微鏡が広く用いられており、観測対象となる分子の蛍光標識が必須であった。一方でラマン顕微鏡では各座標におけるターゲット分子のラマンバンドの強度を測定する。これを座標についてプロットすることで、ラベルフリーで生体分子の分布イメージが得られる。また、ラマンスペクトルには観測位置に存在するあらゆる分子のバンドが観測されるため、異種分子（タンパク、核酸など）の同時イメージングも可能である。タンパク質の液滴を測定する場合は、ディッシュ内に液滴の懸濁液または液滴を形成した細胞を調製し、顕微鏡下で液滴の内部に励起光を照射する ( 図 3A)。ラマン散乱光を同じ対物レンズで集め、スペクトルを測定する。実際に得られるラマンスペクトルの例を図 3B に示した。液滴内部のタンパク質の主鎖・側鎖に由来するラマンバンドのほか、水に由来するバンドも観測される。

近年、ラマン顕微鏡が単一液滴中のタンパク質や核酸の観測に応用されている。Nakabayashi らは神経変性疾患の一つであるマシャド - ジョセフ病の原因タンパク質 ataxin-3 の液滴をラマン顕微鏡を用いて研究した[9]。彼らは ataxin-3 が夾雑環境下で LLPS を起こし、液滴を形成することを明らかにした。この液滴内部のラマンスペクトルを測定したところ、タンパク質に特徴的なスペクトルが得られ、水の O-H 伸縮振動バンドに加えタンパク質主鎖由来の amide I バンドやフェニルアラニンやチロシンなどといったアミノ酸側鎖のバンドが観測された。一方で液滴の外側には夾雑環境を再現するために用いた PEG と水のラマンバンドだけが観測された。これらの結果から、液滴内部に高濃度の ataxin-3 が存在することが確認された。さらに彼ら

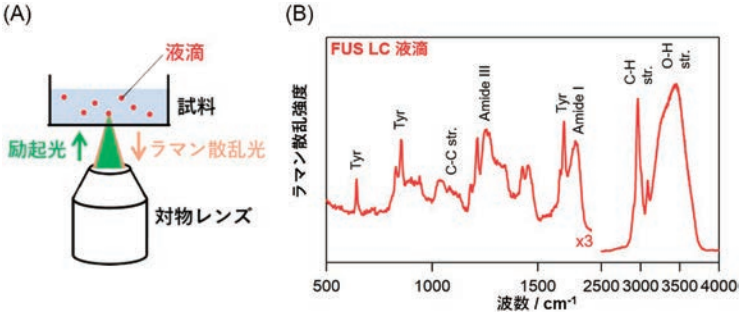


**図 3.** (A) 倒立顕微鏡によるラマン顕微測定の概略図。ディッシュ内に液滴の懸濁液を調製し、対物レンズにより励起光を液滴内部に照射する。ラマン散乱光は同じ対物レンズを通り、分光器と CCD に導入され、ラマンスペクトルが得られる。(B) ALS 原因タンパク質 FUS の部分配列 FUS LC の液滴のラマンスペクトル。励起波長は 532 nm である。500-1900 $cm^{-1}$, 2500-4000 $cm^{-1}$ の領域を示しており、前者は強度を 3 倍したものを示した。Tyr: チロシン、Str.: 伸縮振動。

はラマン散乱強度を用いて液滴内部の ataxin-3 濃度が 13.6 mM にも達することを示し、液滴内のタンパク質濃度の高精度定量法を確立した。この方法を応用し、ALS 原因タンパク質の一つである FUS の天然変性領域 FUS LC や酵母のオートファジー関連タンパク質である Pbp1 の天然変性領域 Pbp1 LC の LLPS がラマン顕微鏡によって研究された[10-11]。pH や塩濃度などが FUS LC の LLPS の至適条件から遠ざかると、液滴内部のタンパク質濃度が徐々に低下し、ある一定の値に達すると液滴が消失することが明らかになった。また、Pbp1 LC のメチオニン側鎖の酸化が進行すると、FUS LC と同様に液滴内のタンパク質濃度が低下し、液滴が消失した。これらの結果から、タンパク質が液滴の内側から外側へと散逸することによって LLPS の抑制が引き起こされ、濃度がある閾値以下に達すると液滴が解消すると考えられる。また、ラマンスペクトルの amide I バンドや amide III バンドが二次構造に鋭敏であることを利用し、液滴内のタンパク質の構造変化が解析された。Lee らは TDP-43 の LLPS 後の線維形成に伴う二次構造変化を観測した[12]。TDP-43 は本来転写やスプライシングを司る重要なタンパク質であるが、線維を形成し、ALS の原因になると考えられている。TDP-43 の C 末端ドメイン（$TDP\text{-}43_{CTD}$）が LLPS を起こすことが知られている。彼女らは $TDP\text{-}43_{CTD}$ の液滴内における構造ダイナミクスを調べることにより、TDP-43 の LLPS と凝集の関係性を考察した。$TDP\text{-}43_{CTD}$ の液滴内のラマンスペクトルの時間変化を測定したところ、二次構造に鋭敏な amide I バンドの形状が徐々に変化した。特に β シートに特徴的な振動数領域でピークの先鋭化が見られたことから、液滴内部で TDP-43 の β シート構造の割合が増大することを示した。また、amide III バンドが低波数シフトしたことからも β シート構造の形成が支持された。TDP-43 の線維は β シート構造を豊富に持つことが知られており、ラマン顕微鏡によって液滴内で線維が形成される過程を可視化することに成功したと考えられる。

以上のようにラマン顕微鏡は液滴内タンパク質の散逸や二次構造変化を解析するための強力なツールになる。ラベルフリーの測定であるため、ありのままに近い状態で液滴を観測することができる。一方でラマンスペクトルは分子の構造変化に敏感でない場合も多く、実際に構造変化を観測できたタンパク質は極めて限られている。また、比較的強いレーザー光を照射する必要があり、液滴内の生体分子にダメージを与えてしまうことも少なくない。

**自家蛍光寿命顕微鏡**

我々は最近、液滴内のタンパク質の構造変化を観測するため、自家蛍光寿命顕微鏡を LLPS に応用した[13]。タンパク質に 300 nm 以下の光を照射すると、蛍光が観測される。この蛍光は主に芳香族アミノ酸（トリプトファン・チロシン・フェニルアラニン）に由来する。特にトリプトファンは、周辺の環境に応じて蛍光波長や蛍光寿命の変化を示すことが知られている。タンパク質が構造変化を起こすと、Trp 残基の接触残基や周辺環境が変化する。このため、蛍光波長と蛍光寿命を観測することにより、タンパク質の構造変化を捉えることが可能となる。本手法はタンパク質が本来持つ Trp 残基を

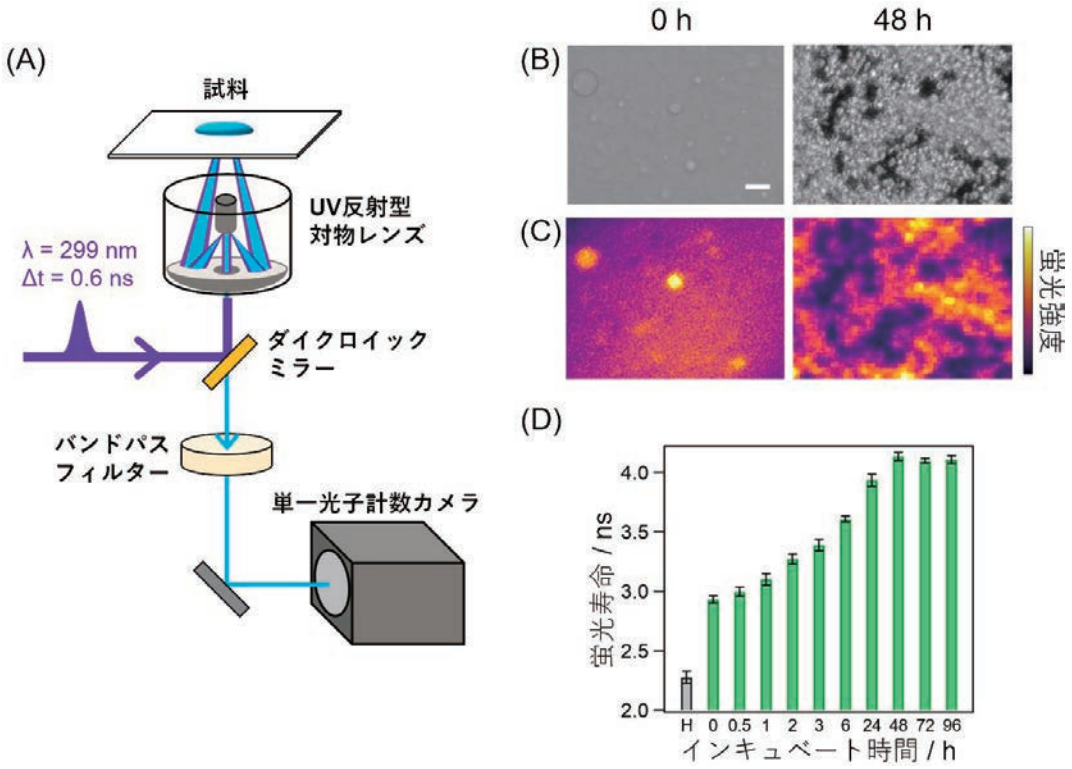


**図 4.**（A）自家蛍光寿命顕微鏡。サブナノ秒パルス紫外 LED を励起光源とし、UV 反射型対物レンズで試料を励起する。単一光子計数カメラを用いて、蛍光強度や蛍光寿命を測定する。（B）インキュベート前後の液滴の明視野画像。スケールバーは 10 μ m。（C）自家蛍光画像。（D）平均蛍光寿命のインキュベートによる変化。H: 均一溶液。

用いるため、ラベルフリーな手法である。顕微鏡の構成は通常の蛍光顕微鏡とほとんど同じであるが、広い波長範囲の紫外光を観測する必要があるため、対物レンズを UV 域強化型の反射型対物レンズにするなどの工夫が必要であった（図 4A）。単一光子計数カメラを用いることで、時間相関単一光子計数法（TCSPC）で試料の各座標における蛍光減衰曲線を同時に取得し、蛍光寿命を計測した。

我々はこの手法を用い、ataxin-3 の液滴形成後の構造変化を捉えた。前述のとおり ataxin-3 は LLPS によって液滴を形成した（図 4B）。液滴を 296 K でインキュベートしたところ、48 時間後には ataxin-3 が凝集体を形成したことが確認された。紫外蛍光寿命イメージング装置を用いて、ataxin-3 の液滴と凝集体の自家蛍光画像を取得した（図 4C）。液滴が強い自発蛍光を示したことから、前述のラマン顕微鏡の結果と一致し、ataxin-3 が液滴内部に濃縮されていることが確認された。Ataxin-3 のアミノ酸組成から、観察された自家蛍光は主に Trp 残基に起因すると考えられる。

LLPS 後の様々なインキュベート時間における液滴内の自家蛍光減衰曲線を測定し、3 つの指数関数の和によるフィッティング解析から平均蛍光寿命を計算した（図 4D）。0 h における液滴内のトリプトファン残基の平均蛍光寿命は、均一溶液中よりも顕著に長かった。液滴をインキュベートしたところ、48 時間までの間、平均蛍光寿命が徐々に増大した。この結果は、Trp 残基の周辺環境が凝集に伴って変化したことを意味している。Ataxin-3 の Trp 残基周辺には消光作用を示すアミノ酸残基が多数存在する。蛍光寿命の増大は、これらの Trp 残基とこれらのアミノ酸との距離が増大したことを示唆しており、LLPS およびインキュベートとともに本来のタンパク質構造が失われたことを意味している。さらに各インキュベート時間における自家蛍光スペクトルを測定したところ、Trp の蛍光波長が時間とともに長波長シフトした。Trp 周辺の環境が親水的であるほど、蛍光のピーク波長が長くなることが知られている。したがって観測されたスペクトルの変化は、液滴中の ataxin-3 の Trp 残基の周辺環境が徐々に親水的になったことを示している。

さらに ataxin-3 の 3 つの Trp 残基 Trp87、Trp120 および Trp130 の周辺環境をそれぞれ解析するため、変異体の測定を行ったところ、Trp120 および Trp130 の周辺環境がそれぞれ異なる時間スケールで親水的になることが明らかになった。天然状態の ataxin-3 では Trp120, Trp130 はタンパク質内部に埋もれているが、時間とともにタンパク質の立体構造が崩壊し、Trp120, Trp130 が水に曝露したことを意味する。それぞれの Trp 残基が互いに異なる時間スケールで蛍光寿命や蛍光波長の変化を示したことから、LLPS を起こした ataxin-3 は液滴から凝集体となる過程で多段階的な構造変化を引き起こすことが示唆された。

さらに Mukherjee らは Trp 残基の蛍光の異方性を応用することで、LLPS によるタンパク質のコンフォメーション変化を解析した[14]。彼らは分子夾雑環境において $\beta$ ラクトグロブリンの液滴を調製したところ、エステラーゼ活性のミカエリス定数 $K_m$ およびターンオーバー数 $k_{cat}$ が均一溶液の状態と比較して数倍程度向上することを発見した。酵素活性が向上した分子メカニズムを明らかにするため、液滴内の β ラクトグロブリンの構造を解析した。液滴を形成した β ラクトグロブリンの Trp 残基の蛍光異方性の緩和時間を測定したところ、均一溶液中よりも短かった。このことから $\beta$ ラクトグロブリンは LLPS を起こすとより柔軟な構造へと変化することが示唆された。円二色性スペクトルから、β シート構造が減少し、ランダムコイル構造が増大することが確認された。すなわち LLPS によって β ラクトグロブリンがランダムコイルに富んだ柔軟なコンフォメーションに変わることで、高いエステラーゼ活性を獲得することが示唆された。

以上のように Trp 残基の蛍光寿命や蛍光波長および異方性を観測することによりタンパク質構造変化を感度良く検出できる。また、タンパク質が本来持っている Trp 残基を利用するため、蛍光標識等が不要なラベルフリー測定である。この手法の欠点は、目的タンパク質以外に紫外光照射によって蛍光を放出する分子が多く含まれる系への適用が困難な点である。特に細胞内には自家蛍光を示す分子が多く存在し、それらの信号に Trp 残基由来の信号が埋もれてしまう可能性がある。

## 3. おわりに

本稿では LLPS によって生成した液滴内部のタンパク質ダイナミクスを調べるための顕微鏡的手法として、FRAP 法、ラマン顕微鏡、自家蛍光顕微鏡について解説した。LLPS がタンパク質の凝集を促進することが多くの実験から明らかになっているが、その詳細な分子メカニズムにせまった研究は非常に少ない。これらの手法を用いることで、液滴内に出現するタンパク質の異常構造の検出や同定が可能となり、凝集体形成のメカニズムについて知見が得られる。それぞれの手法には一長一短があるものの、それぞれユニークかつ異なるダイナミクスの情報を与えることから、これらの手法を併用することでタンパク質の LLPS から凝集までのダイナミクスの全体像を捉えることが可能になるであろう。

**利益相反**

該当なし。

**謝辞**

自家蛍光寿命顕微鏡を用いた ataxin-3 の構造変化の解析は、東北大学大学院薬学研究科生物構造化学分野の中林孝和教授、梶本真司准教授、松浦宇宙君（2023 年度修士課程修了）とともに行った。

**参考文献**

(1) Shin, Y, Brangwynne, C P, Liquid phase condensation in cell physiology and disease. Science, 2017; 357: eaaf4382.
(2) Alberti, S, Gladfelter, A, Mittag, T, Considerations and challenges in studying liquid-liquid phase separation and biomolecular condensates. Cell, 2019; 176: 419-434.
(3) Yoshizawa, T, Nozawa, R-S, Jia, T Z, Saio, T, Mori, E, Biological phase separation: Cell biology meets

biophysics. Biophys Rev, 2020; 12: 519-539.
(4) Glauninger, H, Wong Hickernell, C J, Bard, J A M, Drummond, D A, Stressful steps: Progress and challenges in understanding stress-induced mrna condensation and accumulation in stress granules. Mol Cell, 2022; 82: 2544-2556.
(5) Zbinden, A, Pérez-Berlanga, M, De Rossi, P, Polymenidou, M, Phase separation and neurodegenerative diseases: A disturbance in the force. Dev Cell, 2020; 55: 45-68.
(6) Kanaan, N M, Hamel, C, Grabinski, T, Combs, B, Liquid-liquid phase separation induces pathogenic tau conformations in vitro. Nat Commun, 2020; 11: 2809.
(7) Mateju, D, Franzmann, T M, Patel, A, Kopach, A, Boczek, E E, Maharana, S, Lee, H O, et al., An aberrant phase transition of stress granules triggered by misfolded protein and prevented by chaperone function. EMBO J, 2017; 36: 1669-1687.
(8) Pandey, N K, Varkey, J, Ajayan, A, George, G, Chen, J, Langen, R, Fluorescent protein tagging promotes phase separation and alters the aggregation pathway of huntingtin exon-1. J Biol Chem, 2024; 300: 105585.
(9) Murakami, K, Kajimoto, S, Shibata, D, Kuroi, K, Fujii, F, Nakabayashi, T, Observation of liquid–liquid phase separation of ataxin-3 and quantitative evaluation of its concentration in a single droplet using raman microscopy. Chem Sci, 2021; 12: 7411-7418.
(10) Yokosawa, K, Kajimoto, S, Shibata, D, Kuroi, K, Konno, T, Nakabayashi, T, Concentration quantification of the low-complexity domain of fused in sarcoma inside a single droplet and effects of solution parameters. J Phys Chem Lett, 2022; 13: 5692-5697.
(11) Kageyama, L, Tahara, S, Yokosawa, K, Kamijo, M, Kajimoto, S, Nakabayashi, T, Raman quantitative analysis of methionine oxidation and its promotion effect on dissolution of phase-separated liquid droplets of pbp1. Chem Phys Lett, 2024; 856: 141671.
(12) Shuster, S O, Lee, J C, Watching liquid droplets of TDP-$43_{CTD}$ age by raman spectroscopy. J Biol Chem, 2022; 298.
(13) Matsuura, U, Tahara, S, Kajimoto, S, Nakabayashi, T, Label-free autofluorescence lifetime reveals the structural dynamics of ataxin-3 inside droplets formed via liquid–liquid phase separation. Sci Rep, 2023; 13: 6389.
(14) Rai, S, Pramanik, S, Mukherjee, S, Deciphering the liquid–liquid phase separation induced modulation in the structure, dynamics, and enzymatic activity of an ordered protein β-lactoglobulin. Chem Sci, 2024; 15: 3936-3948.

# The light sources for phototherapy have advanced from lamps to LEDs

Hideyuki Masuda[1,2] and Akimichi Morita[1]

*1 Department of Geriatric and Environmental Dermatology, Nagoya City University, Graduate School of Medical Sciences, Nagoya, Japan*
*2 USHIO INC, Tokyo, Japan*

## Introduction

With the advance of technology and the development of photobiology research, new light sources have been applied, making it possible to treat more effectively, more quickly, and more safely. Phototherapy includes PUVA, UVA1-LED therapy, broadband UVB, narrowband UVB, excimer light, and UVB-LED therapy. In Japan, topical PUVA therapy was first introduced in 1976. While it was effective for refractory psoriasis and other conditions, concerns about carcinogenicity due to the mechanism of action of psoralen, which cross-links to DNA, and the necessity for shielding after irradiation created challenges for broad application in general practice. In 2002, Japan developed its first narrowband UVB treatment device, followed by the excimer light treatment device in 2008. In 2021, the UVA1-LED treatment device was introduced, and in 2022, the UVB-LED treatment device was launched. The light sources used for phototherapy have transitioned from lamps to LEDs.

### 1. Narrowband UVB

Since the 1970s, research on phototherapy for psoriasis has progressed. In 1976, Fischer[1)] and later, in 1981, Parrish[2)] reported that the effective wavelength was around 313 nm. Narrowband refers to devices that utilize lamps with a peak wavelength of approximately 311-312 nm and a very narrow emission spectrum. Because it does not require the photosensitizer psoralen, the treatment procedure is straightforward and can be administered at doses that do not cause erythema, making it easy to handle.

### 2. Excimer Light

Excimer light utilizes an excimer lamp, which is a discharge lamp that emits light generated by excimers formed from noble gases or noble gas-halogen combinations. The emission spectrum can be set according to the discharge gas used. Excimer light uses XeCl as the discharge gas, with a peak wavelength of 308nm. The peak wavelength of excimer light is 3 nm shorter than that of narrowband UVB, resulting in a shorter treatment time due to a lower minimal erythema dose. However this also increases the likelihood of erythema reactions. To minimize treatment effect reduction while suppressing side effects, a short-wavelength cut filter, known as an excimer filter, was developed[3)]. As a result, the TheraBeam® UV308 can safely and effectively irradiate the affected area while reducing risks to healthy skin. It has been reported to achieve higher treatment efficacy for vitiligo[4)].

### 3. UVA1 Therapy

UVA is divided into UVA1 (340-400nm) and UVA2 (320-340nm), with UVA2 having properties similar to UVB, such as inducing erythema. UVA1 penetrates deeper into the skin compared to UVB. Therefore, UVA1 is effective for diseases with dermal pathology, such as atopic dermatitis, cutaneous T-cell lymphoma, prurigo, and scleroderma[5)]. Discharge lamps were used as light sources for UVA1 devices, but with improvements in output, LEDs have become applicable. LEDs have many advantages, such as wavelength selectivity, long life, low power consumption, and mercury-free. With enhanced emission efficiency, LEDs have achieved a level suitable for use as light sources in phototherapy. However, the optimal optical characteristics were not yet clear. Therefore, we researched to develop more effective UVA1 therapy light sources. The results suggested that the most effective wavelength for UVA1 phototherapy is 365nm, and the use of a short-wavelength cut filter could suppress immediate tanning[6)]. Based on these research results, the LED-based UVA1 treatment device (TheraBeam® UVA1) was launched in Japan and can be used as an insured treatment. Due to the different treatment mechanisms, it is expected to be a next step for patients resistant to existing UVB treatments. Significant treatment effects have already been reported for refractory palmoplantar pustulosis[7)] and mycosis fungoides[8)].

### 4. UVB-LED Therapy

UVB-LED output significantly increases following the UVA range, making practical use possible. The half-width of the spectral distribution of narrowband UVB and excimer light is less than 5 nm, while UVB-LEDs have a half-width of approximately 15 nm due to their design principle. The DNA absorption coefficient for ultraviolet light around 300nm varies significantly, leading to substantial differences in clinical effects with slight wavelength characteristic differences. Therefore, research was conducted on the optimal optical characteristics. These results confirmed that the optimal peak wavelength for using UVB-LEDs with a half-width of about 15 nm in ultraviolet therapy devices is around 312nm[9)], and optical processing

such as narrowing the spectrum can slide the peak wavelength to about 308nm, similar to excimer light.

UVB-LED treatment device (TheraBeam® UV308mini LED) was launched as a sustainable and environmentally friendly device, achieving an approximately 70% reduction in power consumption and extending the light source life by about 4-5 times compared to conventional devices.

## Conclusion

The light sources for phototherapy for skin diseases began with lamps, enabling treatments such as PUVA therapy and narrowband UVB. Subsequently, they evolved into LEDs, allowing for more effective, faster, and safer treatments. In the future, further improvements in LED efficiency and narrow spectrum are expected to expand the range of applicable devices. Additionally, new treatment methods such as photodynamic therapy (PDT) using visible light and photosensitizers and extracorporeal photopheresis (ECP), as well as the development of new light sources such as semiconductor lasers (LD: Laser Diode), are expected to contribute to solving unmet medical needs. (4766/5000)


1) Fisher T et al. Ultraviolet-action spectrum and evaluation of ultraviolet lamps for psoriasis healing. *Int J Dermatol*. 1984 Dec;23(10):633-637.
2) Parrish JA, Jaenicke KF. Action spectrum for phototherapy of psoriasis. *J Invest Dermatol*. 1981 May;76(5):359-62.
3) Kobayashi K Morita A et al. The development of a filter to enhance the efficacy and safety of excimer light (308 nm) therapy. *Photodermatol Photoimmunol Photomed*. 2009 Feb;25(1):30-36.
4) Cassacci M et al.: Comparison between 308-nm monochromatic excimer light and narrowband UVB phototherapy (311-313nm) in the treatment of vitiligo a multicentre controlled study. *J Eur Acad Dermatol Venereol*, 2007; 21: 956-963.
5) Krutmann, *J et al:J Invest Dermatol* symp Proc 4:70,1999
6) Masuda H, Morita A, Ultraviolet A1 phototherapy utilizing ultraviolet light-emitting diodes and a short wavelength cutoff filter, *J Dermatol Sci*. 2021 Feb;101(2):138-140.
7) Ikumi K, Kio T, Torii K, Masuda H, Morita A. Successful treatment of dyshidrotic palmoplantar eczema with ultraviolet A1 light-emitting diodes. *J Dermatol*. 2020 Aug;47(8):922-923.
8) Ikumi K, Torii K, Kio T, Masuda H, Kanayama Y, Morita A. A case of mycosis fungoides effectively treated with ultraviolet light A 1-light-emitting diode phototherapy. *Photodermatol Photoimmunol Photomed*. 2023 Jan;39(1):69-71.
9) Masuda H, Kimura M, Morita A. Optimum wavelength characteristics for phototherapy utilizing deep ultraviolet light-emitting diodes. *J Dermatol Sci*. 2019 Mar;93(3):186-188.

# リン脂質ポリマーを用いた難水溶性薬物分子の高効率細胞内導入と光を用いたラベルフリー濃度定量法の確立

古賀 圭祐　梶本真司　金野智浩　中林 孝和

東北大学大学院薬学研究科

## Abstract

Label-free detection of drug molecules is essential for evaluating the uptake, distribution, and metabolism of drug molecules introduced into a cell. Fluorescence labeling methods offer high sensitivity; however, they can impair the properties of small-molecule drugs, making label-free detection crucial. We have established a protocol utilizing Raman imaging that enables the label-free quantification of drug concentrations within a single cell. This review provides an overview of methods for introducing poorly water-soluble drugs into cells and detection techniques using Raman imaging.

**Key words:** Raman imaging, Label-free detection, Drug molecules, Amphiphilic phospholipid polymer

## 1. はじめに

創薬研究において薬物の作用機序を明らかにするには、薬物分子が細胞内のどこに、どのくらいの濃度で存在し、どのように代謝されるのかを知る必要がある。生きている細胞内での薬物分子の動態観測では、薬物分子を蛍光標識し、その蛍光を観測する手法が一般的に用いられている。蛍光標識法は感度が高いものの、薬物分子が小さい場合には蛍光標識による影響を無視することができず、薬物分子本来の性質が損なわれる。そのために、低分子薬物を検出するにはラベルフリーでの検出が不可欠である。我々は、細胞内の薬物分子をラベルフリーで検出するために、ラマンイメージングを用いている（図 1）。ラマン散乱はレーザー光を試料に照射することで得られる非弾性散乱光であり、レーザー光とラマン散乱光のエネルギー差は標的分子の分子振動のエネルギーと一致する。そのため、横軸にエネルギー差、縦軸にラマン散乱強度をプロットすることで標的分子の振動スペクトルを得ることができる。振動スペクトルであるために、生細胞内の標的分子の構造、濃度、分子間相互作用などの情報をラベルフリーで取得でき、ラマンイメージングは低分子薬物の測定に有用な手法である。

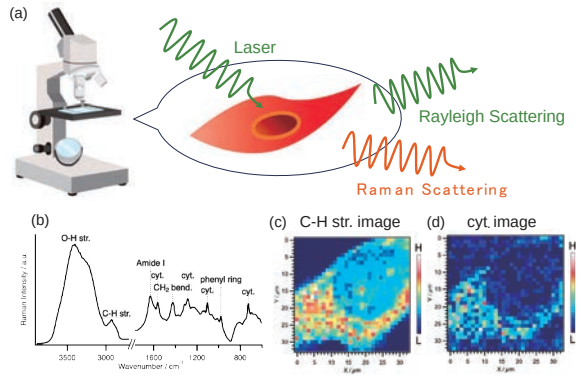


**図 1.** (a) ラマンイメージングの概略図。細胞にレーザーを照射することで細胞内分子の分子振動に対応するラマン散乱光を検出する。(b) 細胞のラマンスペクトルの例。(c,d) ラマン強度をプロットして作成したラマンイメージング。(c) C-H 伸縮振動（C-H str.）バンド、(d) シトクロム（cyt.）のラマンバンドのイメージング。

また、薬物分子を細胞内に導入するには予め水中に分散させる必要がある。しかし、薬物分子の多くは水溶性が低く、最近ではリポソームやナノ粒子を用いた細胞内導入も行われている。本総説ではこれらの実用性についても言及するとともに、我々が提案する両親媒性ポリマー poly[2-methacryloyloxyethyl phosphorylcholine (MPC)-*co*-*n*-butyl methacrylate (BMA)] (PMB) を用いた難水溶性薬物の可溶化、細胞内導入からラマン顕微鏡を用いたラベルフリーでの細胞内分布観測・濃度定量までの一連のプロトコルについて紹介する。

## 2. 難水溶性薬物の可溶化と細胞導入

現在販売されている低分子薬物の多くは難水溶性である [1]。そのため、細胞実験や *in vivo* で薬物を使用するには可溶化剤が必要である。既存の可溶化剤には有機溶媒、ミセル、リポソームなどがあり、以下にそれらについて概説する。細胞実験レベルで最もよく用いられるのは、DMSO やエタノールなどの有機溶媒である。これらの溶媒は薬物分子を単純拡散により迅速に細胞内に移行できるものの、有機溶媒自体の細胞毒性が高いだけではなく、細胞の炎症反応、細胞周期、分化、アポトーシスなどさまざまな細胞プロセスに影響を与えることが報告されており、これらの効果により実験結果を誤って解釈する可能性がある [2]。

界面活性剤は分子構造中に親水基と疎水基を有しており臨界ミセル濃度以上でミセルを形成し、内部に疎水性化合物を取り込むことで可溶化できる。界面活性剤は大きく低分子界面活性剤と高分子界面活性剤に分けることができる。代表的な低分子界面活性剤にアニオン性のドデシル硫酸ナトリウムや非イオン性のポリオキシエチレン硬化ヒマシ油、ポリソルベートなどがある。これらの低分子界面活性剤は細胞膜やタンパク質を変性させるため細胞毒性が無視できない場合があり注意が必要である。低分子界面活性剤の利用例としてパクリタキセルの可溶化がある。パクリタキセルは乳がん、卵巣がん、肺がんの治療のための疎水性抗がん剤であるが、水溶性が低いため、Cremophor EL（ポリ

オキシエチレン硬化ヒマシ油）と脱水エタノールの 1：1 混合物に溶解させる。しかし、Cremophor EL の過敏症、神経毒性、神経障害などさまざまな副作用が報告されている [3]。

一方、疎水性ブロックと親水性ブロックからなる両親媒性ブロックポリマーによって形成される高分子界面活性剤の高分子ミセルは、高い安定性と良好な生体適合性を有しており、さまざまな難水溶性化合物を可溶化することが可能である [4]。リン脂質二重層からなるリポソームは二重層の間の疎水性部位に疎水性化合物を取り込むことで可溶化できる。高分子ミセルやリポソームはサイズが数十～数百 nm のナノ粒子であり、これらのナノ粒子は通常、単純拡散では細胞内に入ることができず、多くがエンドサイトーシスにより取り込まれる [5]。エンドサイトーシスにより取り込まれたナノ粒子はエンドソーム小胞によりリソソームまで輸送され、加水分解を受ける。粒子に内包された薬物分子がエンドソーム内の低 pH 環境や加水分解により分解される場合は、エンドソームからの脱出機構を組み込む必要がある [6]。ナノ粒子を利用した細胞内導入の例として、all-*trans*-retinoic acid (ATRA) を例にあげる。ビタミン A 誘導体の ATRA は急性前骨髄球性白血病（APL）の治療薬として使用され、他にも様々ながん細胞に対する効果が確認されている [7, 8]。ATRA は水溶性が極めて低いため、細胞に取り込ませるための研究が行われている。Zhang らは ATRA とドキソルビシンを送達するために pH 応答性のヒドラゾン結合を介して ATRA 前駆体のレチナールとデキストランを結合させることで高分子ミセルを形成させ、内部にドキソルビシン封入したコンジュゲートを作成した [9]。コンジュゲートがエンドサイトーシスにより取り込まれると、リソソーム内の低 pH によりヒドラゾン結合が切断され、レチナールとドキソルビシンが放出される。放出されたレチナールは ATRA に変換される。導入された ATRA とドキソルビシンが核へ移行することで、がん細胞のアポトーシスとレチノイン酸受容体依存的な細胞老化を引き起こすことが報告されている。

## 3. 細胞膜透過性リン脂質ポリマーによる薬物分子の細胞導入

Ishihara らは安定性と生体適合性を併せ持つ生体材料として細胞膜の表面構造に着目し、側鎖にリン脂質極性基を有するモノマー（2-methacryloyloxyethyl phosphorylcholine (MPC)）を合成した [10]。MPC は通常のラジカル重合反応により他のビニルモノマーと容易に共重合させることができ、目的に応じて高分子の機能を変化させることができる。Konno らは、親水性モノマーの MPC と疎水性モノマーの BMA をランダム共重合した水溶性ポリマーの PMB（図 2）が、難水溶性抗がん剤のパクリタキセルを可溶化できることを報告した [11]。PMB はその両親媒性特性により水中で多分子会合体を形成し、内部に疎水性分子を取り込むことで安定に可溶化できる。PMB 会合体の直径は約 20 nm であり、その内部の疎水性領域の極性はエタノールと同程度であるためエタノールに可溶な疎水性化合物を高濃度で可溶化できる。*In vitro* および *in vivo* において PMB は無視できるほど細胞毒性が小さく、PMB に可溶化したパクリタキセルは従来の Cremophor EL に可溶化したときと同様の活性を有していた [12]。パクリタキセルの他にもシクロスポリン A やベルテポルフィンなどの薬剤分子も同様に可溶化でき、活性も有していることが報告されている [13, 14]。

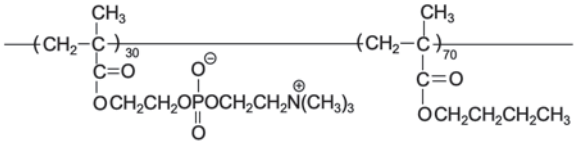

**図 2.** PMB の構造式 [25]。

PMB の性質として可溶化特性の他に細胞膜透過性が Goda らにより報告された [15]。蛍光標識した PMB は 300 秒程度で完全に細胞内に導入され、4℃ や ATP 枯渇といったエンドサイトーシスが阻害される条件においても、常温とあまり変わらない速度で細胞内への取り込みが生じた。この結果は、PMB がエネルギー非依存的な経路で細胞内へ移行できることを示している。PMB は細胞内の特定の領域に局在することはなく、標識した蛍光分子の性質に依存した局在を示す。ローダミン B および Hoechst33258 で標識した PMB はそれぞれミトコンドリアおよび核へ局在し、FITC で標識すると FITC は細胞小器官特異的に局在しないため PMB は細胞全体に分布する。さらに、PMB 導入後、細胞外培地を PMB 不含の緩衝液へ交換し、細胞外から PMB を除くと、細胞内の PMB は細胞外へ漏出する。通常、ナノスケールの水溶性高分子はエンドサイトーシス経路により細胞内に取り込まれるが、PMB はエネルギー非依存的な分子拡散により細胞膜を濃度勾配のみによって双方向に透過し得ることがわかる。PMB の細胞膜透過性の詳しい機構は不明であるが、BMA を持たない MPC のホモポリマーは細胞膜透過性を示さないことから、疎水性の BMA ユニットが大きな役割を果たしていると考えられる。

この分子拡散による細胞膜透過性により、PMB は薬剤分子を水中に分散させるだけではなく、可溶化した低分子化合物の細胞内への効率的な導入を行うことができる。低分子化合物のみならず、PMB の非侵襲的な細胞膜移行性を利用して核酸やペプチドなどを細胞内に送達する研究も行われている。Lin らは HeLa 細胞内で mRNA をリアルタイムで可視化するためにモレキュラービーコン（MB）と poly(MPC-*co*-BMA-*co*-*N*-succinimidyloxycarbonyl tetra (ethylene glycol) methacrylate) (PMBS) とのコンジュゲート（PMBS-MB）を調製した [16]。PMBS-MB は細胞内に浸透でき、従来の MB と比較してタンパク質による非特異的分解を抑制し、特定の mRNA と MB を結合させることができた。PMB は低分子化合物のみならず分子量の大きい生体分子でも細胞内に送達できる可能性を有している。

## 4. ラマン顕微鏡による細胞内導入薬物分子のラベルフリー検出

ラマン顕微鏡による細胞内導入分子のイメージング測定は、蛍光顕微鏡と相補的になるラベルフリー観測

手法として、近年急速に開発･普及されている。ラマン顕微鏡は基本的な光学系は共焦点蛍光顕微鏡と同じであり、蛍光と同じように使用できる（図１）。共焦点蛍光顕微鏡と異なる点は、スペクトル測定のためにラマン散乱光は光学フィルターではなく分光器によってスペクトル分解され検出器に導入されること、微弱光であるために高感度な検出器が用いられることである。Aljakouch らはラマン顕微鏡を用いてチロシンキナーゼ阻害剤であるネラチニブの細胞内分布を測定し、代謝過程に関連するラマンスペクトルの変化を詳細に検討した[17]。ネラチニブは EGFR および HER2 受容体に結合し、受容体とともに細胞内に取り込まれリソソームに局在、その後に代謝を受けることをラベルフリーで示すことができた。さらに、ネラチニブを導入した細胞の LC-MS 測定の結果と密度汎関数法による振動数計算の結果から、代謝物の化学構造を予測することができた。また、Li らはアクチノマイシン D の細胞取り込みと細胞内分布および取り込みに対する細胞応答をラマンイメージングにより観測した[18]。532 nm の励起光によるアクチノマイシン D の自家蛍光から薬剤の細胞導入と局在を可視化することができ、薬剤が導入された細胞では薬剤濃度依存的、時間依存的にシトクロム *c* のラマン強度が減少することを用いて、薬剤の取り込みと細胞毒性を同時に評価した。アクチノマイシン D と核内の DNA の結合に由来するラマンバンドの検出にも成功している。我々のグループではプロドラッグであるコレステロール結合 SN-38 のナノ粒子を細胞内に導入し、自家蛍光イメージングとラマンイメージングからナノ粒子の代謝過程をラベルフリーで観測することに成功した[19]。ナノ粒子として存在するコレステロール結合 SN-38 と代謝生成した SN-38 の自家蛍光スペクトルのピーク位置が異なることを用いて、細胞質に導入されたナノ粒子から SN-38 への代謝を観測し、ナノ粒子と代謝生成物の SN-38 が共局在していることを示した。ラマンイメージングから自家蛍光がナノ粒子または SN-38 由来であることを確認し、SN-38 の薬理作用によるミトコンドリアから細胞質へのシトクロム *c* の放出をも観測することができた。

## 5. 細胞外の水を利用した細胞内薬物分子の濃度定量

上記のように、ラマン顕微鏡は創薬研究において重要なツールになりつつある一方で、ラマン散乱強度は非常に弱く、またラマン顕微鏡による薬剤の分析は、内部標準の無い絶対強度に基づいているため、ラマン強度には必ずしも定量性があるわけではない。そこで我々は、ラマン顕微鏡を用いて細胞内にある分子の濃度定量を行うために、細胞外の水（培地）のラマンバンドを内部標準として用いる方法を提案している。ラマンイメージング測定において同時に観測される細胞外の水の濃度は極めて高く、水中成分がある程度変化しても濃度変化は無視できるほど小さく、水のラマン強度に変化はない。この性質を利用して、細胞外の水のラマンバンドを内部標準として細胞内分子のラマン強度に定量性を与えることができる。初めに緩衝液中の液 - 液相分離（LLPS）によって形成されたタンパク質の液滴を用いて、液滴中のタンパク質の濃度定量を行った[20–23]。予め様々な濃度のタンパク質水溶液を用意し、水の O-H 伸縮振動バンド強度に対するタンパク質のラマン強度の濃度検量線を作成した。次に、液滴内のタンパク質のラマンバンドを液滴外の水の O-H 伸縮振動バンドで規格化し、検量線にあてはめることでタンパク質濃度を算出することができた。この方法を細胞にも適用し、細胞外の水の O-H 伸縮振動バンドを強度標準とすることで、細胞内の核酸濃度を定量することにも成功した[24]。

この水のラマンバンドを用いたラベルフリー単一生細胞濃度定量法を細胞内の薬剤分子に適用した。この総説では、ATRA と *β*- カロテンを PMB によって細胞内に効率的に導入し、生細胞内での濃度分布をその場で明らかにした結果を紹介する[25]。これらの薬剤分子は水にほとんど溶解しないが、PMB により可溶化し高効率に細胞内に導入することができる。ATRA と *β*- カロテンの吸収波長に近い 532 nm の波長の励起レーザー光を用いることで、前期共鳴ラマン効果により 1~100 $\mu$M といった低濃度でも溶液中のラマンスペクトルを検出することができる[26]。

PMB により可溶化した ATRA を 100 $\mu$M で HeLa 細胞の培地に添加し、ラマンイメージングを取得したところ、細胞質において 1580 $cm^{-1}$ に ATRA に由来する C=C 伸縮振動バンドの強度上昇が見られた（図 3）。この C=C 伸縮振動バンド（1548-1588 $cm^{-1}$）の強度をプロットしたラマンイメージでは、強度が高い領域が、脂肪滴を可視化した C-H 伸縮振動バンドのイメージ（2828-2972 $cm^{-1}$）とミトコンドリアに対応するシトクロム（731-758 $cm^{-1}$）のラマン強度イメージの強度が高い領域と一致していた（図 3a-c）。実際に脂肪滴とミトコンドリアのラマンスペクトルにおいて、C=C 伸縮振動バンドのラマン強度が培地のラマン強度と比較して高いことがわかる（図 3d,e）。これらの結果から、ATRA は脂肪滴とミトコンドリアに局在することがわかった。

次に、HeLa 細胞に ATRA を添加し、30 分後に培地を ATRA 不含の緩衝液に交換した。PMB は顕著な細胞

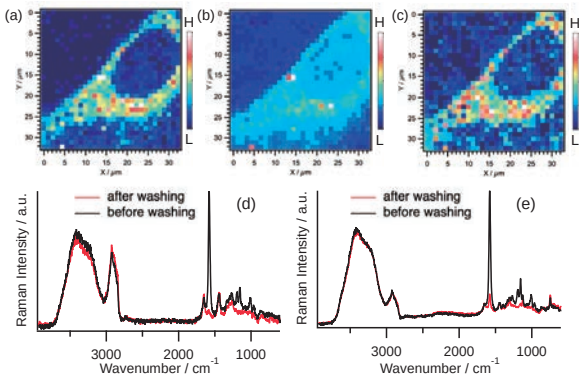


**図 3.** (a-c) PMB で可溶化した ATRA を導入した HeLa 細胞の洗浄前のラマンイメージ。(a) ATRA に対応する C=C 伸縮振動バンド（1548-1588 $cm^{-1}$）のイメージング。(b) C-H 伸縮振動バンド (2828-2972 $cm^{-1}$) のイメージング。白い点が脂肪滴に対応する。(c) ミトコンドリアの分布に対応するシトクロムのラマンバンド（731-758 $cm^{-1}$）のイメージング。(d,e) ATRA を導入した HeLa 細胞の脂肪滴（d）とミトコンドリア（e）のラマンスペクトル。洗浄前（黒）と洗浄後（赤）の比較[25]。

膜透過性により濃度勾配にしたがって、細胞内外を自由に行き来できる。細胞外培地を洗浄して、ATRA を培地から除去すると細胞内の C=C 伸縮振動バンドが減少した。脂肪滴では C=C 伸縮振動バンドがほぼ消失したのに対し、ミトコンドリアでは減少したのみで消失しなかった（図 3d,e）。この結果は、ATRA はミトコンドリアと強く相互作用するために、洗浄後も細胞内に残ることを示している。一方、ATRA と脂肪滴との相互作用は弱く、脂肪滴には濃縮したものの、洗浄により PMB とともに細胞外へ漏出した。

同様の実験を β- カロテンでも行った（図 4）。β- カロテンを PMB で可溶化し HeLa 細胞に添加したところ、ATRA とは異なり細胞内外で β- カロテンのラマンバンド（1006, 1154, 1518 $cm^{-1}$）強度に顕著な変化はなく、強度がほぼ一様な画像が得られた（図 4a,c,e）。この結果は、β- カロテンは PMB とともに細胞内に導入されたが、細胞内には濃縮しないことを示している。さらに、培地を β- カロテンおよび PMB が不含の緩衝液に交換を行うと、細胞内では β- カロテンのラマンバンドは観測されなくなった（図 4b,d,f）。培地中の β- カロテンと PMB が無くなったことで、濃度勾配に従って β- カロテンが細胞内から細胞外へ移動したことを示している。これらのラマンイメージングの結果から、ATRA はミトコンドリアと選択的に強く相互作用することで洗浄後もミトコンドリアに局在するが、β- カロテンはどの細胞内小器官とも相互作用しないため細胞内に濃縮せず、洗浄により細胞外へ漏出したと言える。ラベルフリー測定のため、薬剤本来の性質を反映した結果である。ラマンイメージングを用いることで、薬剤分子の本来の特性を反映した結果を顕微鏡下で単一生細胞を観測しながら得ることができる。

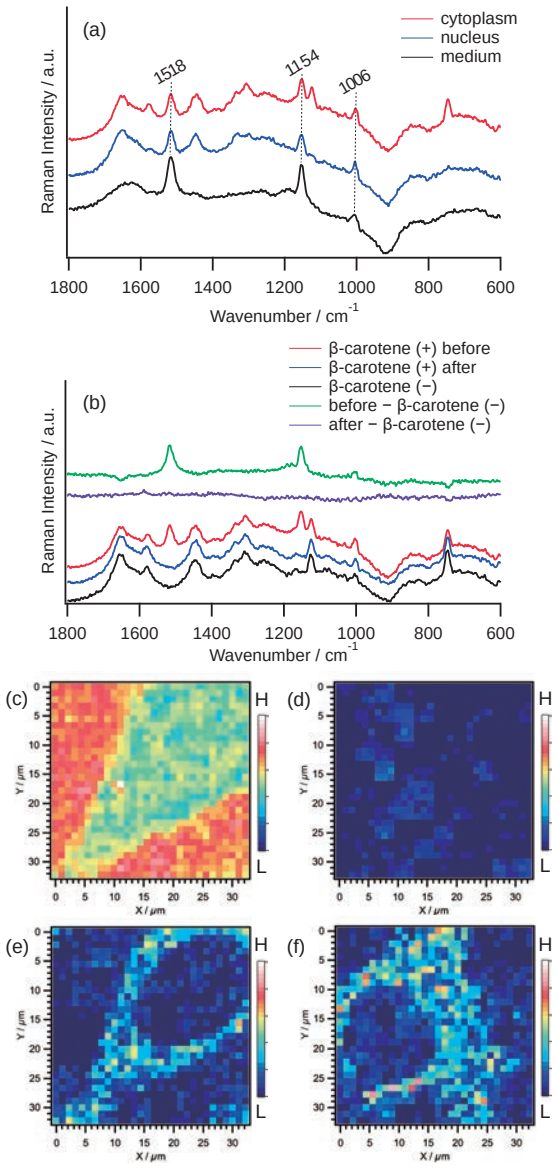


**図 4.** (a,b) PMB で可溶化した β- カロテンを導入した HeLa 細胞のラマンスペクトル。(a) 洗浄前のラマンスペクトル。(b) 洗浄前後の細胞質のラマンスペクトル。(c-h) PMB で可溶化した β- カロテンを導入した HeLa 細胞のラマンイメージ。(c,d) β- カロテンの C-C 伸縮振動ラマンバンド（1174-1138 $cm^{-1}$）、(e,f) シトクロムのラマンバンド（731-758 $cm^{-1}$）のイメージング。(c,e) 洗浄前、(d,f) 洗浄後 [25]。

さらに、ATRA を導入した細胞のラマンイメージングから細胞外の水を強度標準として細胞内の ATRA 濃度を定量した。PMB を使ってさまざまな濃度の ATRA 水溶液を調製し、ラマンスペクトルを取得した（図 5a）。水の O-H 伸縮振動バンドに対する ATRA の C=C 伸縮振動バンドのラマン強度を算出し、ATRA 濃度に対してプロットすることで検量線を作成した（図 5b）。ATRA にも O-H 結合があるが、ATRA の濃度に比べて水の濃度ははるかに高いため、検量線への影響は無視できる。また、PMB は O-H 結合が無いために、水の O-H 伸縮振動バンドへの影響は無い。ATRA を導入した HeLa 細胞の洗浄後のラマンイメージから、細胞外の O-H 伸縮振動バンド強度に対する細胞内の ATRA の C=C 伸縮振動バンドの強度を 1 ピクセルごとに算出した。次に得られた各ピクセルの相対強度を検量線にあてはめ、細胞内の ATRA 濃度を求めることで ATRA の濃度イメージを作成することができた（図 6a）。ATRA 濃度は細胞内の位置によって異なり、細胞質では 50 ～ 200 μ M であることがわかった。また、ATRA の濃度分布はミトコンドリアに対応するシトクロムのラマン強度分布と一致しており、ミトコンドリアにて ATRA が 150~200 μ M も濃縮していることがわかった。以上のように、ラマンイメージングにより細胞内の薬剤分子の濃度分布を顕微鏡下で光をあてるのみで定量的に得ることができる。

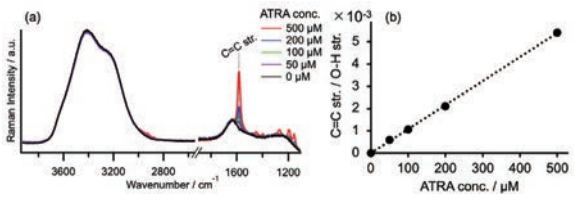


**図 5.** (a) PMB で可溶化した ATRA 水溶液のラマンスペクトル。(b)ATRA の検量線。ATRA 濃度と O-H 伸縮振動バンド（3025-3929 $cm^{-1}$）に対する C=C 伸縮振動バンド（1548-1588 $cm^{-1}$）の強度との関係をプロットした [25]。

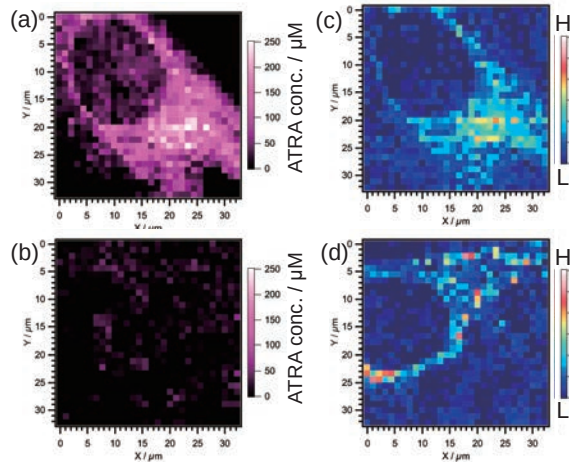


**図 6.** (a,b) ATRA の濃度イメージ。(c,d) シトクロムのラマンバンド（731-758 $cm^{-1}$）に対応するラマンイメージ。(a,c) PMB に可溶化した ATRA を 30 分間インキュベートした後、洗浄により培地から ATRA を除いた。(b,d) ATRA 無添加のコントロール [25]。

## 6. おわりに

本総説では、ラマンイメージングを用いて細胞内に導入した薬剤分子の定量濃度イメージをラベルフリーで得る方法について説明した。光をあてるのみでその場定量を行なうことができ、イメージング測定で同時に得られる細胞外の水のラマンバンドを内部標準とすることが定量測定の肝要となる。また、難水溶性薬剤の可溶化および細胞導入について、従来の方法から我々が用いている膜透過性リン脂質ポリマーを使った方法について概説した。今回紹介した ATRA と $\beta$- カロテンは共鳴ラマン効果によりラマン強度が増強されている。共鳴ラマン効果の条件では無い場合には、細胞内に高濃度で導入する必要があり、優れた可溶化能と細胞膜透過性を持つ PMB は導入キャリアとして有用である。本総説ではラベルフリー濃度イメージングを紹介したが、ラベルフリー測定が今後の生命現象の解析に重要になることは間違いない。ラベルフリーで細胞内分子の情報が得られるラマンイメージングが、生命科学研究における新たな可能性を開いてくれることを確信している。

## References


1. Xie B., Liu Y., Li X., Yang P., He W. Solubilization techniques used for poorly water-soluble drugs. Acta. Pharm. Sin. B, 2024; 14: 4683-4716.
2. Santos C. N., Figueira-Coelho J., Martins-Silva J., Saldanha C. Multidisciplinary utilization of dimethyl sulfoxide: pharmacological, cellular, and molecular aspects. Biochem. Pharmacol., 2003; 65: 1035-1041.
3. Wang Y., Wu K. C., Zhao X. B., et al. A novel paclitaxel microemulsion containing a reduced amount of Cremophor EL: pharmacokinetics, biodistribution, and in vivo antitumor efficacy and safety. J. Biomed. Biotechnol., 2011; 2011: 854872.
4. Hwang D., Ramsey D. J., Kabanov V. A. Polymeric micelles for the delivery of poorly soluble drugs: form nanoformulation to clinical approval. Adv. Drug Deliv. Rev., 2020; 156: 80-118.
5. Rennick J. J., Johnston A. P. R., Parton R. G. Key principles and methods for studying the endocytosis of biological and nanoparticle therapeutics. Nat. Nanotechnol., 2021; 16: 266-276.
6. Chatterjee S., Kon E., Sharma P., Peer D. Endosomal escape: a bottleneck for LNP-mediated therapeutics. Proc. Natl. Acad. Sci., 2024; 121: e2307800120.
7. Ferreira R., Napoli J., Enver T., Bernardino L., Ferreira L. Advances and challenges in retinoid delivery systems in regenerative and therapeutic medicine. Nat. Commun., 2020; 11: 4265.
8. Giuli V. M., Hanieh N. P., Giuliani E., et al. Current trends in ATRA delivery for cancer therapy. Pharmaceutics, 2020; 12: 707.
9. Zhang Y., Li P., Pan H., et al. Retinal-conjugated pH-sensitive micelles induce tumor senescence for boosting breast cancer chemotherapy. Biomaterials, 2016; 83: 219-232.
10. Ishihara K., Ueda T., Nakabayashi N. Preparation of phospholipid polymers and their properties as polymer hydrogel membrane. Polym. J., 1990; 22: 355-360.
11. Konno T., Watanabe J., Ishihara K. Enhanced solubility of paclitaxel using water-soluble and biocompatible 2-methacryloyloxyethyl phosphorylcholine polymers. J. Biomed. Res. A, 2003; 65: 209-214.
12. Wada M., Jinno H., Ueda M., et al. Efficacy of an MPC-BMA co-polymer as a nanotranspoter for paclitaxel. Anticancer Research, 2007; 27: 1431-1436.
13. Suzuki H., Ueno K., Mizumoto T., Seto Y., Sato H., Onoue S. Self-micellizing solid dispersion of cyclosporine A for pulmonary delivery: physicochemical, pharmacokinetic and safety assessments. Eur. J. Pharm. Sci., 2017; 96: 107-114.
14. Shimada K., Matsuda S., Jinno H. The noninvasive treatment for sentinel lymph node metastasis by photodynamic therapy using phospholipid polymer as a nanotranspoter of verteporfin. Biomed. Res. Int., 2017; 74: 12865.
15. Goda T., Goto Y., Ishihara K. Cell-penetrating macromolecules: direct penetration of amphipathic phospholipid polymers across plasma membrane of living cells. Biomaterials, 2010; 31: 2380-2387.
16. Lin X., Konno T., Ishihara K. Cell-membrane-permeable and cytocompatible phospholipid polymer nanoprobes conjugated with molecular beacons. Biomacromolecules, 2014; 15: 150-157.
17. Aljakouch K., Lechtonen T., Yosef H., et al. Raman microspectroscopic evidence for the metabolism of a tyrosine kinase inhibitors, neratinib, in cancer cells. Angew. Chem. Int. Ed., 2018; 57: 7250-7254.
18. Li M., Liao H. X., Bando K., Nawa Y., Fujita S.,

Fujita K. Label-free monitoring of drug-induced cytotoxicity and its molecular fingerprint by live-cell Raman and autofluorescence imaging. Anal. Chem., 2022; 94: 10019-10026.
19. Machida M., Sugimura T., Kajimoto S., et al. Label-free tracking of nanoprodrug cellular uptake and metabolism using Raman and autofluorescence imaging. J. Phys. Chem. B, 2023; 127: 3851-3860.
20. Murakami K., Kajimoto S., Shibata D., Kuroi K., Fujii F., Nakabayashi, T. Observation of liquid-liquid phase separation of ataxin-3 and quantitative evaluation of its concentration in a single droplet using Raman microscopy. Chem. Sci., 2021; 12: 7411.
21. Yokosawa K., Kajimoto S., Shibata D., Kuroi K., Konno T., Nakabayashi T. Concentration quantification of the low-complexity domain of fused in sarcoma inside a single droplet and effects of solution parameters. J. Phys. Chem. Lett., 2022; 13: 5692-5697.
22. Yokosawa K., Tsuruta M., Kajimoto S., Sugimoto N., Miyoshi, N., Nakabayashi T. Quantification of the concentration in a droplet formed by liquid–liquid phase separation of G-quadruplex-forming RNA. Chem. Phys. Lett., 2023; 826: 140634.
23. Kageyama L., Tahara S., Yokosawa K., Kamijo M., Kajimoto S., Nakabayashi, T. Raman quantitative analysis of methionine oxidation and its promotion effect on dissolution of phase-separated liquid droplets of Pbp1. Chem. Phys. Lett., 2024; 856: 141671.
24. Shibuya R, Kajimoto S., Yagimuma H., Ariyoshi T., Okada Y., Nakabayashi T. Nucleic acid-rich stress granules are not merely crowded condensates: a quantitative Raman imaging study. Anal. Chem., 2024; 96: 17078-17085.
25. Koga K., Kajimoto S., Yoshizaki Y. Establishment of a method for the introduction of poorly water-soluble drugs in cells and evaluation of intracellular concentration distribution using resonance Raman imaging. J. Phys. Chem. B, 2024; 128: 1350-1359.
26. Abramczyk H., Imiela A., Surmacki J. Novel strategies of Raman imaging for monitoring intracellular retinoid metabolism in cancer cells. J. Mol. Liq., 2021; 334: 116033.

# Enzymatic synthesis of 4-methylumbelliferyl glycopyranoside-based fluorescence probes with oligosaccharide using the transglycosylation activity of metagenomic β-glucosidase Td2F2

Kyohhei Fujita[1], Mako Kamiya[1,4], Taku Uchiyama[5], Ryosuke Kojima[1], Kiyohiko Igarashi[3,5,6] and Yasuteru Urano[1,2,3 *]

*[1]Graduate School of Medicine, [2]Graduate School of Pharmaceutical Sciences and [3]UT7 Next Life Research Group, The University of Tokyo, 7-3-1 Hongo, Bunkyo-ku, Tokyo 113-0033, Japan.*
*[4]Department of Life Science and Technology, Institute of Science Tokyo, Yokohama, Kanagawa 226-8501, Japan.*
*[5]Department of Biomaterial Sciences, Graduate School of Agricultural and Life Sciences, The University of Tokyo, 1-1-1 Yayoi, Bunkyo-ku, Tokyo 113-8657, Japan.*
*[6]VTT Technical Research Center of Finland Ltd., Tietotie 2, P.O. Box 1000, Espoo, FI-02044 VTT, Finland.*

*e-mail : uranokun@m.u-tokyo.ac.jp

**Key words:** glycosidase, transglycosylation, enzymatic synthesis, fluorescence probe

## ABSTRACT

Activatable glycosidase-reactive fluorescence probes with a glycopyranoside structure are effective analytical tools for the evaluation of various glycosidase activities. However, the chemical synthesis of their substrate moieties is usually challenging due to the need for complicated protection and deprotection steps. As an alternative, enzymatic synthesis offers a more facile approach, and the expansion and functional evaluation of available enzymes are essential. Here, we focused on the β-glucosidase Td2F2 from a compost microbial metagenome, which catalyzes transglycosylation, and evaluated its characteristic and applicability in enzymatic synthesis of fluorescence probes with oligosaccharide substrate moieties. As results, we successfully incorporated a second sugar unit into various 4-methylumbelliferyl glycopyranosides with monosaccharide moiety using Td2F2. Our results suggested that Td2F2 has potential for the applications in enzymatic synthesis of glycopyranoside-based fluorescence probes with oligosaccharide substrate moieties.

## INTRODUCTION

Activatable glycosidase-reactive fluorescence probes with glycopyranoside structure are effective analytical tools for understanding glycobiology and for applications to medical fields.(1-3) For example, 4-methylumbelliferyl glycopyranosides are widely used fluorescence probes for the detection of glycosidase activity.(4-6) Specifically, when the hydroxyl group of 4-methylumbelliferone (4MU) was masked with substrate sugar, the blue fluorescence quenches, but it becomes fluorescent upon the cleavage of the substrate sugar in the presence of the target glycosidase. (5, 7, 8) These probes are commonly used to evaluate glycosidase activity *in vitro*. Chemical probes, including 4MU glycopyranosides, possessing oligosaccharides as substrate moieties are also reported as effective tools to evaluate various glycosidase activities.(9-13) However, the chemical synthesis of oligosaccharide substrate moieties usually requires tedious protection, deprotection and purification steps. (14, 15) In contrast, enzymatic glycosylation provides perfect control of the anomeric configurations and high regio-selectivity without the need for protecting groups and other complicated manipulations.(16-18) So far, enzymatic synthesis of several 4MU glycopyranosides using glycosyltransferases and glycosynthase have been reported.(7, 10) To synthesize fluorescence probes with various oligosaccharide substrate moieties, further expansion and functional evaluation of available enzymes for enzymatic synthesis are required.

Glycosidases are enzymes that hydrolyze glycosidic linkages with net retain or inversion of stereochemistry. (19, 20) It is known that many retaining glycosidase catalyze both a thermodynamically controlled hydrolysis and a kinetically controlled transglycosylation (**Figure 1**).(16, 21) The enzyme active site of retaining glycosidases contains two key catalytic residues such as glutamic acid or aspartic acid. The one side chain acts as a nucleophile, and the other side chain is responsible for general acid/base catalysis in a double-displacement mechanism. In the case of hydrolysis, a covalent glycosyl-enzyme intermediate is formed at first, and then hydrolyzed with general acid/base catalytic assistance. On the other hand, transglycosylation reaction can be achieved by intercepting the reactive glycosyl-enzyme intermediate with an added acceptor sugar instead of a nucleophilic water molecule.

The β-glycosidase Td2F2 encoded by the *td2f2* gene was isolated from a compost microbial metagenomics library.(22, 23) Td2F2 was identified as a member of the

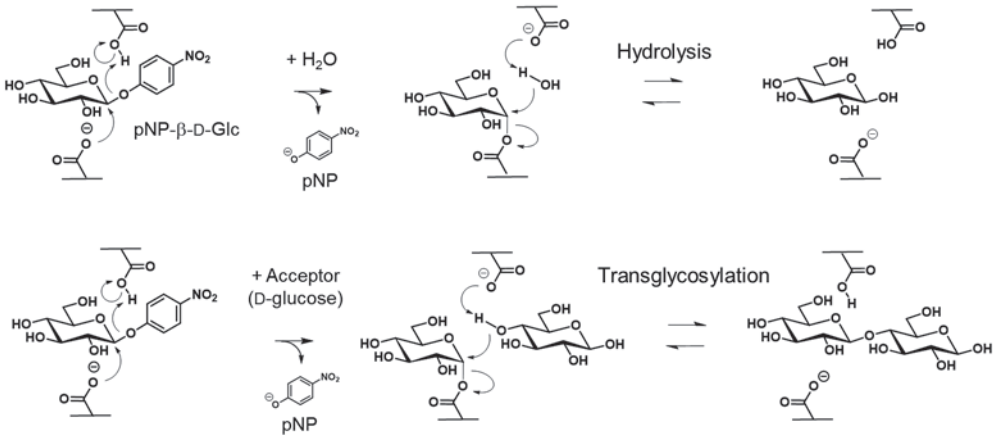


**Figure 1.** Hydrolysis and transglycosylation activities of retaining glycosidase based on a double-displacement mechanism.

glycoside hydrolase family 1 (GH 1), and was classified as a retaining β-glycosidase catalyzing hydrolysis at the nonreducing end and in an exo manner. As an important characteristic of Td2F2, this glycosidase significantly catalyzes transglycosylation with no inhibition by high acceptor concentration, in addition to hydrolysis by a double-displacement mechanism. This strong transglycosylation activity is activated by using *p*-nitrophenyl (pNP) β-glycopyranoside as a donor and D-glucose or D-galactose as an acceptor, leading to the formation of β-glycosidic bond.(22) However, little is known about their acceptor preferences, as well as their potential applications for enzymatic synthesis.

In this study, we aimed to evaluate characteristics and preferences of the transglycosylation activity of Td2F2 and demonstrate its utility in the enzymatic incorporation of oligosaccharide substrate moieties into 4MU glycopyranoside-based fluorescence probes.

## METHODS

**Reagents.** All organic solvents and reagents were commercial products of guaranteed grade, and were used without further purification. Water was doubly distilled and deionized by a Milli-Q water system before use.

**Characterization of compounds.** NMR spectra were recorded on a Bruker AVANCE III and 400 Nanobay at 400 MHz for $^{1}$H NMR. High-resolution mass spectra (HRMS) were measured with a MicroTOF (Bruker).

**Growing *E. coli* cells and plasmid DNA purification.** Plasmid DNA purifications in this experiment were performed by QIAprep Spin Plasmid Kit (QIAGEN). A single colony was picked from a selective antibiotic LB agar plate using a sterile toothpick and inoculated 3 mL of LB medium containing 100 μg/mL ampicillin in a 30 mL tube. The culture was grown overnight at 37°C and then centrifugalized at 12,000 rpm for 1 min. After removing the supernatant, 250 μL of Buffer P1 was added, and the sample was vortexed for mixing. The sample was then added 250 μL of Buffer P2 and tapped for mixing. Following this, 350 μL of Buffer N3 was added, and the sample was tapped for mixing and was centrifugalized at 12,000 rpm for 10 min to form debris. The supernatant (800 μL) was applied to QIAprep spin column, which was then centrifugalized at 12,000 rpm for 1 min. The sample was added 750 μL of Buffer PB and was centrifugalized at 12,000 rpm for 1 min. The sample was added 750 μL of Buffer PE and centrifugalized at 12,000 rpm for 1 min. After centrifugation at 12,000 rpm for 1 min again to completely remove wash buffer, 50 μL of EB buffer was applied to the center of the columns. The spin columns were centrifugalized at 12,000 rpm for 1 min to obtain eluted solutions containing each plasmid. The concentration of plasmid solution was checked by UV-vis measurements.

**Cloning, expression, and purification of the β-glucosidase Td2F2.** *E. coli* BL21 (DE3) harboring pJTtd2f2 were grown in 250 mL of Overnight Express LB Medium (Novagen), supplemented with 100 μg mL$^{-1}$ ampicillin at 37°C for 18 h. After growth, the cells were harvested by centrifugation at 4°C and 4,000 g for 20 min. The resulting cell pellet was frozen overnight at -20°C. The cell pellet was then resuspended in lysis buffer containing Benzonase (QIAGEN). The crude extract was incubated on ice for 30 min. Cell debris was removed by centrifugation at 4°C and 14,000 g for 30 min. The resulting supernatant was purified using Ni-NTA Fast Start Kit (6) (QIAGEN) to obtain the recombinant enzyme, Td2F2. The enzyme fraction was concentrated and substituted by 1 mL of 100 mM $CH_3COONa/CH_3COOH$ buffer, pH 5.5 using an ultrafiltration membrane (Amicon Ultra, Millipore (Billerica, MA)). Expression and concentration of the enzyme stock were checked by SDS-PAGE analysis and BCA protein assay, respectively. All samples were stored at 4°C.

**Evaluation of transglycosylation activity in the presence of acceptor D-glucose.** Transglycosylation activities of Td2F2 (5 μg/mL) was evaluated in the presence of 1,000 mM acceptor D-glucose and 20 mM donor pNP-β-D-Glc, pNP-β-D-Gal or pNP-β-D-Fuc, respectively. The incubations were performed at 70°C for 30 min in 100 mM sodium acetate buffer, pH 5.5-20% DMSO (*v/v*). After 10-fold dilution with 1 M $Na_2CO_3$ a.q.,

the absorbance at 405 nm of each reaction solution was evaluated using Envision plate reader (Perkin Elmer Inc.).

**Evaluation of solvent effects.** Transglycosylation activities of Td2F2 (5 μg/mL) in the presence of 10 mM pNP-β-D-Glc, 500 mM D-glucose and various concentrations of acetonitrile (MeCN), dioxane, dimethyl sulfoxide (DMSO) or tetrahydrofuran (THF) were evaluated. The incubations were performed at 70°C for 30 min in 100 mM sodium acetate buffer, pH 5.5 including each concentration of organic solvent. After 10-fold dilution with 1 M $Na_2CO_3$ a.q., total activities of Td2F2 are evaluated by increase of absorbance at 405 nm derived from pNP production using Envision plate reader (Perkin Elmer Inc.).

**Evaluation of transglycosylation activity using pNP and 4MU glycopyranosides.** Transglycosylation activities in the presence of various concentrations of acceptor 4MU glycopyranosides (50 mM, 10% DMSO; 100 mM, 20% DMSO; 150 mM, 30% DMSO) and 20 mM donor pNP glycopyranosides were evaluated with and without Td2F2 (5 μg/mL). The incubations were carried out at 70°C for 30 min in 100 mM sodium acetate buffer, pH 5.5. Reactions were monitored by TLC and HPLC analysis.

**TLC analysis.** To monitor and evaluate the transglycosylation activity, 2.0 μL of each reaction mixture were applied to silica gel 60 thin layer chromatography (TLC) plates (5 cm x 10 cm) (Merck, Darmstadt, Germany), which were developed with the solvent (AcOEt : AcOH : $H_2O$ = 3 : 2 : 1 by volume for **Figure 2**) or (AcOEt : MeOH : $H_2O$ = 45 : 5 : 3 by volume for **Figures 3 and 4, Table 1**). The products on TLC were detected by heating at 200°C with 10% $H_2SO_4$ and exposing them to 365 nm UV light.

**HPLC analysis.** Transglycosylation reactions were analyzed by analytic reverse-phase HPLC ($C_{18}$ column, 250 x 4.6 mm, pore size: 5 μm) with a gradient of 2-80% MeCN in water (0.1% TFA) over 90 min (a flow rate; 1 mL/min, detection at 254 nm (absorbance) and 400 nm (fluorescence)). For fluorescence chromatograms, excitation and emission were set at 350 nm and 400 nm, respectively.

**Procedure for the enzymatic synthesis of 4MU-β-D-**

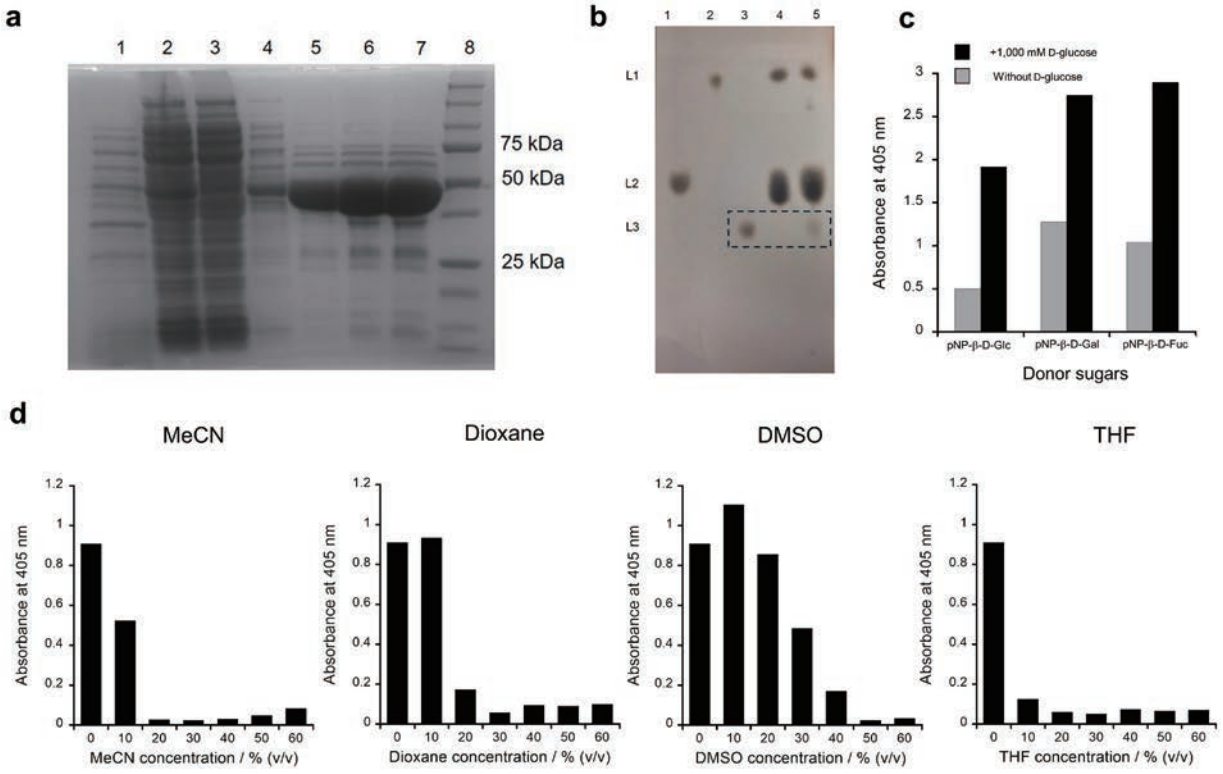


**Figure 2. Evaluation of transglycosylation activities of Td2F2.** (**a**) SDS-PAGE of Td2F2 induced by overnight express LB medium from BL21 (DE3). Lane 1, non-induced; lane 2, induced; lane 3, supernatant; lane 4, wash fraction; lane 5, elution fraction; lane 6 and 7, fraction after buffer substitution, lane 8, molecular marker. (**b**) TLC analysis of D-glucose and pNP-β-D-Glc with and without incubation with Td2F2. Lane 1, D-glucose; lane 2, pNP-β-D-Glc; lane 3, sophorose (disaccharide, putative transglycosylation product); lane4, standards of D-glucose and pNP-β-D-Glc; lane 5, D-glucose and pNP-β-D-Glc incubated with Td2F2; L1, pNP-β-D-Glc; L2, D-glucose; L3, sophorose or transglycosylation products (enclosed with a dotted line). Incubation was carried out in 100 mM sodium acetate buffer, pH 5.5 at 70°C for 120 min. [Td2F2] = 5 μg/mL, [pNP-β-D-Glc] = 20 mM, [D-glucose] = 1,000 mM. (**c**) Absorbance increase at 405 nm derived from pNP produced by transglycosylation and hydrolysis activities of Td2F2, $CH_3COONa/CH_3COOH$ buffer, pH 5.5-20% DMSO (*v/v*), at 70°C. [Td2F2] = 5 μg/mL, [pNP donor sugar] = 10 mM, [D-glucose] = 0 or 1,000 mM. Gray bar represents absorbance increase in the absence of acceptor D-glucose. Black bar represents absorbance increase in the presence of 1,000 mM acceptor D-glucose. (**d**) Absorbance increase at 405 nm derived from pNP produced by hydrolysis and transglycosylation activities of Td2F2 toward pNP-β-D-Glc and D-glucose in the presence of a various concentration of organic solvents, $CH_3COONa/CH_3COOH$ buffer, pH 5.5-0-60% organic solvent (*v/v*), at 70°C. [Td2F2] = 5 μg/mL, [pNP-β-D-Glc] = 10 mM, [D-glucose] = 500 mM.

**Glc-β-D-Fuc.** A mixture of pNP-β-D-Fuc (100 mg, 0.351 mmol), 4MU-β-D-Glc (338 mg, 1.00 mmol) and Td2F2 (46.9 μg) were stirred in 9.00 mL 90% $CH_3COONa$/$CH_3COOH$ buffer, pH 5.5-10% DMSO (*v/v*), at 70°C for 24 h, then the solution was incubated at 95°C for 5 min to quench the reaction. After evaporation, the sample was dissolved in MeOH, then 5.5 g of silica gel 60 was added. After evaporation to dryness, the resulting slurry was subjected to flash column chromatography and eluted with AcOEt : MeOH : $H_2O$ = 45 : 10 : 3 solvent to obtain the product shown in **Figure 3**, L4 spot (8.00 mg, 0.0165 mmol) as a colorless solid in 1.7 % yield (See RESULTS AND DISCUSSION). 4MU-β-D-Glc-β-D-Fuc. $^1$H NMR (400 MHz, DMSO-*d*6): δ 7.72 (d, *J*= 8.4 Hz, 1H), 7.03-7.07 (m, 2H), 6.26 (s, 1H), 5.18 (d, *J*= 7.2 Hz, 1H), 4.35 (d, *J*= 7.2 Hz, 1H), 3.17-3.69 (m, overlaps with HOD), 2.41 (s, 3H), 1.13 (d, *J*= 10.8 Hz, 3H). ESI-HRMS (ESI +) m/z calcd. for [M+Na]+, 507.14730; found, 507.14569.

## RESULTS AND DISCUSSION

### Expressions of Td2F2.

Glycosidase Td2F2 was expressed from *E. coli* BL21 harboring pJTtd2f2 using Overnight Express LB Medium (See METHODS). The expression and purity of Td2F2 (52 kDa) were checked by SDS-PAGE analysis (**Figure 2 (a)**).

### Transglycosylation activity of Td2F2 in the presence of acceptor and donor sugars.

To utilize Td2F2 for enzymatic synthesis, we first examined the TLC detection method for transglycosylation products and the acceptor dependence of several donor sugars. In the TLC analysis, transglycosylation products were observed only in the presence of acceptor D-glucose using the procedure described in the METHODS section (**Figure 2 (b)**). According to the previous research, the observed transglycosylation products were considered to be di-glucose such as sohorose, laminaribiose, cellobiose and gentiobiose.(22, 23) The previous study reported that the pNP production from pNP-β-D-Glc were significantly enhanced as the concentration of the acceptor D-glucose increased, suggesting that high concentrations of the acceptor enhance the transglycosylation activity of Td2F2. (22) When transglycosylation products are produced, pNP

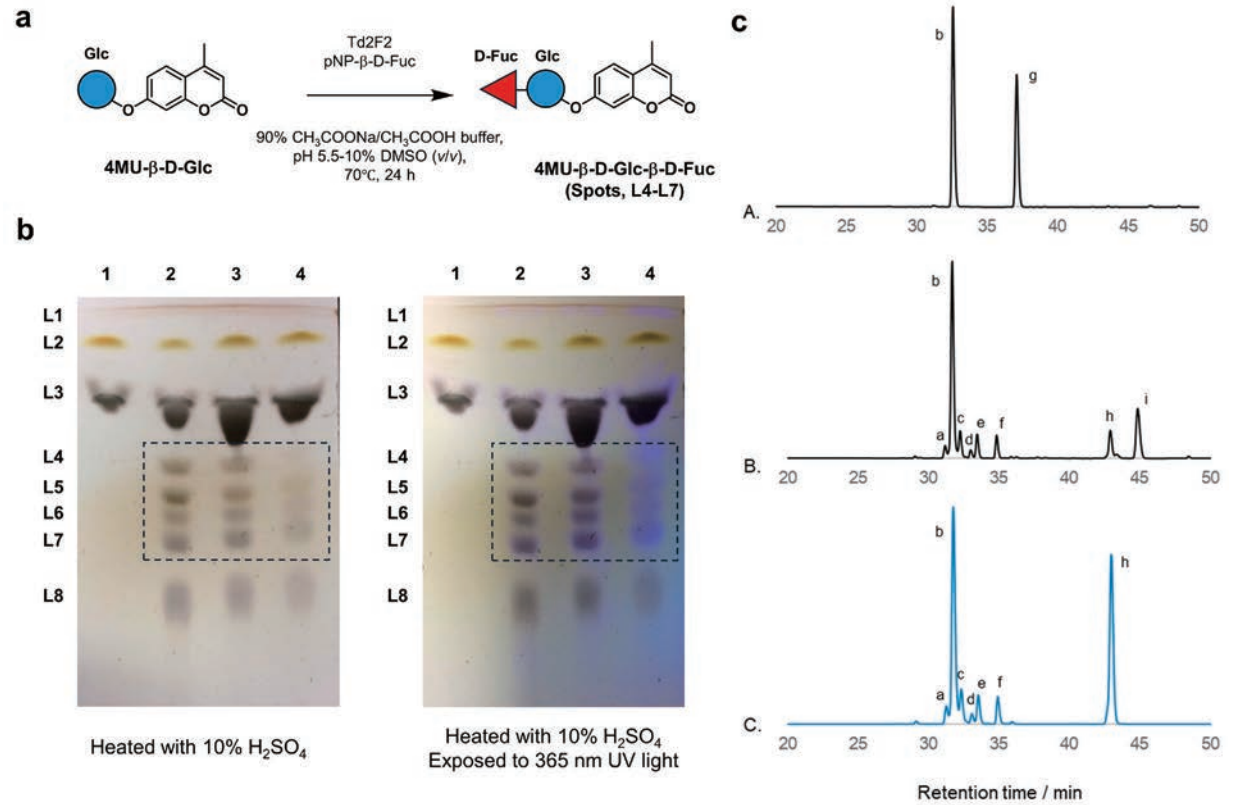


**Figure 3. Enzymatic D-fucosylation of 4MU glucopyranoside.** (**a**) Reaction scheme for the enzymatic installation of D-fucose into 4MU-β-D-Glc. (**b**) TLC analysis of 4MU-β-D-Glc and pNP-β-D-Fuc with and without incubation with Td2F2. Lane 1, standards of 4MU-β-D-Glc and pNP-β-D-Fuc (L2 and L3); lane 2-4, 4MU-β-D-Glc (50 mM, 10% DMSO; 100 mM, 20% DMSO; 150 mM, 30% DMSO) and pNP-β-D-Fuc (20 mM) incubated with Td2F2 (5 μg/mL); L1, 4MU, pNP; L2, pNP-β-D-Fuc; L3, 4MU-β-D-Glc; L4-L7, transglycosylation products derived from 4MU-β-D-Glc (enclosed with a dotted line); L8, D-glucose and D-fucose. Incubation was carried out in 100 mM sodium acetate buffer, pH 5.5 at 70°C for 24 h. (**c**) HPLC analysis of the reaction products of Td2F2. The reaction was performed with 5 μg/mL of Td2F2, 20 mM pNP-β-D-Fuc and 100 mM 4MU-β-D-Glc in 100 mL 90% $CH_3COONa$/$CH_3COOH$ buffer, pH 5.5-10% DMSO (*v/v*), at 70°C for 24 h. Chromatograms are given for (A) standard pNP-β-D-Fuc and 4MU-β-D-Glc (absorbance at 250 nm), (B) pNP-β-D-Fuc and 4MU-β-D-Glc with incubation with Td2F2 (absorbance at 250 nm), and (C) pNP-β-D-Fuc and 4MU-β-D-Glc with incubation with Td2F2 (fluorescence intensity at 400 nm). a, transglycosylation products from 4MU sugar; b, 4MU-β-D-Glc; c-f, transglycosylation products from 4MU sugar; g, pNP-β-D-Fuc; h, 4MU; i, pNP. Ex = 350 nm, Em = 400 nm.

production is expected to be promoted in the presence of the acceptor molecules compared to their absence. We further examined this characteristic of Td2F2 using other donor sugars such as pNP-β-D-Gal and pNP-β-D-Fuc. As well as the case of pNP-β-D-Glc, the same tendency was observed when these pNP glycopyranosides were used as donor sugars (**Figure 2 (c)**). These results indicated that higher concentrations of acceptor are required to efficiently catalyze transglycosylation activity of Td2F2 in the presence of donors pNP-β-D-Glc, pNP-β-D-Gal and pNP-β-D-Fuc.

## Transglycosylation activity of Td2F2 in the presence of various concentrations of organic solvents.

In order to enzymatically synthesize glycopyranoside-based fluorescence probes with oligosaccharide, high

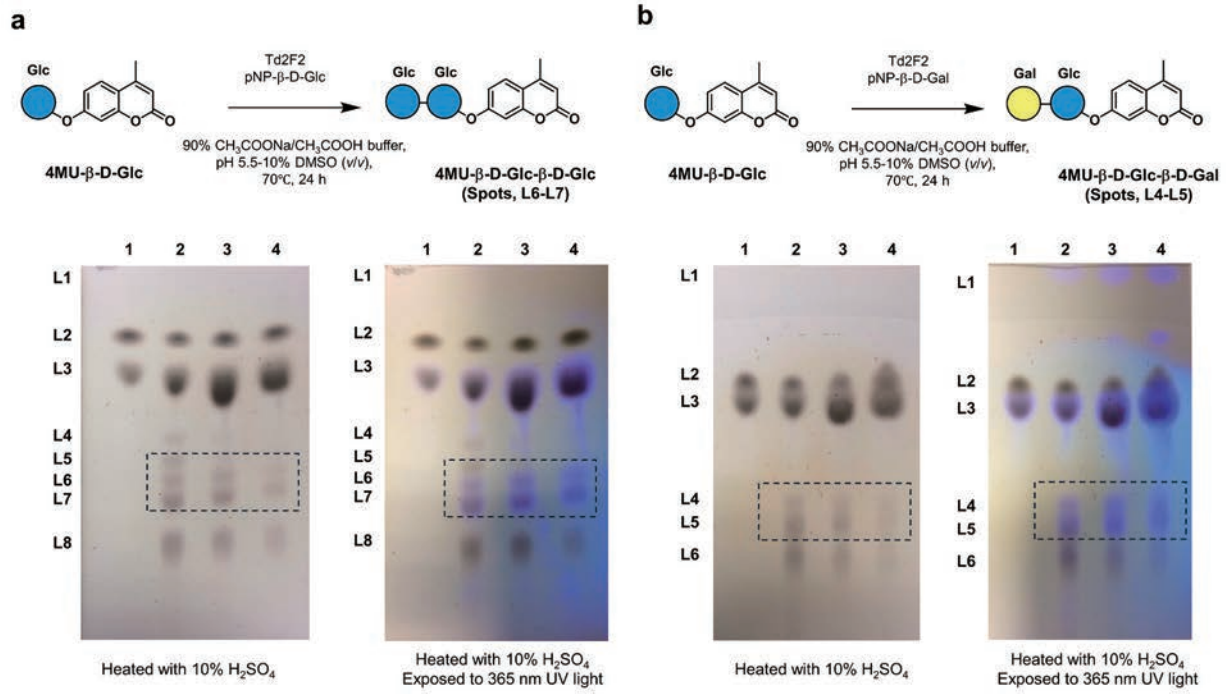


**Figure 4. Enzymatic glucosylation and galactosylation of 4MU glucopyranoside.** (**a**) Reaction scheme for the enzymatic glucosylation of 4MU-β-D-Glc (upper). TLC analysis of 4MU-β-D-Glc and pNP-β-D-Glc with and without incubation with Td2F2 (bottom). Lane 1, standards of 4MU-β-D-Glc (50 mM, 10% DMSO) and pNP-β-D-Glc (L2 and L3); lane 2-4, 4MU-β-D-Glc (50 mM, 10% DMSO; 100 mM, 20% DMSO; 150 mM, 30% DMSO) and pNP-β-D-Glc (20 mM) incubated with Td2F2 (5 μg/mL); L1, 4MU, pNP; L2, pNP-β-D-Glc; L3, 4MU-β-D-Glc; L4 and L5, transglycosylation products derived from pNP-β-D-Glc; L6 and L7, transglycosylation products derived from 4MU-β-D-Glc; L8, D-glucose. Incubation was performed in 100 mM sodium acetate buffer, pH 5.5 at 70°C for 24 h. (**b**) Reaction scheme for the enzymatic galactosylation of 4MU-β-D-Glc (upper). TLC analysis of 4MU-β-D-Glc and pNP-β-D-Gal with and without incubation with Td2F2 (bottom). Lane 1, standards of 4MU-β-D-Glc and pNP-β-D-Gal (L2 and L3); lane 2-4, 4MU-β-D-Glc (50 mM, 10% DMSO; 100 mM, 20% DMSO; 150 mM, 30% DMSO) and pNP-β-D-Gal (20 mM) incubated with Td2F2 (5 μg/mL); L1, 4MU, pNP; L2, pNP-β-D-Gal; L3, 4MU-β-D-Glc; L4-L5, transglycosylation products derived from 4MU-β-D-Glc; L6, D-glucose and D-galactose; L7, transglycosylation product. Incubation was performed in 100 mM sodium acetate buffer, pH 5.5 at 70°C for 24 h.

Acceptor 4MU glycopyranosides

| Donor pNP glycopyranosides | 4MU-β-D-Glc | 4MU-β-D-Gal | 4MU-β-D-Fuc | 4MU-β-D-Man | 4MU-β-D-GlcNAc | 4MU-β-D-Xyl | 4MU |
|---|---|---|---|---|---|---|---|
| pNP-β-D-Glc | ○ | ○ | ND | ○ | ND | ○ | ND |
| pNP-β-D-Gal | ○ | ○ | ND | ○ | ○ | ○ | ND |
| pNP-β-D-Fuc | ○ | ○ | ND | ○ | ○ | ○ | ND |
| pNP-β-D-Man | ND | ND | ND | ○ | ND | ND | ND |
| pNP-β-D-GlcNAc | ND | ND | ND | ND | ND | ND | ND |
| pNP-β-D-GlcUA | ND | ND | ND | ND | ND | ND | ND |
| pNP-β-D-Xyl | ND | ○ | ND | ○ | ND | ND | ND |

Circles ○; transglycosylation products were detected by TLC analysis.
ND; transglycosylation products were not detected by TLC analysis.

**Table 1.** Donor and acceptor preference of Td2F2.

concentrations of the acceptor probe molecules must be dissolved in the buffer solution. However, water solubilities of these organic molecules are usually poor. Therefore, addition of certain amounts of organic solvent to the reaction mixture as a cosolvent is inevitable. Thus, we next examined the solvent effects on transglycosylation activity using pNP-β-D-Glc as a donor and D-glucose as an acceptor in the presence of various non-reactive organic solvents: MeCN, dioxane, DMSO or THF. These non-nucleophilic solvents were selected to avoid attacking the anomeric carbon of donor sugars activated by Td2F2. As a result, Td2F2 can efficiently catalyze transglycosylation in 10-20% DMSO or 10% dioxane conditions, whereas its activity decreased in the presence of 10% MeCN and THF (**Figure 2 (d)**). This solvent effect of DMSO also represented the results of the previous research.(22) The observed behaviors may reflect their differential effects on protein structure and hydration. DMSO and dioxane are moderately polar solvents and are considered to exert minimal effects on protein structure and hydration shells. In contrast, MeCN is highly polar, whereas THF is relatively hydrophobic, both of which may disrupt protein conformation and hydration structures. These results suggested that 10-20% DMSO or 10% dioxane conditions should be useful in enzymatic synthesis using Td2F2.

## Enzymatic glycosylation of 4MU glucopyranoside using transglycosylation activity of Td2F2.

We next examined whether Td2F2 catalyzes transglycosylation toward the 4MU glucopyranoside-based probe. Since Td2F2 especially exhibited significant transglycosylation in the presence of donor pNP-β-D-Fuc and acceptor D-glucose, we first evaluated the pair of donor pNP-β-D-Fuc and acceptor 4MU-β-D-Glc. To dissolved high concentration of 4MU-β-D-Glc (50-150 mM), 10-30% DMSO (v/v) was added to the $CH_3COONa/CH_3COOH$ buffer, pH 5.5 (**Figure 3 (a)**), and transglycosylation reactions were monitored by TLC and HPLC analysis. In the TLC analysis using the procedure described in the METHODS section, four fluorescent spots (L4-L7) were clearly observed after incubation with Td2F2, especially under 10-20% DMSO conditions (**Figure 3 (b)**), as we investigated in **Figure 2 (d)**. In the HPLC analysis, five fluorescent peaks appeared after incubation with Td2F2 (**Figure 3 (c)**). These new spots and peaks were considered to be the transglycosylation products (disaccharides or trisaccharides) derived from 4MU-β-D-Glc, suggesting that Td2F2 catalyzes transglycosylation toward 4MU-β-D-Glc. We also performed this enzymatic reaction on a scale of hundreds milligrams under 10% DMSO conditions and purified the reaction mixture to isolate the L4 spot with 1.7% yield (See METHODS). This spot was identified as D-fucosylated 4MU-β-D-Glc (4MU-β-D-Glc-β-D-Fuc) by $^1$HNMR and ESI-HRMS. Furthermore, using pNP-β-D-Glc or pNP-β-D-Gal as a donor, transglycosylation products derived from 4MU-β-D-Glc were also detected by TLC (**Figures 4 (a)** and **(b)**) and HPLC (data not shown) analysis. These results suggested that Td2F2 can preferentially utilize 4MU-β-D-Glc rather than water as an acceptor for the glycosyl moiety during the catalytic degradation of pNP donor sugars, thereby providing the transglycosylation products. The glycosylation positions of the acceptor sugar were not identified in this study.

## Evaluation of donor and acceptor preference of Td2F2.

Finally, we evaluated the transglycosylation activity of Td2F2 using various combinations of donor pNP glycopyranosides and acceptor 4MU glycopyranosides (Table 1). As a result, Td2F2 was found to catalyze transglycosylation, especially when pNP-β-D-Glc, pNP-β-D-Gal, pNP-β-D-Fuc, pNP-β-D-Man and pNP-β-D-Xyl was used as donors, depending on the acceptor 4MU glycopyranosides. Furthermore, we also found that various 4MU glycopyranosides, such as 4MU-β-D-Glc, 4MU-β-D-Gal, 4MU-β-D-Man, 4MU-β-D-GlcNAc and 4MU-β-D-Xyl can be used as acceptor sugars, depending on the donor sugars. These results suggested that Td2F2 exhibits broader specificity for donor and acceptor sugars compared to typical glycosyltransferases and glycosynthases. It was also suggested that the 4MU fluorophore does not significantly affect the substrate affinity of active site in Td2F2. These results indicated the potential utility of Td2F2 for enzymatic synthesis of the various oligosaccharide substrate moieties of 4MU glycopyranoside-based probes or other fluorescence probes. As a limitation of enzymatic glycosylation using Td2F2, the yield is low due to the simultaneous hydrolysis reactions. In order to further optimize the function of Td2F2 in enzymatic synthesis, additional investigations, such as glycosynthase engineering by genetic modifications, are required.(24) Furthermore, Td2F2 was unable to directly transfer pNP donor sugars to the hydroxy group of 4MU, indicating that 4MU cannot work as an acceptor. This result indicated that Td2F2 particularly prefers sugar structures as acceptor molecules. Our results suggested that Td2F2 is a promising enzyme that can be utilized to introduce sugars into various probes with saccharide moieties.

## CONCLUSION

In order to demonstrate the utility of transglycosylation activity of Td2F2 in enzymatic synthesis of glycosidase-reactive fluorescence probes with oligosaccharide substrate moieties, we evaluated the characteristics of transglycosylation activity of Td2F2. As a result, Td2F2 exhibited high transglycosylation activity in the presence of acceptor molecules under 10-20% DMSO or 10% dioxane conditions. We also found that Td2F2 demonstrated transglycosylation activity with various combinations of donor pNP glycopyranosides and acceptor 4MU glycopyranosides. By optimizing the reaction conditions, we enzymatically incorporated a

second sugar unit into various 4MU glycopyranosides with a monosaccharide moiety using Td2F2, and successfully synthesized various 4MU glycopyranoside-based probes with a disaccharide moiety without the need for protecting groups. These results suggested that Td2F2 exhibits uniquely broad substrate specificity toward donor pNP and acceptor 4MU glycopyranosides, compared to typical glycosyltransferases and glycosynthases. Its transglycosylation activity has potential for the application in enzymatic synthesis of the oligosaccharide substrate moieties of various glycosidase-reactive fluorescence probes.

## Data Availability

All data and materials are available upon request.

## Acknowledgements

This research was supported in part by AMED under grant number JP19gm0710008 (to Y.U.), by MEXT/JSPS KAKENHI grants JP16H02606, JP26111012 and JP19H05632 (to Y.U.). JSPS KAKENHI grant number JP22K20528 and JP23K14317 (to K. F.). JST, ACT-X grant number JPMJAX222G and Masason Foundation (to K.F.).

## Author contributions

K.F., M.K. and Y.U. designed the project. K.F. performed the experimental work. T. U. and K. I. provided pJTtd2f2. K.F., M.K., R.K. and Y.U. analyzed the results. K.F. wrote the manuscript with input from all the authors. The authors declare no competing interests.

## References

1. Fujita K, Urano Y. Activity-Based Fluorescence Diagnostics for Cancer. Chemical Reviews. 2024;124(7):4021-78.
2. Fujita K, Kamiya M, Yoshioka T, Ogasawara A, Hino R, Kojima R, et al. Rapid and Accurate Visualization of Breast Tumors with a Fluorescent Probe Targeting α-Mannosidase 2C1. ACS Central Science. 2020;6(12):2217-27.
3. Burke HM, Gunnlaugsson T, Scanlan EM. Recent advances in the development of synthetic chemical probes for glycosidase enzymes. Chemical Communications. 2015;51(53):10576-88.
4. Park S, Shin I. Profiling of Glycosidase Activities Using Coumarin-Conjugated Glycoside Cocktails. Organic Letters. 2007;9(4):619-22.
5. Li Y, Deng B, Chen H, Yang S, Sun B. A ratiometric fluorescent probe for the detection of β-galactosidase and its application. RSC Advances. 2021;11(22):13341-7.
6. Chen H-M, Armstrong Z, Hallam SJ, Withers SG. Synthesis and evaluation of a series of 6-chloro-4-methylumbelliferyl glycosides as fluorogenic reagents for screening metagenomic libraries for glycosidase activity. Carbohydrate Research. 2016;421:33-9.
7. Williams GJ, Zhang C, Thorson JS. Expanding the promiscuity of a natural-product glycosyltransferase by directed evolution. Nature chemical biology. 2007;3(10):657-62.
8. Giovannini G, Hall AJ, Gubala V. Coumarin-based, switchable fluorescent substrates for enzymatic bacterial detection. Talanta. 2018;188:448-53.
9. Eneyskaya EV, Ivanen DR, Shabalin KA, Kulminskaya AA, Backinowsky LV, Brumer Iii H, et al. Chemo-enzymatic synthesis of 4-methylumbelliferyl β-(1→4)-d-xylooligosides: new substrates for β-d-xylanase assays. Organic & Biomolecular Chemistry. 2005;3(1):146-51.
10. Kwan DH, Ernst S, Kötzler MP, Withers SG. Chemoenzymatic Synthesis of a Type 2 Blood Group A Tetrasaccharide and Development of High-throughput Assays Enables a Platform for Screening Blood Group Antigen-cleaving Enzymes. Glycobiology. 2015;25(8):806-11.
11. Foo AY, Bais R. Amylase measurement with 2-chloro-4-nitrophenyl maltotrioside as substrate. Clinica Chimica Acta. 1998;272(2):137-47.
12. Malet C, Vallés J, Bou J, Planas A. A specific chromophoric substrate for activity assays of 1,3-1,4-β-d-glucan 4-glucanohydrolases. Journal of Biotechnology. 1996;48(3):209-19.
13. Singh M, Watkinson M, Scanlan EM, Miller GJ. Illuminating glycoscience: synthetic strategies for FRET-enabled carbohydrate active enzyme probes. RSC Chemical Biology. 2020;1(5):352-68.
14. Bennett CS. Principles of modern solid-phase oligosaccharide synthesis. Organic & Biomolecular Chemistry. 2014;12(11):1686-98.
15. Das R, Mukhopadhyay B. Chemical O-Glycosylations: An Overview. ChemistryOpen. 2016;5(5):401-33.
16. Wang L-X, Huang W. Enzymatic transglycosylation for glycoconjugate synthesis. Current Opinion in Chemical Biology. 2009;13(5):592-600.
17. Hancock SM, Vaughan MD, Withers SG. Engineering of glycosidases and glycosyltransferases. Current Opinion in Chemical Biology. 2006;10(5):509-19.
18. Rich JR, Cunningham A-M, Gilbert M, Withers SG. Glycosphingolipid synthesis employing a combination of recombinant glycosyltransferases and an endoglycoceramidase glycosynthase. Chemical Communications. 2011;47(38):10806-8.
19. Bojarová P, Křen V. Glycosidases: a key to tailored carbohydrates. Trends in Biotechnology. 2009;27(4):199-209.
20. Vocadlo DJ, Davies GJ. Mechanistic insights into glycosidase chemistry. Current Opinion in Chemical Biology. 2008;12(5):539-55.
21. Vester-Christensen MB, Holck J, Rejzek M, Perrin L, Tovborg M, Svensson B, et al. Exploration of the Transglycosylation Activity of Barley Limit

Dextrinase for Production of Novel Glycoconjugates. Molecules. 2023;28(10):4111.
22. Uchiyama T, Miyazaki K, Yaoi K. Characterization of a Novel β-Glucosidase from a Compost Microbial Metagenome with Strong Transglycosylation Activity*. Journal of Biological Chemistry. 2013;288(25):18325-34.
23. Matsuzawa T, Jo T, Uchiyama T, Manninen JA, Arakawa T, Miyazaki K, et al. Crystal structure and identification of a key amino acid for glucose tolerance, substrate specificity, and transglycosylation activity of metagenomic β-glucosidase Td2F2. The FEBS journal. 2016;283(12):2340-53.
24. Mackenzie LF, Wang Q, Warren RAJ, Withers SG. Glycosynthases: Mutant Glycosidases for Oligosaccharide Synthesis. Journal of the American Chemical Society. 1998;120(22):5583-4.

# Photocytotoxicity for HeLa cells by tetrakis(alkoxyphenyl)porphyrin phosphorus(V) complexes

Kazutaka Hirakawa,[1,2,3*] Hiroko Hasegawa,[2] and Shiho Hirohara[4,5]

[1] *Applied Chemistry and Biochemical Engineering Course, Department of Engineering, Graduate School of Integrated Science and Technology, Shizuoka University, Johoku 3-5-1, Chuo-ku, Hamamatsu, Shizuoka 432-8561, Japan*
[2] *Department of Optoelectronics and Nanostructure Science, Graduate School of Science and Technology, Shizuoka University, Johoku 3-5-1, Chuo-ku, Hamamatsu, Shizuoka 432-8561, Japan*
[3] *Cooperative Major in Medical Photonics, Shizuoka University, Johoku 3-5-1, Chuo-ku, Hamamatsu, Shizuoka 432-8561, Japan*
[4] *Department of Chemical and Biological Engineering, National Institute of Technology, Ube College, Tokiwadai, Ube, Yamaguchi 755-8555, Japan*
[5] *Department of Bioresources Engineering, National Institute of Technology, Okinawa College 905 Henoko, Nago-shi, Okinawa, Japan 905-2192, Japan*

***Corresponding author:**
Kazutaka Hirakawa
Applied Chemistry and Biochemical Engineering Course, Department of Engineering, Graduate School of Integrated Science and Technology, Shizuoka University, Johoku 3-5-1, Chuo-ku, Hamamatsu, Shizuoka 432-8561, Japan
Tel/Fax: +81-53-478-1287, E-mail: hirakawa.kazutaka@shizuoka.ac.jp

**Abstract:**

Photodynamic therapy is a less invasive cancer therapy based on the cytotoxicity by photoexcited medicines. In this study, photocytotoxicity of four types of porphyrin phosphorus(V) complexes for HeLa cells were examined. The reciprocal values of half-maximal inhibitory concentration (IC50) showed the good relationship (correlation coefficient: 0.8622) with the lowest unoccupied molecular orbital energy of these photosensitizers. The relationship between singlet oxygen production quantum yields and the reciprocal values of IC50 was not significant (correlation coefficient: 0.0199). These results suggest that electron transfer-mediated mechanism mainly contribute to photocytotoxicity of these porphyrin phosphorus(V) complexes.

**Keywords:** Porphyrin phosphorus(V) complex; Photocytotoxicity; HeLa cells; Electron transfer; Singlet oxygen

## INTRODUCTION

Porphyrin derivatives and their complexes have been studied as the photosensitizers for photodynamic therapy (PDT), which is a less invasive cancer therapy [1-3]. Singlet oxygen ($^1O_2$) production under visible-light irradiation is an important mechanism for PDT. Furthermore, electron transfer-mediated oxidation of biomolecules has been also reported as the mechanism of biomolecules oxidation [4,5]. Specifically, porphyrin phosphorus(V) complexes can easily oxidize protein [6,7] and DNA [8] through electron transfer. Since tumor tissue is under a hypoxic condition [9,10], the electron transfer mechanism may be an important process to preserve the PDT effect. Recently, we have reported the photosensitized biomolecule oxidation activity of tetrakis(alkoxyphenyl)porphyrin phosphorus(V) complexes (Fig. 1) through $^1O_2$ production and electron transfer mechanisms [11]. The photochemical parameters related to the photooxidation of biomolecules showed good relationship with photochemical oxidation quantum yield of nicotinamide adenine dinucleotide derivative [11]. In this study, photocytotoxicity for HeLa cells by these porphyrin phosphorus(V) complexes was

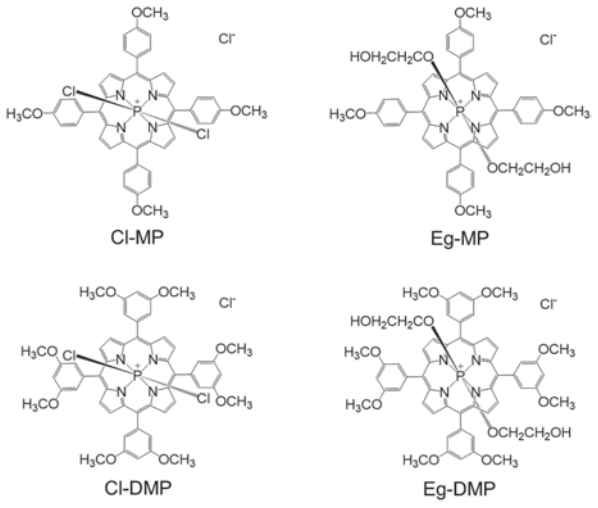


**Fig. 1.** Structures of porphyrin phosphorus(V) complexes.

examined. The relationship between these photocytotoxic effects and photochemical parameters, $^1O_2$ production activity, and molecular orbital energy levels, was also investigated.

## EXPERIMENTAL

**Chemicals.**

Porphyrin phosphorus(V) complexes, dichloro-phosphorus(V)tetrakis(4-methoxyphenyl)porphyrin (Cl-MP) and bis(2-hydroxyethoxy)-phosphorus(V) tetrakis(4-methoxyphenyl)porphyrin (Eg-MP), were synthesized according to the literature [6]; and dichloro-phosphorus(V)tetrakis(3,5-dimethoxyphenyl) porphyrin (Cl-DMP) and bis(2-hydroxyethoxy)-phosphorus(V)tetrakis(3,5-dimethoxyphenyl)porphyrin (Eg-DMP) were synthesized by the previously reported method [11]. Ethanol was obtained from FUJIFILM Wako Pure Chemical Co., Ltd (Osaka, Japan). Spectroscopic-grade water was purchased from Dojin Chemicals Co. (Kumamoto, Japan).

**Cell Culture.**

HeLa human cervical cell line, HeLa (ATCC CCL-2), was obtained from Sumitomo Pharma Co., Ltd. (Osaka, Japan). HeLa cells were grown in Dulbecco's modified Eagle's medium (DMEM, Shimadzu Co., Tokyo, Japan) supplemented with 10% fetal calf serum (FCS, Hyclone Labratories, Inc., Logan, UT, USA) and 1% Antibiotic-Antimycotic (Life Technologies Japan Ltd., Tokyo, Japan).

**Cytotoxicity Test.**

The cytotoxicity of dark and photocytotoxicity of porphyrin phosphorus(V) complexes in cancer cells were examined as follows: Cells ($5\times10^3$ cells/well) in 100 μL of culture medium were plated in 96-well plate (Thermo Fisher Scientific, Inc., Tokyo, Japan) and incubated for overnight (37 °C, 5% $CO_2$). The plate was then incubated at 24 h in the presence of the photosensitizers. The photosensitizer concentration was varied from 0.001 μM to 0.5 μM in culture medium (final ethanol content was 1% in all cases). The cells were washed twice with phosphate-buffered saline, and 100 μL of the fresh culture medium was added. The cells were exposed to light from a 100-W halogen lamp (Luminar Ace LA-150UE, Hayashi-Repic Co., Ltd., Tokyo, Japan) equipped with a water jacket and a Y-50 cut off filter ($\lambda > 500$ nm, Toshiba Co., Tokyo, Japan). The light intensity was measured by using a power mater (power meter: StarLife Meter RoHS, thermopile sensor: 2A-BB-9, Ophir Optronics Ltd., Jerusalem, Israel). The irradiation time was adjusted to obtain the desired light dose of 15 J $cm^{-2}$. The mitochondrial activity of NADH dehydrogenase of the cells in each well was measured at 24 h after photoirradiation using WST-8 reagent (8 μL) from Cell Counting Kit-8 (Dojindo, Tokyo, Japan) according to the manufacturer's instructions. The absorbance at 450 nm was measured using a plate reader (Multiskan Sky, Thermo Fisher Scientific Co., Yokohama, Japan). The percentage of cell survival was calculated by normalization with respect to the value for no drug treatment.

**Calculation.**

The optimized structures and molecular orbital energy levels of these porphyrins were calculated by the density functional theory (DFT) at ωB97X-D level utilized with Spartan'20 (Wavefunction Inc., CA, USA).

## RESULTS AND DISCUSSION

These porphyrin phosphorus(V) complexes demonstrated photocytotoxicity to HeLa cells (Fig. 2A). The observed half-maximal inhibitory concentration (IC50) values were as follows: 0.058 μM (Cl-MP), 0.042 μM (Eg-MP), 0.052 μM (Cl-DMP), and 0.033 μM (Eg-DMP). Therefore, the photocytotoxicity of these porphyrin phosphorus(V) complexes becomes the following order: Eg-DMP > Eg-MP > Cl-DMP > Cl-MP. These results showed that the photocytotoxicity of these hydrophobic porphyrin phosphorus(V) complexes for HeLa cells is smaller than those of highly water-soluble glycosylated free base porphyrins (IC50: 0.5-1 nM) under a similar experimental condition [12]. However, these porphyrin phosphorus(V) complexes showed comparable photocytotoxicity to 5,10,15,20-tetrakis(pentafluorophen yl)porphyrins [13]; and showed stronger photocytotoxicity than those of 5,10,15,20-tetrakis(pentafluorophenyl) porphyrin bearing 2-hydroxyethylthio groups (IC50: larger than μM order) [14]. In general, previous reports suggest that water-soluble porphyrin shows relatively stronger photocytotoxicity than hydrophobic porphyrins [12-14]. The present results showed the relatively strong PDT activity of these porphyrin phosphorus(V) complexes, though these porphins are hydrophobic compounds. Specifically, newly synthesized porphyrin, Eg-DMP, was most active photosensitizer in these porphyrins under the present experimental condition. Dark cytotoxicity of porphyrin phosphorus(V) complexes was also examined using relatively high concentration (0.5 μM) (Fig. 2B). Eg-DMP and Eg-MP showed relatively strong dark toxicity. The dark toxicity of Cl-DMP was lowest in these porphyrins.

Relationship between the photocytotoxicity of porphyrin phosphorus(V) complexes and their photochemical parameters was evaluated (Fig. 3). These porphyrin phosphorus(V) complexes can oxidize biomolecules through photoinduced electron transfer [6,11]. The $^1O_2$ production activity of these porphyrins has been evaluated. The reported values of $^1O_2$ production quantum yield ($\Phi_\Delta$) of these porphyrin phosphorus(V) complexes in ethanol are as follows: 0.68 (Cl-MP) [6], 0.61 (Eg-MP) [6], 0.24 (Cl-DMP) [11], and 0.47 (Eg-DMP) [11]. The calculated values of the lowest unoccupied molecular orbital (LUMO) for these porphyrin phosphorus(V) complexes were as follows: -4.13 eV (Cl-MP), -3.97 eV (Eg-MP), -4.09 eV (Cl-DMP), and -3.96 eV (Eg-DMP). The higher LUMO energy level indicates the higher redox

potential of photosensitizer; and high redox potential is effective for the electron transfer-mediated oxidation [15]. To evaluate the photocytotoxic effect of photosensitizers, the reciprocal value of IC50 was used as an indicator. Relatively good relationship between the LUMO values and the reciprocal values of IC50 (correlation coefficient: 0.8622) was observed (Fig. 3A), whereas a significant relationship between their $\Phi_\Delta$ values and the reciprocal values of IC50 was not observed (correlation coefficient: 0.0199) (Fig. 3B). These results suggest that electron transfer mechanism contributes to the photocytotoxic effect of these porphyrin phosphorus(V) complexes.

## CONCLUSIONS

Photocytotoxicity of porphyrin phosphorus(V) complexes, Cl-MP, Eg-MP, Cl-DMP, and Eg-DMP, for HeLa cells were confirmed. Eg-MP and Eg-DMP showed relatively strong dark toxicity, whereas those of Cl-MP and Cl-DMP were relatively small. The reciprocal values of IC50 showed the good relationship with the LUMO energy of these photosensitizers. The relationship between the $\Phi_\Delta$ values and the reciprocal values of IC50 was not significant. These results suggest that electron transfer-mediated mechanism mainly contribute to photocytotoxicity of these porphyrin phosphorus(V) complexes.

## Acknowledgments

This work was supported in part by Grant-in-Aid for Scientific Research (B) from Japanese Society for the Promotion of Science (JSPS KAKENHI 17H03086), The Futaba Research Grant Program of the Futaba Foundation (No. 10407), and Takahashi Industrial and Economic Research Foundation.

## Notes

The authors declare no conflict of interests.

## References

1. Dolmans DEJGJ, Fukumura D, Jain RK. Photodynamic therapy for cancer. Nat Rev Cancer, 2003;3:380-387.
2. Tian J, Huang B, Nawaz MH, Zhang W. Recent advances of multi-dimensional porphyrin-based functional materials in photodynamic therapy. Coord Chem Rev, 2020;420:213410.
3. Ji B, Wei M, Yang B. Recent advances in nanomedicines for photodynamic therapy (PDT)-driven cancer immunotherapy. Theranostics, 2022;12:434-458.
4. Ouyang D, Hirakawa K. Photosensitized enzyme deactivation and protein oxidation by axial-substituted phosphorus(V) tetraphenylporphyrins. J Photochem Photobiol B, 2017;175:125-131.
5. Hirakawa K, Takai S, Horiuchi H, Okazaki S. Photooxidation activity control of dimethylaminoph enyltris-(*N*-methyl-4-pridinio)porphyrin by pH. ACS Omega, 2020;5:27702-27708.
6. Hirakawa K, Ouyang D, Ibuki Y, Hirohara S, Okazaki S, Kono E, Kanayama N, Nakazaki J, Segawa H. Photosensitized protein-damaging activity, cytotoxicity, and antitumor effects of P(V)porphyrins using long-wavelength visible light through electron transfer. Chem Res Toxicol, 2018;31:371-379.
7. Hirakawa K, Yoshida M, Hirano T, Nakazaki J, Segawa H. Photosensitized protein damage by

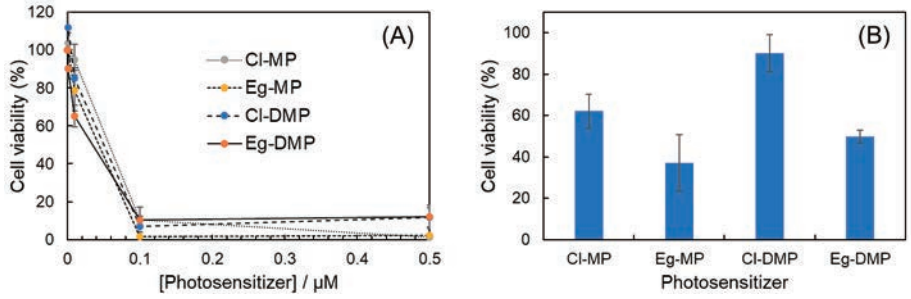


**Fig. 2.** Cell viability of HeLa cells with (A) and without (B) light irradiation in the presence of porphyrin phosphorus(V) complexes. The concentration of porphyrin phosphorus(V) complexes for dark-toxicity assay was 0.5 μM (B). The experimental condition was described in the Experimental section.

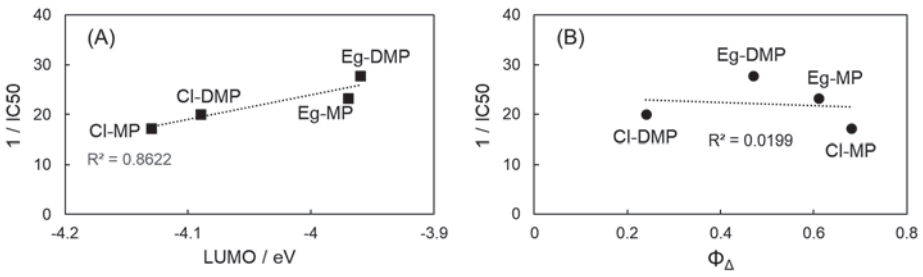


**Fig. 3.** The relationship between the reciprocal values of IC50 and the photochemical parameters.

diethyleneglycoxyP(V)tetrakis(*p*-*n*-butoxyphenyl) porphyrin through electron transfer: activity control through self-aggregation and dissociation. Photochem Photobiol, 2022;98:434-441.
8. Hirakawa K, Kawanishi S, Hirano T, Segawa H. Guanine-specific DNA oxidation photosensitized by the tetraphenylporphyrin phosphorus(V) complex via singlet oxygen generation and electron transfer. J Photochem Photobiol B, 2007;87:209-217.
9. Yoshihara T, Hirakawa Y, Hosaka M, Nangaku M, Tobita S. Oxygen imaging of living cells and tissues using luminescent molecular probes. J Photochem Photobiol C, 2017;30:71-95.
10. Li Y, Zhao L, Li XF. Hypoxia and the tumor microenvironment. Technol Cancer Res Treat, 2021;20:15330338211036304.
11. Hasegawa H, Hirakawa K. Evaluation of the photosensitizer activity of hydrophobic phosphorus(V)porphyrins using the absorption spectral change of 1-benzyl-1,4-dihydronicotinamide. Spectrochim Acta A, 2024;308:123765.
12. Hirohara S, Oka C, Totani M, Obata M, Yuasa J, Ito H, Tamura M, Matsui H, Kakiuchi K, Kawai T, Kawaichi M, Tanihara M. Synthesis, photophysical properties, and biological evaluation of trans-bisthioglycosylated tetrakis(fluorophenyl)chlorin for photodynamic therapy. J Med Chem, 2015;58:8658-8670.
13. Hirohara S, Sharyo K, Kawasaki Y, Totani M, Tomotsuka A, Funasako R, Yasui N, Hasegawa Y, Yuasa J, Nakashima T, Kawai T, Oka C, Kawaichi M, Obata M, Tanihara M. trans-Bisglycoconjugation is an efficient and robust architecture for PDT photosensitizers based on 5,10,15,20-tetrakis(penta fluorophenyl)porphyrin derivatives. Bull Chem Soc Jpn, 2013;86:1295-1308.
14. Obata M, Hirohara S. Syntheses, photophysical properties, and photocytotoxicities of tetrakis(fluorophenyl)porphyrin derivatives bearing 2-hydroxyethylthio groups. J Photochem Photobiol B, 2016;162:324-331.
15. Hirakawa K, Ishikawa T. Phenothiazine dyes photosensitize protein damage through electron transfer and singlet oxygen generation. Dyes Pigmt, 2017;142:183-188.

# Effect of *meso*-phenyl substituents on the photochemical and electrochemical properties of tetrakis(methoxyphenyl)porphyrin phosphorus(V) complexes

Kazutaka Hirakawa,[1,2,3*] Daiki Miyake,[1] Tomoki Matsui,[1] Shota Nomura,[1] and Shigetoshi Okazaki[4]

[1] *Applied Chemistry and Biochemical Engineering Course, Department of Engineering, Graduate School of Integrated Science and Technology, Shizuoka University, Johoku 3-5-1, Chuo-ku, Hamamatsu, Shizuoka 432-8561, Japan*
[2] *Department of Optoelectronics and Nanostructure Science, Graduate School of Science and Technology, Shizuoka University, Johoku 3-5-1, Chuo-ku, Hamamatsu, Shizuoka 432-8561, Japan*
[3] *Cooperative Major in Medical Photonics, Shizuoka University, Johoku 3-5-1, Chuo-ku, Hamamatsu, Shizuoka 432-8561, Japan*
[4] *Preeminent Medical Photonics Education and Research Center, Hamamatsu University School of Medicine, Handayama 1-20-1, Chuo-ku, Hamamatsu, Shizuoka 431-3192, Japan*

***Corresponding author:**

Kazutaka Hirakawa
Applied Chemistry and Biochemical Engineering Course, Department of Engineering, Graduate School of Integrated Science and Technology, Shizuoka University, Johoku 3-5-1, Chuo-ku, Hamamatsu, Shizuoka 432-8561, Japan
Tel/Fax: +81-53-478-1287, E-mail: hirakawa.kazutaka@shizuoka.ac.jp

**Abstract:**

Tetrakis(methoxyphenyl)porphyrin phosphorus(V) complexes were synthesized to investigate the effect of *meso*-phenyl substituents on their photosensitizer properties. Redox potentials and photochemical properties, absorption and fluorescence spectra, and singlet oxygen production activities of these porphyrins were examined. Tetrakis(*p*-methoxyphenyl)porphyrin phosphorus(V) complex (***p*-OCH$_3$**) showed the smallest photoexcitation energy among the porphyrins used in this study and its redox potential of one-electron reduction was relatively large. The low-excitation-energy photosensitizer is suitable for photodynamic therapy, since longer wavelength visible light can penetrate deeply into human tissues. The higher redox potential of one-electron reduction is an effective property of the photosensitizer to photooxidize biomolecules via the electron transfer mechanism. The quantum yield of protein photodamage by ***p*-OCH$_3$** was largest in the porphyrin phosphorus(V) complexes used in this study. In conclusion, this study suggests that the tetrakis(*p*-alkoxyphenyl)porphyrin phosphorus(V) complex, a *p*-alkoxy substituted derivative of phosphorus(V) tetraphenylporphyrin, is a suitable electron transfer photosensitizer for photodynamic therapy.

**Keywords:** Porphyrin phosphorus(V) complex; *meso*-Substituent; Redox potential; Excitation energy; Protein damage

## INTRODUCTION

The molecular design of photosensitizer is one of the most important topics in the foundation of photodynamic therapy (PDT), a less invasive form of cancer phototherapy [1-3]. Porphyrins are clinically used compounds for PDT photosensitizers and their derivatives have been extensively studied [4-6]. In general, administered porphyrin molecules induce oxidative damage to biomolecules in cancer cells through production of reactive oxygen species such as singlet oxygen ($^1O_2$) under illumination. Furthermore, porphyrin phosphorus(V) complexes can damage biomolecules through an electron transfer mechanism as $^1O_2$ production mechanism does [7-9]. Since the tumor microenvironment is under hypoxia [10-12], the electron transfer-mediated biomolecule oxidation should become an important mechanism of PDT [7]. Tetraphenylporphyrin can be easily synthesized and this type of porphyrin is photochemically stable, and substitution of the phenyl group of this porphyrin can improve the photochemical and electrochemical property of the porphyrin ring [7]. The lower energy level of the singlet excited ($S_1$) state is an advantageous property for PDT photosensitizer, since longer wavelength visible light or near infrared radiation can penetrate deeply into human tissues [13,14]. In addition, the redox potential of the photosensitizer is an important factor for the activity of the photosensitizer to induce biomolecule damage through electron transfer [7]. The higher redox potential of the one-electron reduction of the photosensitizer is advantageous for this electron transfer-induced oxidation. However, the low $S_1$ energy of the photosensitizer is traded off with the strong photooxidative activity via electron transfer. In this study, several types of tetraphenylporphyrin phosphorus(V) complexes (Fig. 1) were synthesized to evaluate their

photochemical and electrochemical properties. Previously reported similar types of phosphorus(V) porphyrins [9,15] were also used in this study.

## EXPERIMENTAL

Acetonitrile, ethanol, phosphoryl chloride, pyrrole, pyridine (anhydrous), and spectroscopic-grade distilled water were purchased from FUJIFILM Wako Pure Chemical Co., Ltd., (Osaka, Japan). Human serum albumin (HSA) was obtained from Sigma-Aldrich Co. LLC. (St. Louis, MO, USA). Sodium phosphate buffer (0.1 M, pH 7.6) was obtained from Nacalai Tesque Inc. (Kyoto, Japan). Porphyrin phosphorus(V) complexes, dichloro *meso*-tetraphenylporphyrin phosphorus(V) chloride (**H**) [15], dichloro *meso*-tetrakis(4-methoxyphenyl)porphyrin phosphorus(V) chloride (***p*-OCH$_3$**) [9], and dichloro *meso*-tetrakis(3,5-dimethoxyphenyl)porphyrin phosphorus(V) chloride (***m*-di-OCH$_3$**) [16] were synthesized according to the reported previously.

**Synthesis of *o*-di-OCH$_3$:** *meso*-Tetrakis(2,6-dimethoxyphenyl)porphyrin was synthesized using 2,6-dimethoxybenzaldehyde (Tokyo Chemical Industry Co., Ltd., Tokyo, Japan) and pyrrole according to the literature [17]. Dichloro *meso*-tetrakis(2,6-dimethoxyphenyl)porphyrin phosphorus(V) chloride (***o*-di-OCH$_3$**) was synthesized by refluxing in 5 mL of dry pyridine with *meso*-tetrakis(2,6-dimethoxyphenyl) porphyrin (100 mg) and phosphoryl chloride (9 g) for 290 h, as the similar method of the literature [18]. The solvent was removed in vacuo after reaction. The product was purified by column chromatography on silica gel with a chloroform-methanol (75/25, vol/vol) as an eluent. The yield of ***o*-di-OCH$_3$** was 91% (100 mg). $^1$H-NMR (300 MHz, $CDCl_3$, δ in ppm) δ 8.85 (8H, d, $J_{P\text{-}H}$ =3.0 Hz, *β*H), 7.72 (4H, d, $J_{H\text{-}H}$ = 9.0 Hz, *p*-phenyl-H), 6.66 (8H, d, $J_{H\text{-}H}$ =9.0 Hz, *m*-phenyl-H), δ 4.13 (12H, s, methoxy-H), δ 2.98 (12H, s, methoxy-H), FAB-MS m/z: 953.2 (calcd.), 953.3 (observed).

**Synthesis of *o,p*-di-OCH$_3$:** *meso*-Tetrakis(2,4-dimethoxyphenyl)porphyrin was synthesized using 2,4-dimethoxybenzaldehyde (Tokyo Chemical Industry Co., Ltd.) and pyrrole according to the literature [17]. Dichloro *meso*-tetrakis(2,4-dimethoxyphenyl) porphyrin phosphorus(V) chloride (***o,p*-di-OCH$_3$**) was synthesized by refluxing in 5 mL of dry pyridine with *meso*-tetrakis(2,4-dimethoxyphenyl)porphyrin (80 mg) and phosphoryl chloride (1.4 g) for 120 h, as the similar method of the literature [18]. The solvent was removed in vacuo after reaction. The product was purified by column chromatography on silica gel with a chloroform-methanol (80/20, vol/vol) as an eluent. The yield of **o,*p*-di-OCH$_3$** was 10% (9 mg). $^1$H-NMR (300 MHz, $CDCl_3$, δ in ppm): δ 8.96 (8H, d, $J_{P\text{-}H}$=1.5 Hz, *β*H), 7.28 (4H, d, $J_{H\text{-}H}$=10.2 Hz, phenyl-H), 6.90 (4H, d, $J_{H\text{-}H}$=8.4 Hz, phenyl-H), 6.79 (4H, s, phenyl-H), 4.03 (12H, s, methoxy-H), 3.99 (12H, s, methoxy-H), $^{13}$C-NMR (300 MHz, $CDCl_3$, δ in ppm) δ 163.08, 159.42, 140.47, 134.88, 132.27, 99.05, 77.24, 55.95, 55.68. ESI-HR TOF-MS m/z: 953.2269 (calcd.), 953.2330 (observed).

**Synthesis of *m,p*-tri-OCH$_3$:** Tetrakis(*3,4,5*-trimethoxyphenyl)porphyrin was synthesized using *3,4,5*-trimethoxybenzaldehyde (Tokyo Chemical Industry Co., Ltd.) and pyrrole according to the literature [17]. Dichloro 5,10,15,20-tetrakis(3',4',5'-dimethoxy) phenylporphyrin phosphorus(V) chloride (***m,p*-tri-OCH$_3$**) was synthesized by refluxing in 2 mL of dry pyridine with tetrakis(*3,4,5*-trimethoxyphenyl)porphyrin (160 mg) and phosphoryl chloride (2.4 g) for 96 h, as the similar method of the literature [18]. The solvent was removed in vacuo after reaction. The product was purified by column chromatography on silica gel with a chloroform-methanol (75/25, vol/vol) as an eluent. The yield of ***m,p*-tri-OCH$_3$** was 55% (90 mg).$^1$H NMR (300 MHz, $CDCL_3$, δ in ppm): δ 9.01 (8H, d, $J_{P\text{-}H}$ = 9.0 Hz, *β*H), 7.27 (8H, s, *o*-phenyl-H), 4.03 (12H, d, $J_{H\text{-}H}$ =3.0 Hz, methoxy-H), 3.88 (24H, d, $J_{H\text{-}H}$ =12 Hz, methoxy-H), FAB-MS m/z: 1041.3 (calcd.), 1041.3 (observed).

**Measurements:** The absorption spectra of samples were measured with the UV-Vis spectrophotometer UV-1650PC (Shimadzu, Kyoto, Japan). The fluorescence

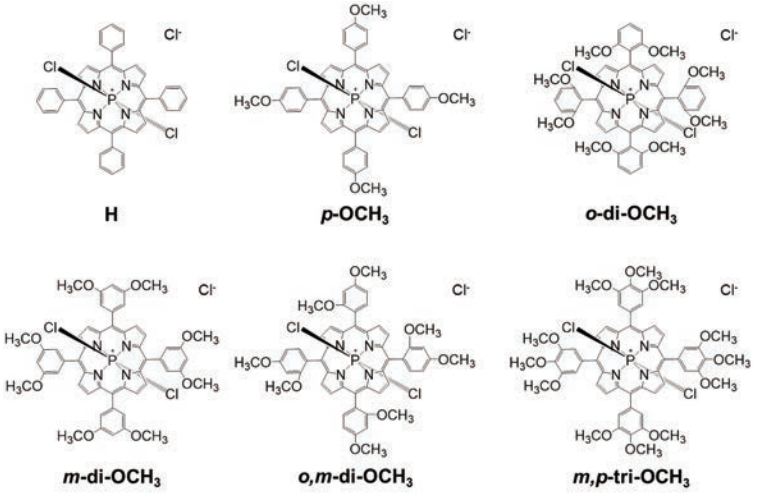


**Fig. 1.** Structures of porphyrin phosphorus(V) complexes.

spectra of samples were measured with an F-4500 fluorescence spectrophotometer (Hitachi, Tokyo, Japan). The fluorescence lifetime ($\tau_f$), which equals the $S_1$ state lifetime of porphyrin was measured with a Fluorescence Lifetime System TemPro (HORIBA, Kyoto, Japan). The excitation wavelength for the $\tau_f$ measurements was 402 nm. The sample solutions for the absorption and fluorescence measurements contained 5 μM porphyrin phosphorus(V) complexes in ethanol. Redox potentials of the porphyrin phosphorus(V) complexes (1 mg $mL^{-1}$) in dry acetonitrile including 0.1 M tetrabutylammonium hexafluorophosphate (supporting electrolyte) were measured with a potentiostat/galvanostat (HA-301, Hokuto Denko Co., Tokyo, Japan), a digital function generator (DF1906, NF Co., Yokohama, Japan), and a midi logger (GL900-4, Graphtec Co., Yokohama, Japan), using a platinum working electrode (ALS Co., Ltd., Tokyo, Japan), a platinum counter electrode (ALS Co., Ltd.), and saturated calomel electrode (SCE, ALS Co., Ltd). The quantum yield of $^1O_2$ production ($\Phi_\Delta$) by these porphyrins (5 μM) in ethanol was examined by the method reported previously [19].

**Calculation:** The optimized structure of porphyrin phosphorus(V) complex was calculated by the density functional theory (DFT) at the ωB97X-D/6-31G* level utilizing the Spartan 20' (Wavefunction Inc., CA).

**Evaluation of protein photodamage:** To evaluate protein photodamaging activity of porphyrin phosphorus(V) complexes, the sample solution containing 10 μM porphyrins and 10 μM HSA was prepared in a 10 mM sodium phosphate buffer (pH 7.6) including 5% ethanol. The binding interaction between HSA and porphyrin phosphorus(V) complex was analyzed by the absorption spectrum measurement according to the previous report [9]. The sample solution was irradiated with a light-emitting diode (LED, $\lambda_{max}$= 585 or 659 nm, 2.0 mW $cm^{-2}$, CCS Inc., Kyoto, Japan). The intensity of the LED was measured with an 8230E optical power meter (ADC Corporation, Tokyo, Japan). The fluorescence intensity of HSA at 350 nm, assigned to the emission from tryptophan [20], was measured with a Hitachi 650-60 fluorescence photometer (Hitachi, Tokyo, Japan). The excitation wavelength for this assay was 298 nm. HSA photodamage was analyzed by the results of fluorometry based on the diminishment of the intrinsic fluorescence of tryptophan residue, as reported previously [9].

## RESULTS AND DISCUSSION

The absorption spectra of the phosphorus(V) porphyrins were affected by the *meso*-substituents. The wavelengths of the absorption maxima of these phosphorus(V) porphyrins are listed in Table 1. The $S_1$ energy of ***p*-OCH*3*** ($E_{0\text{-}0}$) was the smallest in these phosphorus(V) porphyrins. The low excitation energy is suitable for PDT photosensitizer, since the window region of wavelength is between around 650~900 nm and longer wavelength visible light can penetrate deeply into human tissues [13,14]. However, the higher excitation energy is advantageous for the greater oxidative capacity of photosensitizer through the electron transfer mechanism [7]. The redox potentials of photosensitizers are also important characteristics of PDT photosensitizers. The higher redox potentials of one-electron reduction ($E_{red}$) and oxidation ($E_{ox}$) of the photosensitizer are advantageous for the electron transfer-mediated oxidation of biomolecules. In general, the photosensitizer with the larger gap between $E_{red}$ and $E_{ox}$ (larger $S_1$ energy) shows stronger photooxidative activity [7]. The redox potentials and the energy gaps of these porphyrins are shown in Fig. 2. The large energy gap and large $E_{red}$ (small absolute value) should be the important factors for the electron transfer photosensitizer. The $E_{red}$ values of these phosphorus(V) porphyrins are listed in Table 1. The $E_{red}$ value of **H** is the highest (smallest absolute value) in these porphyrins. The $E_{red}$ value of ***p*-OCH$_3$** is also relatively large in these phosphorus(V) porphyrins. It is suggested that the results for ***p*-OCH$_3$** can be explained by the electron-donating property of the methoxy group substituted at the *para*-position of phenyl ring. The $E_{red}$ values of ***o*-di-OCH$_3$**, ***m*-di-OCH$_3$**, ***o,p*-di-OCH$_3$**, and ***m,p*-tri-OCH$_3$** were relatively small. These results demonstrated that the methoxy group in the *meta*-position decreases the $E_{red}$ of the porphyrin ring. Therefore, the *meta*-substituted tetraphenylporphyrin phosphorus(V) complex may not be effective for the electron transfer-mediated photooxidation of biomolecules. These results can be explained by the effect of the *meta*-position substitutions and suggest that the *meta*-alkoxy substitution of the phenyl group suppresses the photooxidative activity

**Table 1.** Photochemical property and redox potential of porphyrin P(V) complexes

| Porphyrin | $\lambda_{Ab}$ / nm [a] | $E_{0\text{-}0}$ / eV [a] | $E_{red}$ / V vs. SCE [b] |
|---|---|---|---|
| **H** | 437, 565, 610 | 2.04 | -0.30 |
| ***p*-OCH$_3$** | 456, 576, 628 | 1.94 | -0.33 |
| ***o*-di-OCH$_3$** | 436, 563, 604 | 2.08 | -0.47 |
| ***m*-di-OCH$_3$** | 446, 569, 614 | 2.01 | -0.46 |
| ***o,p*-di-OCH$_3$** | 448, 571, 621 | 2.03 | -0.40 |
| ***m,p*-tri-OCH$_3$** | 433, 557, 605 | 2.06 | -0.49 |

$\lambda_{Ab}$: absorption maximum. [a]: in ethanol. [b]: in acetonitrile.

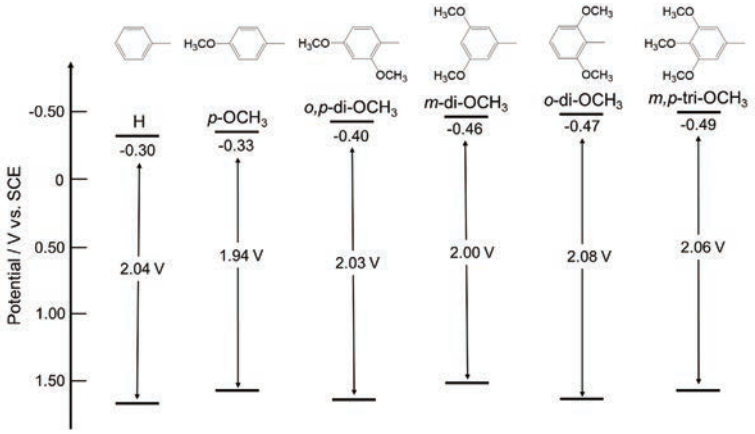


**Fig. 2.** Redox potentials and the scheme of energy gap of porphyrin phosphorus(V) complexes.

of the porphyrin phosphorus(V) complex via the electron transfer mechanism. Based on the results for the *para*-substituted compounds, it was predicted that the *ortho*-substituent would also increase the $E_{red}$ value of the porphyrins, because of the similar effects of the *ortho* and *para* substitution. However, the observed $E_{red}$ values of ***o*-di-OCH$_3$** and ***o,p*-di-OCH$_3$** were significantly smaller than those of **H** and ***p*-OCH$_3$**. Furthermore, the $E_{0\text{-}0}$ of these porphyrins are relatively large. These results can be explained by the steric effect of the *ortho* substituent. The optimized structure of *ortho*-substituted porphyrin is shown in Fig. 3. The porphyrin ring and the phenyl ring of the *ortho*-substituted porphyrin become orthogonal to each other due to a steric hindrance of this methoxy-group at the *ortho*-position of the phenyl group. This steric effect should reduce an electronic interaction between these porphyrins and their phenyl rings. These findings suggest that the electron-donating interaction from the *meso*-phenyl moiety to the porphyrin ring plays an important

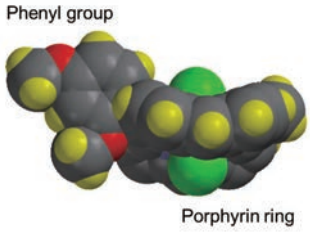


**Fig. 3.** The optimized structure of ***o,p*-di-OCH$_3$**.

role in the decrease of $E_{0\text{-}0}$; however, this substitution does not strongly decrease the redox potential of the porphyrin ring.

The methoxy substitution decreased the fluorescence quantum yield ($\Phi_f$) and fluorescence lifetime ($\tau_f$) (Table 2). The shorter lifetime of the photoexcited state is not advantageous from a kinetic point of view for the photooxidation of the biomolecule via the electron transfer mechanism. The $^1O_2$ production quantum yields

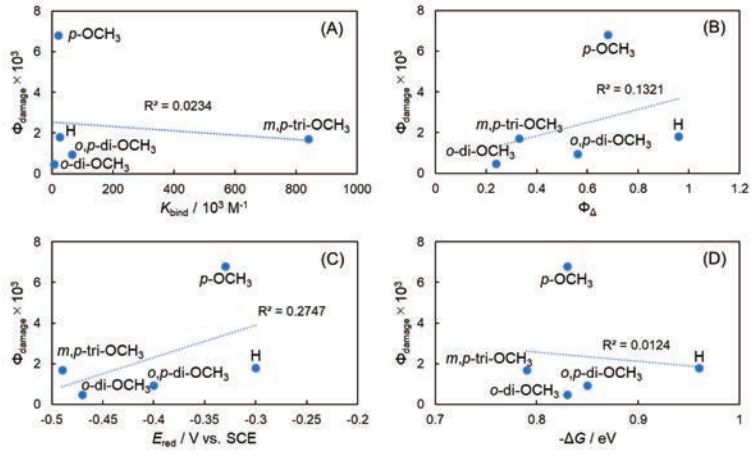


**Fig. 4.** Relationship between the quantum yield of protein photodamage and the related parameters of porphyrin phosphorus(V) complexes. $\Phi_{damage}$ and $K_{bind}$ (A), $\Phi_{damage}$ and $\Phi_\Delta$ (B), $\Phi_{damage}$ and $E_{red}$ (C), and $\Phi_{damage}$ and the Gibbs energy of electron transfer from tryptophan to photoexcited porphyrin ($-\Delta G$) (D). $\Delta G = e(E_{ox} - E_{red}) - E_{0\text{-}0}$. $e$: elementary charge ($1.602\times10^{-19}$ C). $E_{ox}$: redox potential of one-electron oxidation of tryptophan (0.78 V vs. SCE) [22]. $R^2$: correlation coefficient.

**Table 2.** The binding constants between HSA and porphyrin phosphorus(V) complexes, their fluorescence quantum yields, fluorescence lifetimes, quantum yields of $^1O_2$ production, and quantum yields of protein photodamage

| Porphyrin | $K_{bind}$ / $M^{-1}$ [a] | $\Phi_f$ [b] | $\tau_f$ / ns | $\Phi_\Delta$ [b, c] | $\Phi_{damage}$ [a] |
|---|---|---|---|---|---|
| **H** | $2.6\times10^5$ | 0.045 | 5.7 (0.79), 3.6 (0.21) [d] | 0.96 | $1.8\times10^{-3}$ |
| ***p*-OCH$_3$** | $2.1\times10^6$ | 0.026 | 2.05 [b] | 0.68 | $6.8\times10^{-3}$ |
| ***o*-di-OCH$_3$** | $7.9\times10^4$ | 0.032 | ND | 0.24 | $4.7\times10^{-4}$ |
| ***m*-di-OCH$_3$** | ND | 0.037 | 3.73 [b] | 0.17 | ND |
| ***o,p*-di-OCH$_3$** | $6.6\times10^5$ | 0.023 | 0.63 (0.61), 3.43 (0.39) [b] | 0.56 | $9.4\times10^{-4}$ |
| ***m,p*-tri-OCH$_3$** | $8.4\times10^6$ | 0.028 | ND | 0.33 | $1.7\times10^{-3}$ |

[a]: in 10 mM sodium phosphate buffer plus 5% ethanol. [b]: in ethanol. [c]: These values were determined using a reference photosensitizer (methylene blue: 0.52 in ethanol) [21]. [d]: in 10 mM sodium phosphate buffer [16]. ND: not determined.

($\Phi_\Delta$) of these phosphorus(V) porphyrins were also decreased by the methoxy substitution (Table 2). These results suggest that the methoxy substitution of the phenyl group of the porphyrin phosphorus(V) complex reduces its photosensitizing activity. However, the quantum yield of protein photodamage ($\Phi_{damage}$) of ***p*-OCH$_3$** was largest in these porphyrins (Table 2). The binding constant between these porphyrins and HSA ($K_{bind}$), which can be determined from the previous report [9], is also listed in Table 2. The following relationships between "$\Phi_{damage}$ and $K_{bind}$" and "$\Phi_{damage}$ and $\Delta G$" are not significant, though the "$\Phi_{damage}$ and $E_{red}$", and "$\Phi_{damage}$ and $\Phi_\Delta$" showed a weak relationship (Fig. 4). The factors governing the protein photodamage are complicated. In this study, ***p*-OCH$_3$** demonstrated relatively strong protein photodamaging activity and the reason for this is unclear; however, these results suggest that the *para*-alkoxy-substituted porphyrin phosphorus(V) complex has superior photosensitizing activity for PDT in practical use. The observed value of $\Phi_{damage}$ by ***m,p*-tri-OCH$_3$**, of which the $E_{red}$ was smallest in these porphyrins, was relatively large (Fig. 4C). This result may be explained by that the large $K_{bind}$ between ***m,p*-tri-OCH$_3$** and HSA enhances the possibility of photosensitized tryptophan oxidation.

## CONCLUSIONS

The methoxy-substituted tetraphenylporphyrin phosphorus(V) complexes were synthesized to evaluate their redox potentials and photochemical properties. ***p*-OCH$_3$** showed relatively large $E_{red}$ value and its $E_{0\text{-}0}$ was the smallest among the porphyrins used in this study. Furthermore, the protein photodamaging activity of ***p*-OCH$_3$** was greatest in these porphyrins. The large $E_{red}$ and small $E_{0\text{-}0}$ of the PDT photosensitizer are advantageous for the mechanism of biomolecule oxidation via photoinduced electron transfer. These results demonstrate that the *p*-alkoxy-substituted tetraphenylporphyrin phosphorus(V) complex is a suitable electron transfer photosensitizer for inducing oxidative biomolecule damage.

## Acknowledgments

This work was supported in part by Grant-in-Aid for Scientific Research from Japanese Society for the Promotion of Science (JSPS KAKENHI, 24K08600).

## Notes

The authors declare no conflict of interests.

## References

1. Dolmans DEJGJ, Fukumura D, Jain RK. Photodynamic therapy for cancer. Nat Rev Cancer, 2003;3:380-387.
2. Obaid G, Celli JP, Broekgaarden M, Bulin A-L, Uusimaa P, Pogue B, Hasan T, Huang H-C. Engineering photodynamics for treatment, priming and imaging. Nat Rev Bioeng, 2024;2: 752-769.
3. Allamyradov Y, ben Yosef J, Annamuradov B, Ateyeh M, Street C, Whipple H, Er AO. Photodynamic therapy review: past, present, future, opportunities and challenges. Photochem, 2024;4:434-461.
4. Lang K, Mosinger J, Wagnerová DM. Photophysical properties of porphyrinoid sensitizers non-covalently bound to host molecules; models for photodynamic therapy. Coord Chem Rev, 2004;248:321-350.
5. Fadlan A, Tanimoto H, Ito T, Aritomi Y, Ueno M, Tokuda M, Hirohara S, Obata M, Morimoto T, Kakiuchi K. Synthesis, photophysical properties, and photodynamic activity of positional isomers of TFPP-glucose conjugates. Bioorg Med Chem, 2018;26:1848-1858.
6. Lan M, Zhao S, Liu W, Lee CS, Zhang W, Wang P. Photosensitizers for Photodynamic Therapy. Adv Healthc Mater, 2019:e1900132.
7. Hirakawa K, Electron transfer-supported photodynamic therapy. In: Photodynamic Therapy-from Basic Science to Clinical Research (Edited by Inada N.) Intech Open: London, 2020;1-25.
8. Hirakawa K, Kishimoto N, Nishimura Y, Ibuki Y, Fuki M, Okazaki S. Protein photodamaging activity and photocytotoxic effect of an axial-connecting phosphorus(V)porphyrin trimer. Chem Res Toxicol,

2023;36:1622-1630.
9. Hirakawa K, Ouyang D, Ibuki Y, Hirohara S, Okazaki S, Kono E, Kanayama N, Nakazaki J, Segawa H. Photosensitized protein-damaging activity, cytotoxicity, and antitumor effects of P(V)porphyrins using long-wavelength visible light through electron transfer. Chem Res Toxicol, 2018;31:371-379.
10. Zhang S, Hosaka M, Yoshihara T, Negishi K, Iida Y, Tobita S, Takeuchi T. Phosphorescent light-emitting iridium complexes serve as a hypoxia-sensing probe for tumor imaging in living animals. Cancer Res, 2010;70:4490-4498.
11. Meng W, Hao Y, He C, Li L, Zhu G. Exosome-orchestrated hypoxic tumor microenvironment. Mol Cancer, 2019;18:57.
12. Emami NA, Najafgholian S, Rostami A, Sistani A, Shojaeifar S, Esparvarinha M, Nedaeinia R, Haghjooy JS, Taherian M, Ahmadlou M, Salehi R, Sadeghi B, Manian M. The role of hypoxia in the tumor microenvironment and development of cancer stem cell: a novel approach to developing treatment. Cancer Cell Int, 2021;21:62.
13. Ansari MA, Mohajerani E. Mechanisms of lasertissue interaction: I. optical properties of tissue. J Lasers Med Sci, 2011;2:119-125.
14. Pansare V, Hejazi S, Faenza W, Prud'homme RK. Review of long-wavelength optical and NIR imaging materials: contrast agents, fluorophores and multifunctional nano carriers. Chem Mater, 2012;24:812-827.
15. Ouyang D, Hirakawa K. Photosensitized oxidative damage of human serum albumin by water-soluble dichlorophosphorus(V) tetraphenylporphyrin. Rapid Commun Photosci, 2015;4:41-44.
16. Hasegawa H, Hirakawa K. Evaluation of the photosensitizer activity of hydrophobic phosphorus(V) porphyrins using the absorption spectral change of 1-benzyl-1,4-dihydronicotinamide. Spectrochim Acta A Mol Biomol Spectrosc, 2024;308:123765.
17. Adler AD, Longo FR, Finarelli JD, Goldmacher J, Assour J, Korsakoff L. A simplified synthesis for meso-Tetraphenylporphine. J Org Chem, 1967;32:476.
18. Marrese CA, Carrano CJ. Synthesis, characterization, and electrochemistry of (5,10,15,20-tetraphenylporp hinato)dichlorophosphorus(V) chloride Inorg Chem, 1983;22:1858-1862.
19. Hirakawa K, Nishimura Y, Arai T, Okazaki S. Singlet oxygen generating activity of an electron donor connecting porphyrin photosensitizer can be controlled by DNA. J Phys Chem B, 2013;117:13490-13496.
20. He XM, Carter DC. Atomic structure and chemistry of human serum albumin. Nature, 1992;358:209-215.
21. Usui Y, Kamogawa K. A standard system to determine the quantum yield of singlet oxygen formation in aqueous solution. Photochem Photobiol, 1974;19:245-247.
22. Sakura S. Chemiluminescence of tryptophan enhanced by electrochemical energy. Electrochimica Acta, 1992;37:2731-2735.

# Effects of pH and solvents on photosensitizer properties of pyridine-connecting P(V)porphyrin

# ピリジン結合型P(V)ポルフィリンの光増感剤特性におけるpHおよび溶媒効果

Yuma Hiraiwa[1], Shigetoshi Okazaki[2], Kazuhiro Takeda[1], and Kazutaka Hirakawa[1,3,4*]

[1] *Applied Chemistry and Biochemical Engineering Course, Department of Engineering, Graduate School of Integrated Science and Technology, Shizuoka University, Johoku 3-5-1, Chuo-ku, Hamamatsu, Shizuoka 432-8561, Japan*
[2] *Preeminent Medical Photonics Education and Research Center, Hamamatsu University School of Medicine, Handayama 1-20-1, Chuo-ku, Hamamatsu, Shizuoka 431-3192, Japan*
[3] *Department of Optoelectronics and Nanostructure Science, Graduate School of Integrated Science and Technology, Shizuoka University, Johoku 3-5-1, Chuo-ku, Hamamatsu, Shizuoka 432-8561, Japan*
[4] *Cooperate Major in Medical Photonics, Shizuoka University, Johoku 3-5-1, Chuo-ku, Hamamatsu, Shizuoka 432-8561, Japan*

***Corresponding author:**

Kazutaka Hirakawa
Applied Chemistry and Biochemical Engineering Course, Department of Engineering, Graduate School of Integrated Science and Technology, Shizuoka University, Johoku 3-5-1, Chuo-ku, Hamamatsu, Shizuoka 432-8561, Japan
Tel/Fax: 81-53-478-1287, E-mail: hirakawa.kazutaka@shizuoka.ac.jp

**Abstract:**

Photodynamic therapy (PDT), a minimally invasive cancer treatment, has attracted attention for its low physical burden on patients. In this study, we aimed to overcome a phototoxicity for normal tissues, a side effect of PDT, by activity control of photosensitizers using the acidic environment around tumor tissues. For this purpose, P(V)porphyrins, in which a phosphorus atom was introduced into the center of the porphyrin ring, were synthesized. To control the photosensitizer activity of P(V)porphyrin through intramolecular electron transfer and aggregation, pyridine-connecting P(V)porphyrin was designed to evaluate the protein photodamaging activity under different pH conditions. Under an acidic condition, the protonation of the pyridine moiety, an electron donating group, suppressed the intramolecular electron transfer quenching of photoexcited P(V)porphyrins, resulting in the enhancement of protein photodamage. In conclusion, a pH-responsive electron donor can be used to control the photosensitizer activity of P(V)porphyrin in an acidic environment and these findings show the possibility of developing the tumor tissue-selective photosensitizers using a pyridyl group.

**Keywords:** P(V)porphyrin; Photodynamic therapy; Aggregation; Electron transfer; Protein photodamage

## 1. 緒言

光線力学的療法（Photodynamic Therapy: PDT）とは、特定の波長の光を吸収して活性を示す光増感剤を静脈注射で投与し、光増感剤の蓄積した腫瘍に内視鏡を利用して可視光照射する手順の低侵襲ながん治療法である（1）。一般に PDT では、光照射された光増感剤により一重項酸素（$^1O_2$）生成（タイプⅡ機構）や腫瘍細胞内の生体分子からの電子引抜きによる酸化損傷（タイプⅠ機構）でがん細胞をアポトーシスやネクローシスへ誘導する（2,3）。PDT では、外科的切除や副作用の強い薬剤投与を必要とせずに腫瘍組織選択的な治療が可能である（4,5）。しかし、一部の光増感剤は正常組織にも蓄積し、術後に生活光の暴露によって正常組織を損傷する光線過敏症の副作用が問題となっている（4,5）。

そこで、本研究では、特定の条件下で光増感剤が機能することを利用した光増感剤の活性制御を試みた。一般に、光増感剤は、凝集すると分子間の電子的相互作用により励起状態の失活が促進される（6）。また、分子内に電子のドナーやアクセプターとなる部分を導入した光増感剤は、励起状態での分子内電子移動によって、基底状態に速やかに失活することで生体分子の損傷活性の抑制が可能である。具体的には分子内電子移動による励起状態の失活過程は、一般に数ナノ秒（～$10^{-9}$ s）から数ピコ秒（1～$10^{-12}$ s）で進行し、数ナノ秒で進行する通常の電子移動を介さない他の光化学過程と比較して短時間で進行するため、光化学的な活性を示すことなく失活できると考えられる（6-8）。そこで、腫瘍組織選択的な PDT を目指すため、この凝集体の形成と分子内電子移動を制御することで腫瘍組織周辺でのみ光増感活性を示す光増感剤の開発を行った。

腫瘍組織は急速な細胞増殖のため、解糖系を用いた代謝が盛んであり、ピルビン酸や乳酸など酸性の代謝産物のため、腫瘍組織周辺は正常組織よりも酸性になっていることが知られている（9,10）。本研究では、この腫瘍組織周辺に特有な酸性環境を利用し、光増感剤の活性制御を試みた。

**Figure 1** に、本研究で合成したポルフィリン環の中心にリン原子を導入したP(V)ポルフィリン誘導体を示す。これらのポルフィリンでは、*meso*- 位のフェニル基にペンチルオキシ基を導入することで疎水性を高めている。また、ポルフィリン環の中心リン原子から上下に伸びる軸配位子として、窒素原子をもつピリジル基を電子供与性の配位子に導入している。合成したポルフィリンは、正常組織内では疎水性の高さのため凝集体を形成し、また分子内電子移動によって光増感剤活性を示さないが、腫瘍組織周辺では配位子の窒素原子のプロトン化により、分子間での静電的な反発による凝集の解除、配位子の電子供与能力の低下による分子内電子移動の抑制によって活性が回復すると期待される（8）。本研究では、これら活性制御のトリガーを用いたポルフィリンの光増感特性の制御機能を評価した。

## 2．実験方法

### 2.1. 試薬

エタノール（特級および脱水）と脱水ピリジン、酢酸、酢酸ナトリウム、無水硫酸ナトリウム、アセトニトリル、ヘキサフルオロリン酸テトラブチルアンモニウムは富士フィルム和光純薬工業株式会社、0.1 mol/L リン酸緩衝液（pH 7.6）および緩衝液の調製に用いたリン酸三ナトリウム・12 水和物、リン酸水素二ナトリウム・12 水和物、リン酸二水素ナトリウム二水和物はナカライテスク株式会社、0.05 mol/L リン酸は関東化学工業株式会社、2- ピリジンメタノールは東京化成工業株式会社製からそれぞれ購入した。ヒト血清アルブミン（HSA）は Sigma-Aldrich Japan 合同会社から購入した。

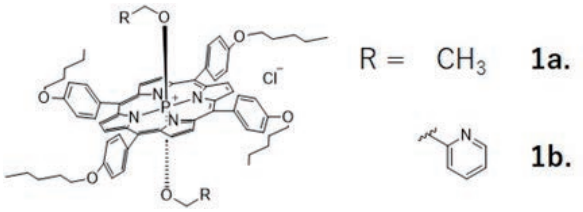


**Figure 1** Structures of P(V)porphyrins synthesized in this study.

### 2.2. 測定

NMR は AvanceIII HD400（Bruker）、質量分析は microTOF（Bruker）、吸収スペクトルは UV-1900i 紫外可視分光光度計（株式会社島津製作所）、蛍光スペクトルは F-4500 蛍光分光光度計（株式会社日立製作所）を用いてそれぞれ測定した。光増感剤の酸化還元電位は Potentiostat/Galvanostat（HA-301、北斗電工株式会社）、Function generator（DF1906、NF 株式会社）、Midi Loger（GL900-4、GRAPHTEC 株式会社）を用いて測定した。溶媒には、アセトニトリル、電解質にはヘキサフルオロリン酸テトラブチルアンモニウムを用いた。参照電極として飽和カロメル電極（SCE）、作用極および対極には白金電極を用いた。

### 2.3. 計算

ポルフィリンおよび電子ドナーのピリジン誘導体の最適構造およびエネルギーは、ソフトウェア Spartan'20（Wavefunction Inc.）を用いて密度汎関数法（DFT、基底関数ωB97XD、6-31* レベル）にて計算した。

### 2.4. 合成

定法（10）に基づき dichloro P(V)tetrakis(4'-pentyloxyphenyl)porphyrin（Cl P(V)TPOPP）を合成した。次に Cl P(V)TPOPP 21.38 mg を脱水ピリジンと脱水エタノールの混合溶媒に溶かし、24 時間加熱還流した。生成物はシリカゲルカラムクロマトグラフィー（展開溶媒、メタノール：クロロホルム = 1 : 4 にて 1 回、1 : 6 にて 1 回）で精製し、diethoxy P(V)tetrakis(4-pentyloxyphenyl)porphyrin（EthoxyP(V)TPOPP: **1a.**）を収率 98.6% で得た。また、Cl P(V)TPOPP 18.27 mg を脱水ピリジンと硫酸ナトリウムで脱水した 2- ピリジンメタノールの混合溶媒に溶かし、4 時間加熱還流した。生成物はシリカゲルカラムクロマトグラフィー（展開溶媒　メタノール：クロロホルム = 1 : 6 にて 2 回、1 : 5 にて 1 回、1 : 4 にて 1 回）で精製し、Bis-2-pyridil methoxy P(V)tetrakis(4-pentyloxyphenyl)porphyrin（Pyr P(V)TPOPP: **1b.**）を収率 41.5% で得た。

合成した光増感剤の NMR および質量分析の結果を以下に示す。

**1a. EthoxyP(V)TPOPP:** $^{1}$H NMR ($CDCl_3$, 400 MHz): $\delta$ 9.05 (d, $J_{P\text{-}H}$ = 2.9 Hz, 8H, βH), 7.63 (d, $J_{H\text{-}H}$ = 4.8 Hz, 2H, *o*-phenyl-H), 7.27 (d, $J_{H\text{-}H}$ = 9.5 Hz, 8H, *m*-phenyl-H), 4.18 (t, $J_{H\text{-}H}$ = 6.5Hz, 8H, phenyl-OC$\underline{H}_3$-), 3.64 (br, 4H, $CH_3CH_2CH_2$ $CH_2C\underline{H}_2O$-), 1.94 (m, $J_{H\text{-}H}$ = 5.3 Hz, 8H, $CH_3CH_2CH_2C\underline{H}_2CH_2O$-), 1.55 (br, 8H, $CH_3CH_2C\underline{H}_2CH_2CH_2O$-), 1.48 (m, 8H, $CH_3C\underline{H}_2CH_2CH_2CH_2O$-), 1.00 (t, $J_{H\text{-}H}$ = 7.2 Hz, 12H, $C\underline{H}_3CH_2CH_2CH_2CH_2O$-), -1.76 (t, $J_{H\text{-}H}$ = 7.4 Hz, 4H, P-O-C$\underline{H}_2$-$CH_3$), -2.33 (m, $J_{H\text{-}H}$ = 7.0 Hz, 6H, P-O-$CH_2$-C$\underline{H}_3$). $^{31}$P NMR ($CDCl_3$, 160 MHz): δ -180.1285. ESI-HR TOF-MS calcd. for $C_{68}H_{78}N_4O_6P^+$ [$M^+$]: 1077.5659, found: 1077.5596.

**1b. PyrP(V)TPOPP:** $^{1}$H NMR ($CDCl_3$, 400 MHz): δ 9.05 (d, $J_{P\text{-}H}$ = 2.8 Hz, 8H, *β*H), 7.63 (d, $J_{H\text{-}H}$ = 8.6 Hz, 8H, *o*-pyridine-H), 7.58 (d, $J_{H\text{-}H}$ = 9.0 Hz, 8H, *o*-phenyl-H), 7.18 (d, $J_{H\text{-}H}$ = 8.8Hz, 8H, *m*-phenyl-H), 6.70 (t, $J_{H\text{-}H}$ = 7,7 Hz, 2H, *m*-pyridine-H), 6.54 (t, $J_{H\text{-}H}$ = 6.2 Hz, 2H, *m*-pyridine-H), 4.16 (t, 8H, $J_{H\text{-}H}$ = 6.5 Hz, phenyl-OC$\underline{H}_3$-), 1.92 (m, $J_{H\text{-}H}$ = 7.0 Hz, 8H, $CH_3CH_2CH_2C\underline{H}_2CH_2O$-), 1.54 (m, 8H, $CH_3CH_2C\underline{H}_2CH_2CH_2O$-), 1.47 (m, 7.6 Hz 8H, $CH_3C\underline{H}_2CH_2CH_2CH_2O$-), 0.99 (t, $J_{H\text{-}H}$ = 7.2 Hz, 12H, $C\underline{H}_3CH_2CH_2CH_2CH_2O$-), -1.06 (d, $J_{H\text{-}H}$ = 14.3 Hz, 4H, P-OC$\underline{H}_2$-Pyridine). $^{31}$P NMR ($CDCl_3$, 160 MHz): δ -181.9752. ESI-HR TOF-MS calcd. for $C_{76}H_{80}N_6O_6P^+$ [$M^+$]: 1203.5871, found: 1203.6020.

## 3．結果および考察

### 3.1. P(V) ポルフィリンの水溶性

合成した各光増感剤のエタノールまたは 1 % エタノールを含む水溶液中での吸収スペクトルおよび蛍光スペクトルを **Figure 2** に示す。**1a.**、**1b.** ともに水溶液中では吸光度、蛍光強度が大幅に減少していることがわかる。これは水溶液中では、光増感剤分子が疎水性の高さから凝集体を形成することで、光の吸収断面積の低下や、分子間での電子的な相互作用のためであると説明できる（2）。

また、ポルフィリン化合物には、波長 400–450 nm

付近に第二励起一重項状態への電子遷移に帰属される Soret 帯と波長 500–700 nm 付近に第一励起一重項（$S_1$）状態への電子遷移に帰属される Q 帯と呼ばれる特徴的な吸収波長域が知られている（11）。吸収スペクトルでは、**1a.**、**1b.** ともに Soret 帯、Q 帯を確認できたが、エタノール溶液から水の割合を増やしていくと次第に Soret 帯、Q 帯ともに赤方偏移した（**1a.** (Soret: 446 → 448 nm, Q: 569 → 573 nm, 616 → 621 nm）,**1b.** (Soret: 450 → 453 nm, Q: 572 → 575 nm, 619 → 624 nm) ) 。一般に、ポルフィリンは会合体の形成により、吸収帯の偏移が知られている（12）。特に、光増感剤分子が T 字型に会合する J 会合では吸収帯は赤方偏移を示す（12）。従って、本研究で合成した P(V) ポルフィリン **1a.**、**1b.** はいずれも水溶液中にて J 会合体を形成する可能性が示唆された。

### 3.2. P(V) ポルフィリンの光化学的物性における pH 依存性

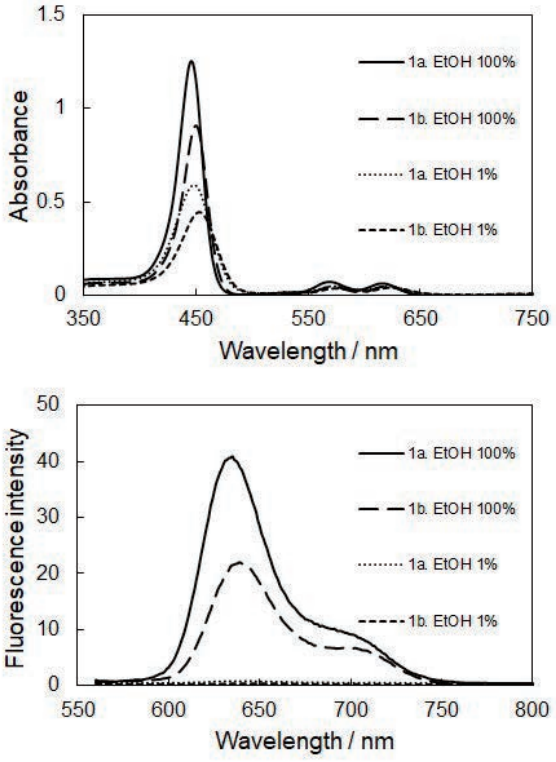


**Figure 2** Absorption spectra of **1a.** (top) and **1b.** (bottom) in ethanol or distilled water including 1% ethanol.

電子供与性の配位子をもつ **1b.** の吸収スペクトルおよび蛍光スペクトルを、エタノールを 30 % 含む pH の異なる緩衝液（pH 10.8, 7.0, 3.0 のリン酸緩衝液および pH 5.0 の酢酸緩衝液、濃度はともに 10 mM）中で測定した。緩衝液の pH の上昇に従い、吸光度の上昇と蛍光強度の顕著な増大を観測した。この結果は、配位子のもつピリジンのプロトン化による脱凝集と光化学的物性の変化で説明される。高 pH 条件（pH 10.8）では、ピリジン部分からの分子内電子移動のため、**1b.** は失活するが、低 pH 条件（pH 3.0）では、ピリジンのプロトン化による電子ドナー性の低下に基づく励起状態の失活抑制が示唆された。（**Figure 3**）

詳細な解析を行うため、**1b.** の p$K_a$ の解析を行った。ピリジン部位のプロトンとの化学平衡は、中性状態のポルフィリンを Por、プロトン化したポルフィリンを Por – $H^+$ と表すと以下のように示すことができる。

$$\mathrm{Por-H^+} \rightleftarrows \mathrm{Por} + \mathrm{H^+} \qquad [1]$$

ここで酸解離定数 $K_a$ および p$K_a$ はポルフィリン、プロトン化ポルフィリンの割合をそれぞれ $R_{Por}$、$R_{H\text{-}Por}$ とすると、以下の式のようになる。

$$K_a = \frac{[\mathrm{Por}][\mathrm{H^+}]}{[\mathrm{Por-H^+}]} = \frac{R_{\mathrm{Por}}[\mathrm{H^+}]}{R_{\mathrm{H-Por}}} \qquad [2]$$

$$pK_a = -\log_{10} K_a \qquad [3]$$

また、$K_a$ および p$K_a$ は蛍光量子収率の実測値（$\phi_f^{ob}$）および脱プロトン化状態のポルフィリンとプロトン化ポルフィリンの蛍光量子収率（それぞれ$\phi_f^{Por}$と$\phi_f^{H-Por}$）を用いて以下のように示すことができる。

$$\begin{aligned}\phi_f^{ob} &= \phi_f^{Por} \times R_{Por} + \phi_f^{H-Por} \times R_{H-Por} \\ &= \frac{\phi_f^{Por} K_a + \phi_f^{H-Por}[H^+]}{K_a + [H^+]}\end{aligned} \qquad [4]$$

なお、$K_a$ は上記の [3] のように、[$H^+$] は以下の [5] の式のように表される。

$$pH = -\log_{10}[H^+] \qquad [5]$$

この関係を用いて、pH = 10.8 ~ 2.0 での蛍光量子収率の実測値をプロットし、最小二乗法によるカーブフィッティングで p$K_a$ を解析したところ、p$K_a$ は 4.7 であった。配位子として導入したピリジンの p$K_a$ の文献値が 5.19 であり（13）、両者が比較的近い値であることから、光化学的物性の変化が配位子のプロトン化に起因していると考えられる。

### 3.3. 分子内電子移動の論理的な考察

合成したポルフィリンの酸化側における酸化還元位電位の測定が困難であったため、**1b.** の分子内電子移動について、DFT 計算による熱力学的な 評価を行った。光照射されたポルフィリンは、ポルフィリン環の最高被占分子軌道（HOMO）に相当する軌道の電子が最低空軌道（LUMO）に遷移して励起状態になる。従って、電子ドナーとして結合した配位子であるピリジン部位の HOMO に相当するエネルギー準位がポルフィリン環の HOMO に相当するエネルギー準位よりも高ければ、ピリジン部位の HOMO に相当する電子が、光励起によってポルフィリン環の HOMO に相当する軌道に生じた電子の空席へ分子内電子移動することが期待できる。このピリジン部位は、ポルフィリン環に近接しているため、熱力学的に許容であるなら分子内電子移動はすみやかに進行し、励起状態のポルフィリンが生体分子損傷の活性を示すことなく失活すると考えられる（14-15）。そこで、ポルフィリンおよびピリジン部位のエネルギー準位（それぞれ $E_{Por,HOMO}$ および $E_{Lig,HOMO}$）を DFT 計算（$\omega$B97XD、6-31G* レベル）によって求めた。

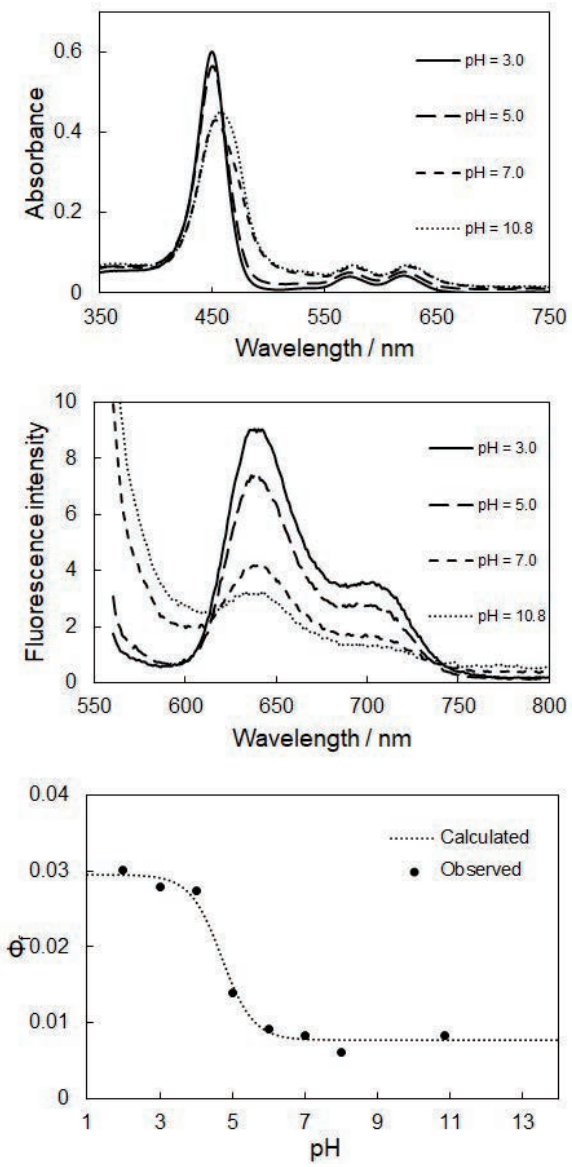


**Figure 3** Absorption (top) and fluorescence (middle) spectra of **1b.** and the relationship between the fluorescence quantum yield and pH in a 10 mM sodium phosphate buffer (pH 10.8 ~ 6.0, 3.0, 2.0, 10 mM, 30% ethanol) or acetate buffer (pH 5.0, 4.0, 10 mM, 30% ethanol).

なお、**1b.** のポルフィリン環とピリジンのエネルギーを直接計算すると、真空中での計算では、中心リン原子の正電荷の影響が過大評価されるため、本研究ではポルフィリン環とピリジン部位を別々に計算した。そこで、それぞれのモデルとしてポルフィリン環には **1a.**、ピリジン部位には 2- メチルピリジンを用いた。その結果、$E_{\mathrm{Lig,HOMO}}$ = -8.84 eV、$E_{\mathrm{Por,HOMO}}$ = -9.92 eV であった。従って、$E_{\mathrm{Lig,HOMO}}$ の方が $E_{\mathrm{Por,HOMO}}$ よりもエネルギー準位は高く、励起状態において配位子からポルフィリン環への分子内電子移動が起こる可能性が示唆された。さらに、ピリジンがプロトン化した際は、$E_{\mathrm{Lig,HOMO}}$ = -14.46 eV となり、$E_{\mathrm{Por,HOMO}}$ よりもエネルギー準位が低くなるため、酸性条件でピリジン部位がプロトン化すると、電子移動が抑制され、活性制御に利用できる可能性が示された。

### 3.4. P(V) ポルフィリンのタンパク質との相互作用

PDT においてターゲットとなるタンパク質と P(V) ポルフィリンとの相互作用を評価するために、水溶性タンパク質である HSA 存在下での P(V) ポルフィリンの光化学的物性および HSA への光損傷作用を評価した。

ポルフィリンは HSA と結合することによって吸収、蛍光スペクトルが変化することが知られており（9）、本研究でも pH 7.6 および 3.2 のリン酸緩衝液中、pH 5.0 の酢酸緩衝液中において、HSA 添加で明らかな濃色効果が確認できた（Abs. at 455 nm, **1a.** pH 7.6: 0.13 → 0.44, pH 5.0: 0.46 → 0.51, pH 3.2: 0.37 → 0.48、**1b.** pH 7.6: 0.13 → 0.44 pH 5.0: 0.46 → 0.51, pH 3.2: 0.37 → 0.48）。これは、水溶液中において凝集していた P(V) ポルフィリン分子が HSA の疎水性ポケット内へ結合することにより、脱凝集され、電子状態が変化したことで説明できる。

また、HSA の存在下においても、**1b.** は、中性環境よりも酸性環境において、高い蛍光量子収率（pH 7.6: $\Phi_f$ = 0.012, pH 5.0: $\Phi_f$ = 0.016, pH 3.2: $\Phi_f$ = 0.025, [HSA] = 10 μM）を示したことから、HSA に結合した状態でも分子内電子移動による光化学的物性の制御が可能であることがわかった。

次に、HSA 濃度に依存したポルフィリンの吸収スペクトル変化から結合定数（$K_b$、$M^{-1}$）を解析した。ポルフィリンと HSA が 1 : 1 で結合すると仮定したときの $K_b$ は、ポルフィリンと HSA の複合体を Por–HSA として、以下のようになる。

$$K_{\mathrm{b}} = \frac{[\mathrm{Por-HSA}]}{[\mathrm{Por}][\mathrm{HSA}]} \qquad [6]$$

また、ポルフィリン分子の HSA との結合率を $R_{\mathrm{HSA\text{-}Por}}$ とすると、$K_b$ は、$R_{\mathrm{HSA\text{-}Por}}$ および、ポルフィリンと HSA の初濃度をそれぞれ表す $[\mathrm{Por}]_0$ と $[\mathrm{HSA}]_0$ を用いて、次のように表すことができる。

$$K_{\mathrm{b}} = \frac{[\mathrm{Por}]_0 R_{\mathrm{HSA-Por}}}{[\mathrm{Por}]_0(1 - R_{\mathrm{HSA-Por}})([\mathrm{HSA}]_0 - [\mathrm{Por}]_0 R_{\mathrm{HSA-Por}})} \qquad [7]$$

そこで、濃度 0, 0.2, 0.5, 1.0, 2.0, 5.0, 10, 20 μM の HSA と 5 μM の P(V) ポルフィリンを 1%のエタノールを含む 10 mM リン酸緩衝液（pH 7.6 または 3.2）または酢酸緩衝液（pH 5.0）中に調製した。これらの吸光度の実測値 $A_{ob}$ は、HSA と結合したポルフィリンの吸光度 $A_b$、未結合状態のポルフィリンの吸光度 $A_f$ を用いて以下のように表せる。

$$A_{\mathrm{ob}} = A_{\mathrm{b}}x + A_{\mathrm{f}}(1 - R_{\mathrm{HSA-Por}}) \qquad [8]$$

式 [6] および [7] を用い、$A_{ob}$ と $[\mathrm{HSA}]_0$ の関係を非線形最小二乗法（2）により解析することで $K_b$ を算出した（**Table 1**）。**1a.** の $K_b$ に注目すると、pH 7.6 および 5.0 ではほとんど変化しなかったが、pH 3.2 では 2 倍近く増大した。HSA は酸性環境において二次構造の変化、すなわち $\alpha$ – ヘリックス構造の割合が減少し、$\beta$ – シート構造の割合が増加することが知られており（16）、この $K_b$ の変化はその影響に起因するものと考えられる。また、これに伴い HSA は、楕円形に畳み込まれた構造か

ら平面的な構造へと三次構造が変化する（16）。HSA の構造変化はポルフィリンとの結合サイトである疎水ポケットへのアクセスを向上させ、ポルフィリンは HSA と結合しやすくなり、$K_b$ が増大したと考えられる。対照的に、**1b.** の $K_b$ は、pH 7.6 に比べ、酸性環境である pH 5.0 および 3.2 では半分以下に減少した。これは酸性環境では HSA とポルフィリンがともにプロトン化しているため、両者の静電的な反発で説明できる。

以上の情報を踏まえて P(V) ポルフィリンの HSA の光損傷を評価した。HSA は分子内にトリプトファンを 1 つもつことから、本研究では HSA 中のトリプトファンをターゲットにして、P(V) ポルフィリンへの光照射による損傷を解析した（2,3,8）。HSA の光酸化損傷の程度は、トリプトファンの自家蛍光強度（17）の減少から、次の式で評価した。

$$[\text{Damaged HSA}] = \frac{F_0 - F}{F_0}[\text{HSA}]_0 \qquad [9]$$

ここで、[Damaged HSA] は、HSA 損傷量（トリプトファン残基が酸化された HSA の濃度）、$F_0$ は、初期の蛍光強度、$F$ は、光照射後の蛍光強度である。式 [8] によって求めた損傷量から算出した初期の光酸化損傷速度とポルフィリンの吸収光子数、照射断面積から、次の式 [9] を用いてタンパク質損傷量子収率（$\Phi_D$）を算出した。

$$\Phi_D = \frac{\nu}{NA} \qquad [10]$$

ここで、ν は、初期の酸化損傷速度 [nM min$^{-1}$]、$N$ は、ポルフィリンに吸収された単位時間当たりの光子数 [nM cm$^{-2}$ min$^{-1}$]、$A$ は、サンプルの光照射面積 [cm$^2$] である。各条件での HSA との結合定数、タンパク質損傷量子収率、pH 7.6 を基準としたときの pH 5.0 および 3.2 における損傷量子収率の比を活性制御比 $r_{\text{on-off}}$ として **Table 1** に示す。

**Table 1** Binding constant, protein photodamaging quantum yields, and controlled activity ratio by **1a.** and **1b.**

| Compound | pH | $K_b$ / $10^6$ M$^{-1}$ | $\Phi_D$ $\times 10^3$ | $r_{\text{on-off}}$ |
|---|---|---|---|---|
| **1a.** | 7.6 | 2.6 | 3.4 | - |
| | 5.0 | 2.5 | 4.1 | 1.2 |
| | 3.2 | 4.3 | 11 | 3.3 |
| **1b.** | 7.6 | 13 | 6.2 | - |
| | 5.0 | 5.4 | 19 | 3.1 |
| | 3.2 | 5.6 | 23 | 3.8 |

なお、リン酸緩衝液中での **1a.**、**1b.** の $^1O_2$ 生成量子収率（エタノール中でのメチレンブルーの $^1O_2$ 生成量子収率 0.52（18）と比較することで算出）は、それぞれ **1a.** が pH 7.6 にて 0.013、pH 3.2 にて 0.019、**1b.** が pH 7.6 にて 0.007、pH 3.2 にて 0.005 であり、$^1O_2$ の生成によるタンパク質の損傷がある程度は可能であると考えられる。

続いて、両化合物のタンパク質からの電子の引抜きによる酸化損傷を熱力学的に考察する。これまでの研究から、P(V) ポルフィリンは、$S_1$ 状態における電子移動で HSA を酸化損傷すると考えられる（19）。P(V) ポルフィリンの一電子還元の酸化還元電位を $E^-$、電子ドナー（タンパク質の酸化損傷のターゲットであるトリプトファン）の一電子酸化の酸化還元電位を $E^+$、P(V) ポルフィリンの吸収および蛍光スペクトルから求めた励起エネルギーを $E_{0\text{-}0}$ とすると素電荷 $e$ を用いて、タンパク質からの電子の引抜きのギブズエネルギー（$\Delta G_d$）は以下の式で求められる。

$$\Delta G_d = e(E^- - E^+) - E_{0-0} \qquad [11]$$

**1a.** および **1b.** の一電子還元の酸化還元電位 $E^-$ は、それぞれ -0.60 および -0.54 V vs. SCE であり、励起エネルギー $E_{0\text{-}0}$ は、それぞれ 1.98 および 1.97 eV であった。トリプトファンの一電子酸化の酸化還元電位の文献値である $E^+$ = 0.78 V vs. SCE（20）を用いると、**1a.**、**1b.** の $\Delta G_d$ は、それぞれ = -0.61、-0.65 eV であり、負の値であることから両化合物が生体分子を電子の引抜きによって酸化損傷できることが熱力学的に確認できた。両化合物による光増感反応で $^1O_2$ の物理的な消去作用をもつアジ化ナトリウムを共存させた条件でもタンパク質の光損傷を確認できたことから両化合物がタンパク質を電子引抜きによって酸化損傷できることが示された。

**1a.**、**1b.** の活性制御比に注目すると、**1a.** では、電子ドナー部位をもたないにも関わらず、低 pH 環境では損傷量子収率が顕著に増大した。これは、先述した **1a.** と HSA の $K_b$ が増大することで説明できる。pH 3.2 における **1a.** の $K_b$ は、pH 7.6 と比較して約 1.7 倍に増加するため、酸性条件では、より多くの **1a.** 分子が HSA と結合し、ターゲットとなるトリプトファン残基の近傍に存在していると考えられる。一般に、光損傷は、ターゲットと光増感剤との距離や結合の仕方に大きく依存するため、標的となるアミノ酸残基の付近に光増感剤が存在するほど損傷が起こりやすい。従って、電子供与性の配位子をもたない **1a.** においても、酸性環境では HSA との結合が促進されることで、損傷量子収率が増大したと考えられる。また、**1b.** においては、電子供与性の配位子をもっているにも関わらず、中性条件（pH 7.6）でも同条件下の **1a.** と比較して高い損傷量子収率を示した。**1b.** では励起状態における分子内電子移動により光損傷が抑えられることが予想されたが、HSA との結合による疎水環境で分子内電子移動が抑制されたことで説明できる。pH 7.6 における **1b.** の HSA との $K_b$ は $1.3 \times 10^7$ M$^{-1}$ と、今回の測定条件で最も大きな値を示しており、他の条件と比べても多くの分子が HSA に結合し、トリプトファン残基の近傍に存在していると考えられる。また、P(V) ポルフィリンの HSA との結合部位は疎水的環境であり、そのような周囲の比誘電率が低い環境において、P(V) ポルフィリンは電荷分離状態（配位子からの電子移動が起こった状態）のエネルギー準位が上昇することが知られている（21）。その結果、分子内電子移動が抑制され、中性付近の pH でも多くの分子が活性を示したと考えられる。HSA の電子移動機構による光酸化も疎水的環境の効果で同様に抑制されるが、トリプトファンから励起状態ポルフィリ

ンへの電子移動の駆動力である $-\Delta G_d$ が十分に大きいため、光酸化の活性は維持されたと考えられる。以上の要因で、**1b.** は同条件下の **1a.** と比較して高い損傷量子収率を示したと考えられる。

また、**1b.** は、pH 5.0 および 3.2 において損傷量子収率の大幅な増大が確認できた。**1b.** は、酸性環境において HSA との $K_b$ は半分以下にまで減少しており、結合しにくい状態であることから、この活性上昇は配位子のプロトン化によるポルフィリンの光増感剤としての活性の回復による効果が大きいと考えられる。以上から、窒素原子を含む pH 応答性の電子供与性の配位子をもつ P(V) ポルフィリンは、生体分子の光損傷作用において、pH による活性制御が可能であることが示された。特に、本研究で合成したピリジン結合型の P(V) ポルフィリンである **1b.** は腫瘍組織周辺の pH 環境に近い pH 5.0 にて優れた活性制御比を示したことから、生体分子の光損傷における pH 制御が可能であり、PDT の副作用の解決に寄与できる可能性が示唆された。

## 総括

本研究では、PDT における副作用である光線過敏症の解決のために、弱酸性環境である腫瘍組織周辺を標的として、P(V) ポルフィリンの親水性環境における凝集体の形成および分子内電子移動による失活機構を利用した光化学的物性の制御機能を評価した。ClP(V) TPOPP を原料に P(V) ポルフィリンの軸配位子として、pH による活性制御機能のないエトキシ基をもつ **1a.** と pH 応答性の活性制御機能をもつピリジンを配位子として結合した **1b.** を合成した。両化合物によるタンパク質光損傷作用において、腫瘍組織周辺の pH に近い pH 5.0 の環境 (6) では、**1a.** は大きな活性制御比を示さなかったのに対して、pH 応答性の軸配位子をもつ **1b.** は中性条件に比べて優れた損傷効率の増大を示した。このことから、P(V) ポルフィリンの軸配位子における窒素原子のプロトン化を利用した光化学的物性の制御が可能であることが示された。ピリジンを配位子にもつ **1b.** は腫瘍組織周辺に近い pH 環境での活性制御が可能であったため、PDT における副作用の解決に利用できる可能性が示唆された。

## 謝辞

本研究は JSPS 科研費（24K08600）の助成を受けて行われました。また、NMR および質量分析でご協力頂きました早川敏弘技術専門職員（静岡大学技術部）に厚く御礼申し上げます。

## 参考文献

1. Asif MI, Milan P, Sri GP, Balaram G, Swati B. Nanotherapeutic intervention in photodynamic therapy for cancer. ACS Omega, 2022;7:45882-45909.
2. Hirakawa K, Ounyang D, Hirohara S et al. Photosensitized protein-damaging activity, cytotoxicity, and antitumor effects of P(V)porphyrins using long-wavelength visible light through electron transfer. Chem Res Toxical, 2018;31:371-379.
3. Hirakawa K, Katayama A, Yamaoka S, Ikeue T, Okazaki S. Photosensitized protein damage by water-soluble phthalocyanine zinc(II) and gallium(III) complexes through electron transfer and singlet oxygen production. Chem Phys Lett, 2022;802:139764.
4. Usuda J, Tsutsui H, Honda H et al. Photodynamic therapy for lung cancers based on novel photodynamic diagnosis using talaporfin sodium (NPe6) and autofluorescence bronchoscopy. Lung Cancer, 2007;58:317-323.
5. Karolina W, Gillstedt M, Tovi J et al. Optimizing treatment of acne with photodynamic therapy (PDT) to achieve long-term remission and reduce side effects. A prospective randomized controlled trial. J Photochem Photobiol B, 2021;223:112299.
6. Costa-Tuna A, Chaves O, Loureieo R, Pinto S, Pina J, Serpa C. Interaction between a water-soluble anionic porphyrin and human serum albumin unexpectedly stimulates the aggregation of the photosensitizer at the surface of the albumin. Int J Biol Macromol, 2024;255:128210.
7. Hasegawa H, Hirakawa K. Evaluation of the photosensitizer activity of hydrophobic phosphorus(V) porphyrins using the absorption spectral change of 1-benzyl-1,4-dihydronicotinamide. Spectrochim Acta A: Mol Biomol Spectrosc, 2024;308:123765.
8. Yamaoka S, Okazaki S, Hirakawa K. Activity control of pH-responsive photosensitizer bis(6-quinolinoxy) P(V)tetrakis(4-chlorophenyl)porphyrin through intramolecular electron transfer. Chem Phys Lett, 2022;788:139285.
9. Bogdanov A, Bogdanov A, Chubenko V, Volkov N, Moiseenko F, Moiseyenko V. Tumor acidity: From hallmark of cancer to target of treatment. Front Oncol, 2022;12:979154.
10. 大村健二. がん細胞の代謝と栄養, 日本静脈経腸栄養学会雑誌, 2015;30;907-910.
11. Giovannetti R. The use of Spectrophotometry UV-Vis for Study of Porphyrins. Macro to Nano Spectrosc, 2012;20:87-108.
12. Zannotti M, Giovannetti R, Minofar B et al. Aggregation and metal-complexation behaviour of THPP porphyrin in ethanol/water solutions as function of pH. Spectrochim Acta A: Mol Biomol Spectrosc, 2018;193:235-248.
13. Hayers W. CRC Handbook of Chemistry and Physics, 92nd Edition. CRC Press, 2011.
14. Quan T, Darius K, Su L et al. Dynamics of Photoinduced electron transfer in a carotenoid–porphyrin- dinitronaphthalenedicarboximide molecular triad. J Phys Chem B, 1997;101:5214-5223.
15. Christopher BL, George AF, Liam DS et al. Solvent-mediated activation/deactivation of photoinduced electron-transfer in a molecular dyad. Inorg Chem, 2020;59:10430-10438.
16. Michael D, Daniel CC, Florian R. Conformational

transitions of the three recombinant domains of human serum albumin depending on pH. J Biol Chem, 2000;275:3042-3050.
17. Moriyama Y, Ohta D, Hachiya K, Mitsui Y, Takeda K. Fluorescence behavior of tryptophan residues of bovine and human serum albumins in ionic surfactant solutions: A comparative study of the two and one tryptophan(s) of bovine and human albumins. J Protein Chem, 1996;15:265-272.
18. Robert WR, Janet NG. A compilation of singlet oxygen yields from biologically relevant molecules. Photochem Photobiol, 1999;70:391-475.
19. Hirakawa K, Umemoto H, Kikuchi R et al. Determination of singlet oxygen and electron transfer mediated mechanisms of photosensitized protein damage by phosphorus(V)porphyrins. Chem Res Toxical, 2015;29:262-267.
20. Sakura S. Chemiluminescence of tryptophan enhanced by electrochemical energy. Electrochim Acta, 1992;37:2731-2735.
21. Hirakawa K, Segawa H. Excitation energy transfer and photo-induced electron transfer in axial bispyrenyl phosphorus porphyrin derivatives: Factors governing the competition between energy and electron transfer processes under the existence of intramolecular π-π interaction. J Photochem Photobiol A, 1999;123:67-76.

# Binding interaction between free base porphyrin photosensitizers and human serum albumin responsible for protein photodamaging activity

Kazutaka Hirakawa,[1,2,3*] Daiki Machida,[1] and Shigetoshi Okazaki[4]

[1] *Applied Chemistry and Biochemical Engineering Course, Department of Engineering, Graduate School of Integrated Science and Technology, Shizuoka University, Johoku 3-5-1, Chuo-ku, Hamamatsu, Shizuoka 432-8561, Japan*

[2] *Department of Optoelectronics and Nanostructure Science, Graduate School of Science and Technology, Shizuoka University, Johoku 3-5-1, Chuo-ku, Hamamatsu, Shizuoka 432-8561, Japan*

[3] *Cooperative Major in Medical Photonics, Shizuoka University, Johoku 3-5-1, Chuo-ku, Hamamatsu, Shizuoka 432-8561, Japan*

[4] *Preeminent Medical Photonics Education and Research Center, Hamamatsu University School of Medicine, Handayama 1-20-1, Chuo-ku, Hamamatsu, Shizuoka 431-3192, Japan*

***Corresponding author:**

Kazutaka Hirakawa

Applied Chemistry and Biochemical Engineering Course, Department of Engineering, Graduate School of Integrated Science and Technology, Shizuoka University, Johoku 3-5-1, Chuo-ku, Hamamatsu, Shizuoka 432-8561, Japan

Tel/Fax: +81-53-478-1287, E-mail: hirakawa.kazutaka@shizuoka.ac.jp

**Abstract:**

Photosensitized protein damage is one of the most important mechanisms of photodynamic therapy (PDT). Porphyrins and its derivatives are used as the photosensitizers for PDT. Association between photosensitizer and protein is an important factor of the PDT activity of porphyrin photosensitizer. Thus, a binding interaction between free-base porphyrins and a water-soluble protein, human serum albumin (HSA), was examined. As porphyrin photosensitizers, α,β,γ,δ-tetrakis(3,4,5-trimethoxyphenyl)porphyrin (TMPP; neutral hydrophobic porphyrin), α,β,γ,δ-tetrakis(4-hydroxyphenyl)porphyrin (TOHPP; neutral water-soluble porphyrin), α,β,γ,δ-tetrakis(4-sulphonatophenyl)porphyrin tetrasodium salt (TPPS; anionic water-soluble porphyrin), and α,β,γ,δ-tetrakis(1-methylpyridinium-4-yl)porphyrin tetrachloride (TMPyP; cationic water-soluble porphyrin) were used. The thermodynamic analysis showed that the driving forces for the cases of TMPP and TPPS are Van der Waal's force and electrostatic force, respectively, and that of OHTPP and TMPyP is the entropy, possibly due to a release of water molecules from the binding position of protein. The difference of the photosensitized protein damaging activity of these porphyrins could be explained by the binding constant between HSA and porphyrin molecules and the singlet oxygen production activity of these porphyrins. These results suggest that the thermodynamic analysis can be used for the design of porphyrin photosensitizers for PDT.

**Keywords:** Free base porphyrins; Human serum albumin; Binding interaction; Protein photodamage; Singlet oxygen

## INTRODUCTION

Porphyrins are important photosensitizers that can produce singlet oxygen ($^1O_2$) under visible-light irradiation [1-3]. Specifically, free base porphyrins, such as talaporfin sodium [4,5] and porfimer sodium [6] are clinically used for the photosensitizers of photodynamic therapy (PDT), which is a less-invasive cancer therapy [7-9]. Furthermore, PDT can elicit immunogenic effect on cancer therapy [10]. In general, $^1O_2$ production is an important mechanism of biomolecule oxidation by photoexcited porphyrins [1,2,11]. An interaction between porphyrin photosensitizer and target biomolecules, such as protein, is an important factor for PDT [12-14]. Physical and chemical characteristics affect the PDT activity of photosensitizer; and the characteristic of free base porphyrin can be altered by a substituent [1,12]. A water-solubility and electrostatic characteristics of free base porphyrins can be controlled by the substituents [1]. For example, neutral, anionic, and cationic characteristics are closely related to a water-solubility of compound; and an introduction of hydrophilic or hydrophobic groups also controls the characteristics of neutral porphyrins [1]. In this study, the binding interaction between human serum albumin (HSA), a water-soluble protein, and the following four types of free base porphyrins: neutral hydrophobic (α,β,γ,δ-tetrakis(3,4,5-trimethoxyphenyl) porphyrin, TMPP), neutral hydrophilic (α,β,γ,δ-tetrakis(4-hydroxyphenyl)porphyrin, TOHPP), anionic (α,β,γ,δ-tetrakis(4-sulphonatophenyl)porphyrin tetrasodium salt, TPPS), and cationic (α,β,γ,δ-tetrakis(1-methylpyridinium-4-yl)porphyrin tetrachloride, TMPyP) porphyrins (Fig. 1) was examined. The thermodynamic analysis of the binding interaction and photosensitized protein damaging activity was also performed.

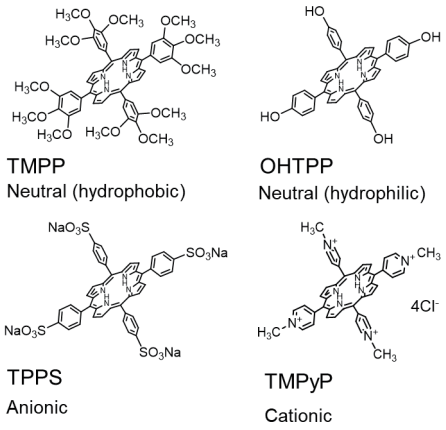


**Fig. 1.** Structures of free base porphyrins.

## EXPERIMENTAL

TMPP was synthesized using 3,4,5-trimethoxybenzaldehyde and pyrrole (FUJIFILM Wako Pure Chemical Co., Ltd., Osaka, Japan) according to the literature [15]. $^1$H NMR (300 MHz, $CDCl_3$) δ 8.96 (s, 8H, pyrrole-H), 7.48 (s, 8H, *ortho*-phenyl-H), 4.19 (s, 12H, *para*-phenyl-$OCH_3$), 3.97 (s, 24H, *meta*-phenyl-$OCH_3$), -2.78 (s, 2H, N-H). M/Z = 975.5 ($M^+$). HSA, OHTPP, and TMPyP were purchased from Sigma-Aldrich Co. LLC. (St. Louis, MO, USA). TPPS was purchased from Tokyo Chemical Industry Co., Ltd. (Tokyo, Japan). Ethanol was obtained from FUJIFILM Wako Pure Chemical Co., Ltd. Spectroscopic-grade water was purchased from Dojin Chemicals Co. (Kumamoto, Japan). Methylene blue was obtained from Kanto Chemical, Co., Inc. (Tokyo, Japan). Sodium phosphate buffer (0.1 M, pH 7.6) was obtained from Nacalai Tesque Inc. (Kyoto, Japan). These chemical agents were used as received.

The absorption spectra of samples were measured with the UV-Vis spectrophotometer UV-1650PC (Shimadzu, Kyoto, Japan). The fluorescence lifetime ($\tau_f$), which equals the singlet excited-state ($S_1$) lifetime, of HSA was measured with a Fluorescence Lifetime System TemPro (HORIBA, Kyoto, Japan). The excitation wavelength for the $\tau_f$ measurements for porphyrins was 402 nm. The $^1O_2$ production was directly measured by near-infrared luminescence at around 1,270 nm from $^1O_2$ relaxation, which corresponds to the $^1O_2$ ($^1\Delta_g$)-$^3O_2$($^3\Sigma_g^-$) transition, as reported previously [16].

To evaluate the HSA damage, the sample solution containing 5 μM porphyrins and 10 μM HSA was prepared in a 10 mM sodium phosphate buffer (pH 7.6) including 5% ethanol. The sample solution was irradiated with a light-emitting diode (LED, $\lambda_{max}$= 585 nm, 2.0 mW $cm^{-2}$, CCS Inc., Kyoto, Japan). The intensity of the LED was measured with an 8230E optical power meter (ADC Corporation, Tokyo, Japan). The fluorescence intensity of HSA at 350 nm was measured with a Hitachi 650-60 fluorescence photometer (Hitachi, Tokyo, Japan). The excitation wavelength for this assay was 298 nm. The amount of damaged HSA was estimated from the results of fluorometry based on the diminishment of the intrinsic fluorescence of tryptophan residue of HSA by photooxidation, as reported previously [13,14].

## RESULTS AND DISCUSSION

### Interaction between human serum albumin and porphyrins

The absorption spectra of the porphyrins were changed by the addition of HSA (Fig. 2). This absorption spectral change can be explained by the interaction between porphyrin molecules and HSA [17,18]. The fitting curves in

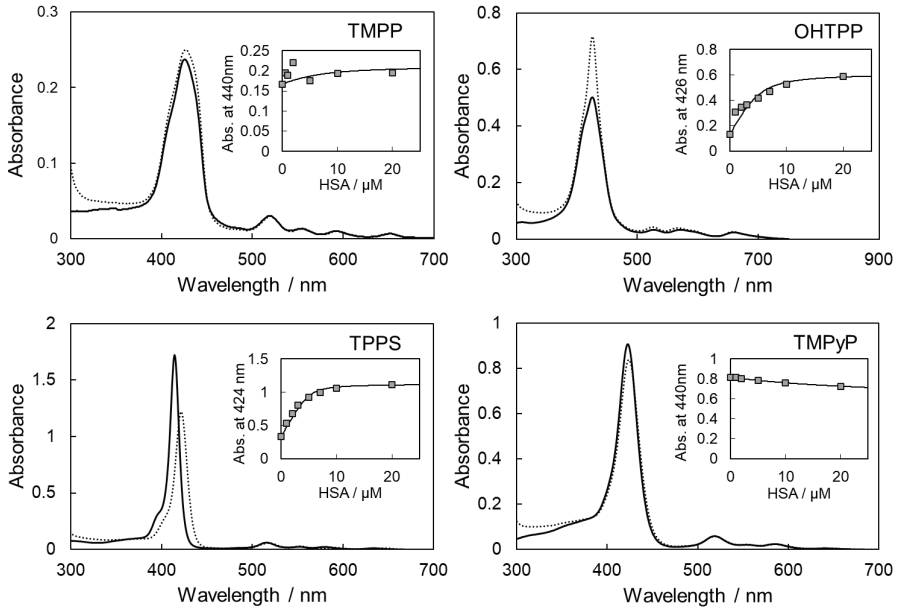


**Fig. 2.** Absorption spectra of free base porphyrins with or without HSA. The sample solution contained 5 μM porphyrins with (dotted) or without (straight) 20 μM HSA in a 10 mM sodium phosphate buffer (pH 7.6) including 5% ethanol. Inset: Relationship between the absorbance of porphyrin at certain wavelength around the Soret band and the concentration of HSA.

the inset of these figures were calculated by the simple 1:1 complex model [13,14]. The absorbance change of TMPP and OHTPP with relatively small HSA concentration (0.5 ~ 2 μM) could not be analyzed by this simple 1:1 model (insert of Fig. 2); and indicates that many porphyrin molecules bind to one HSA molecule. This result suggests the aggregation of porphyrin molecules on HSA surface. However, in the presence of relatively large concentration of HSA (≥5 μM) and in the cases of TPPS and TMPyP, the absorbance change with HSA concentration was simple. Therefore, the apparent binding constant ($K_{bind}$) between porphyrins and HSA could be estimated from these absorbance changes under the condition of relatively large concentration of HSA, according to the reported previously under the assumption that one porphyrin molecule binds to HSA (1:1 complex) [13,14]. The obtained $K_{bind}$ values at 298 K for TMPP, OHTPP, TPPS, and TMPyP were $4.8\times10^5$ $M^{-1}$, $1.0\times10^6$ $M^{-1}$, $2.9\times10^6$ $M^{-1}$, and $4.0\times10^4$ $M^{-1}$, respectively. An anionic porphyrin, TPPS showed the relatively large $K_{bind}$ value, suggesting the electrostatic interaction between the positive charge of HSA surface and TPPS. These $K_{bind}$ values depended on the temperature, and the thermodynamic parameters could be calculated by the van 't Hoff plot (Fig. 3, Table 1). The enthalpy change ($\Delta H^o$) and the entropy change ($\Delta S^o$) of the binding interaction was calculated by the following equation:

$$\mathrm{Ln}\, K_{bind} = -\frac{\Delta H^\circ}{RT} + \frac{\Delta S^\circ}{R} \quad (1)$$

where $R$ is the gas constant and $T$ is the absolute temperature. The Gibbs energy of the binding interaction ($\Delta G^o$) was calculated by the following equation:

$$\Delta G^o = -RT\,\mathrm{Ln}\, K_{bind} \quad (2)$$

The driving force of the binding interaction between protein and molecules can be speculated from these thermodynamic parameters [19,20]. The estimated $\Delta H^o$ values of TMPP and TPPS were negative and the $\Delta S^o$ values for these porphyrins were positive and relatively small, suggesting that the binding interaction between these porphyrin molecules and HSA is enthalpy driven. Because TMPP is a neutral molecule, the Van der Waal's force should be the main driving force of the binding interaction. As mentioned above, TPPS is an anionic

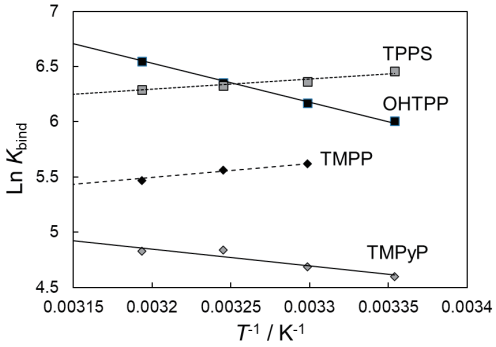


**Fig. 3.** The van 't Hoff plot of the binding constant between free base porphyrins and HSA and the temperature.

molecule and an electrostatic interaction may be a driving force for the binding interaction between TPPS and HSA. Relevantly, it has been reported that the interaction between HSA and α,β,γ,δ-tetrakis(2,6-difluoro-3-sulfophenyl) porphyrin, an anionic porphyrin, is enthalpically driven ($\Delta H^\circ = -70.1 \pm 3.3$ kJ mol$^{-1}$) into subdomain IIA of HSA [21]. In the cases of OHTPP and TMPyP, the obtained $\Delta H^\circ$ values were positive and relatively large $\Delta S^o$ values were estimated. Therefore, the binding interaction between these porphyrins, OHTPP and TMPyP, and HSA is entropy driven. These results suggest that the repulsive force between a cationic molecule or a molecule with hydroxyl group such as OHTPP and the HSA surface exists. However, relatively large $\Delta S^o$ values for these porphyrins suggest that a release of water molecules in the pocket of HSA or around the HSA surface becomes the driving force of the binding interaction.

The binding position of these porphyrins on HSA was roughly estimated using the Förster resonance energy transfer (FRET) method based on the energy-transfer theory [22] with a previously reported procedure [12]. The critical distances of the FRET from the tryptophan to these porphyrin molecules, which were calculated from the fluorescence spectrum of tryptophan and the absorption spectrum of these porphyrins, were 99.6 Å (TMPP), 105 Å (OHTPP), 114 Å (TMPyP), and 115 Å (TPPS). The estimated distance between the tryptophan and these porphyrins were 117 Å (TMPP), 106 Å (OHTPP), 114 Å (TMPyP), and 115 Å (TPPS). The average diameter of HSA is about 80 Å [23], and the tryptophan residue is located almost at the center of HSA [24]. These results suggest that these porphyrin molecules mainly bind to the HSA surface (not subdomain IIA). The difference of

**Table 1** The binding constants and thermodynamic parameters of the binding interaction between free base porphyrins and HSA

| Porphyrin | $K_{bind}$ / $M^{-1}$ | $\Delta H^o$ / kJ mol$^{-1}$ | $\Delta S^o$ / J mol$^{-1}$ K$^{-1}$ | $\Delta G^o$ / kJ mol$^{-1}$ | Driving force |
|---|---|---|---|---|---|
| TMPP | $4.8\times10^5$ | -24.0 | +28.2 | -32.4 | van der Waal's force |
| OHTPP | $1.0\times10^6$ | +67.3 | +340.5 | -34.0 | entropy* |
| TPPS | $2.9\times10^6$ | -17.8 | +63.5 | -36.7 | electrostatic force |
| TMPyP | $4.0\times10^4$ | +28.8 | +185.0 | -26.3 | entropy* |

*: release of water molecules from HSA.

the binding potion between the case of abovementioned α,β,γ,δ-tetrakis(2,6-difluoro-3-sulfophenyl)porphyrin, which binds into subdomain IIA of HSA [21], and that of TPPS is possibly due to the difference of their substituents.

## Fluorescence lifetime of porphyrins in the presence of HSA

The time profile of fluorescence intensity of TMPP could be analyzed by a triple exponential function (Table 2). The short lifetime components suggest the aggregation of porphyrins molecules. In the presence of 20 μM HSA, almost porphyrins are binding on HSA and the three components were observed for $\tau_f$ values. The longest $\tau_f$ value is longer than that without HSA. This result can be explained by the assumption that the interaction with HSA resolves the aggregation of porphyrin molecules and an inhibition of vibrational deactivation of the excited state of porphyrin through a binding interaction with HSA. In the case of OHTPP, the time profile of fluorescence intensity was analyzed by a double exponential function. The shorter lifetime component suggests an aggregation of OHTPP molecules, since OHTPP is a neutral molecule and shows slightly hydrophobic character. Similarly to the case of TMPP, the $\tau_f$ of OHTPP was elongated through an interaction with HSA. These results can be explained by that the interaction with protein environment resolves the aggregation of OHTPP molecules. In the cases of TPPS and TMPyP, water-soluble porphyrins, these time profiles of fluorescence intensity were almost single exponential functions, however, these decay curves were well fitted by double exponential function and small components of short lifetime were observed. These results can be explained by the difference of conformation of these porphyrins. In the presence of HSA, these time profiles could be analyzed by triple exponential functions. The observed longer lifetime components can be explained by the abovementioned stabilization of their photoexcited state in the microenvironment of protein. The shorter lifetime component showed the enhancement of the deactivation of photoexcited state through electron transfer interaction with HSA [13,14].

## Photosensitized HSA oxidation by free base porphyrins

The photosensitized HSA damage by these porphyrins was evaluated using the fluorescence intensity of the tryptophan residue of HSA, which shows the typical fluorescence as being around 350 nm, as reported previously [13,14]. HSA photodamage by TMPP was barely observed, whereas OHTPP, TPPS, and TMPyP photosensitized the HSA damage (Table 3). The quantum yield of HSA photodamage by these porphyrins ($\Phi_D$), estimated from the initial decomposition rate and the absorbed photon fluence, and the $^1O_2$ production quantum

**Table 2** Fluorescence lifetime of porphyrins

| Porphyrins | HSA | $\tau_f$ / ns (relative amplitude) | average value / ns |
|---|---|---|---|
| TMPP | - | 3.88 (0.41), 1.02 (0.44), 0.23 (0.15) | 2.07 |
| | + | 6.08 (0.19), 1.09 (0.61), 0.14 (0.20) | 1.85 |
| OHTPP | - | 6.56 (0.32), 0.02 (0.68) | 2.11 |
| | + | 10.41 (0.89), 2.32 (0.07), 0.21 (0.04) | 9.43 |
| TPPS | - | 10.69 (0.97), 5.16 (0.03) | 10.52 |
| | + | 12.21 (0.96), 2.2 (0.03), 0.12 (0.01) | 11.79 |
| TMPyP | - | 5.50 (0.96), 1.93 (0.04) | 5.36 |
| | + | 9.18 (0.43), 4.62 (0.55), 0.06 (0.02) | 6.49 |

The sample solution contained 5 μM porphyrins with or without 20 μM HSA in a 10 mM sodium phosphate buffer (pH 7.6) including 5% ethanol.

**Table 3** Quantum yields of photosensitized HSA damage and $^1O_2$ production by porphyrins

| Porphyrin | $\Phi_D$ | $\Phi_\Delta$ [b] |
|---|---|---|
| TMPP | ND [a] | 0.052 |
| OHTPP | $2.6\times10^{-5}$ | 0.034 |
| TPPS | $4.9\times10^{-5}$ | 0.82 |
| TMPyP | $5.6\times10^{-5}$ | 0.96 |

[a]: HSA damage was not observed. [b]: in 10 mM phosphate buffer (pH 7.6) including 5% ethanol (reference: methylene blue in water, $\Phi_\Delta$ = 0.52 [25]).

yields ($\Phi_\Delta$) are shown in Table 3. Photooxidation ability of neutral and anionic free base porphyrins through electron transfer is small, because of their low redox potentials [26,27]. Indeed, neutral porphyrins with relatively low redox potentials barely photooxidize HSA through electron transfer [28]. Therefore, the $^1O_2$ production becomes an important mechanism of protein photooxidation by neutral and anionic porphyrins. The non-photodamaging activity of TMPP is attributed to the small $\Phi_\Delta$ value. The HSA photodamaging activity of TPPS is possibly due to the relatively large $K_{bind}$ and $\Phi_\Delta$ values. TMPyP showed the largest values of $\Phi_D$ and $\Phi_\Delta$ in these porphyrins. These results show that the $^1O_2$ production is important mechanism for free base porphyrins. In the case of TMPyP, the electron transfer-mediated mechanism should also contribute to the HSA photodamage as the previous report [29]. Because of relatively high redox potential of TMPyP, a cationic porphyrin [26], this porphyrin has strong ability of electron transfer-mediated oxidation [30]. Although the $\Phi_\Delta$ of OHTPP is significantly smaller than those of TPPS and TMPyP, the $\Phi_D$ of OHTPP is relatively large and of the same order as those of TPPS and TMPyP. This result can be explained by the relatively large $K_{bind}$ value of OHTPP and the fact that the slightly shorter distance between OHTPP molecule and the tryptophan of HSA than those of the other porphyrins.

## CONCLUSIONS

Free base porphyrins, TMPP, OHTPP, TPPS, and TMPyP, bind to HSA. The thermodynamic parameters for the binding interaction were analyzed. The driving force of the binding interaction depends on the water-solubility and electrostatic character of these porphyrins. TMPP, a neutral hydrophobic porphyrin, binds to HSA through the Van der Waal's force. TPPS, an anionic porphyrin, binds to HSA through an electrostatic force. The driving force of these porphyrins is an enthalpy change. In the cases of OHTPP, a neutral hydrophilic porphyrin, and TMPyP, a cationic porphyrin, the driving force of binding interaction with HSA is an entropy, possibly due to the release of water molecules from the pocket or surface of HSA through an association of these porphyrins. The repulsive force between a cationic TMPyP molecule and a positive charge of HSA surface may inhibit the binding interaction. Indeed, the observed $K_{bind}$ value of TMPyP is smaller than other three kinds of porphyrins. The FRET analysis showed the binding positions of these porphyrins on HSA are almost the same; these porphyrins bind to the surface of HSA. The photooxidation of tryptophan residue of HSA by these porphyrins depended on the $K_{bind}$ and $^1O_2$ production activity. This study showed that $^1O_2$ production is the important mechanism for the protein photooxidation by free base porphyrins and the association between the porphyrins and target protein becomes the key factor of photodynamic activity of porphyrin agents. The thermodynamic analysis may be used for a molecular design of PDT photosensitizer.


## Acknowledgments

This work was supported in part by Grant-in-Aid for Scientific Research (B) from Japanese Society for the Promotion of Science (JSPS KAKENHI 17H03086), The Futaba Research Grant Program of the Futaba Foundation (No. 10407), and Takahashi Industrial and Economic Research Foundation.


## Notes

The authors declare no conflict of interests.

## References


1. Lang K, Mosinger J, Wagnerová DM. Photophysical properties of porphyrinoid sensitizers non-covalently bound to host molecules; models for photodynamic therapy. Coord Chem Rev, 2004;248:321-350.
2. DeRosa MC, Crutchley RJ. Photosensitized singlet oxygen and its applications. Coord Chem Rev, 2002;233-234:351-371.
3. Kou J, Dou D, Yang L. Porphyrin photosensitizers in photodynamic therapy and its applications. Oncotarget, 2017;46:81591-81603.
4. Saito T, Tsukahara T, Suzuki T, Nojima I, Tadano H, Kawai N, Kubo T, Hirohashi Y, Kanaseki T, Torigoe T, Li L. Spatiotemporal metabolic dynamics of the photosensitizer talaporfin sodium in carcinoma and sarcoma. Cancer Sci, 2021;112:550-562.
5. Kataoka H, Nishie H, Tanaka M, Sasaki M, Nomoto A, Osaki T, Okamoto Y, Yano S. Potential of photodynamic therapy based on sugar-conjugated photosensitizers. J Clin Med, 2021;10:841.
6. Hosokawa S, Takahashi G, Sugiyama K, Takebayashi S, Okamura J, Takizawa Y, Mineta H. Porfimer sodium-mediated photodynamic therapy in patients with head and neck squamous cell carcinoma. Photodiagnosis Photodyn Ther, 2020;29:101627.
7. Dolmans DEJGJ, Fukumura D, Jain RK. Photodynamic therapy for cancer. Nat Rev Cancer, 2003;3:380-387.
8. Kwiatkowski S, Knap B, Przystupski D, Saczko J, Kędzierska E, Knap-Czop K, Kotlińska J, Michel O, Kotowski K, Kulbacka J. Photodynamic therapy-mechanisms, photosensitizers and combinations. Biomed Pharmacother, 2018;106:1098-1107.
9. Tian J, Huang B, Nawaz MH, Zhang W. Recent advances of multi-dimensional porphyrin-based functional materials in photodynamic therapy. Coord Chem Rev, 2020;420:213410.
10. Ji B, Wei M, Yang B. Recent advances in nanomedicines for photodynamic therapy (PDT)-driven cancer immunotherapy. Theranostics, 2022;12:434-458.
11. Akbar A, Khan S, Chatterjee T, Ghosh M. Unleashing the power of porphyrin photosensitizers: Illuminating breakthroughs in photodynamic therapy. J Photochem Photobiol B, 2023;248:112796.

12. Hirakawa K, Takai S, Horiuchi H, Okazaki S. Photooxidation activity control of dimethylaminoph enyltris-(*N*-methyl-4-pridinio)porphyrin by pH. ACS Omega, 2020;5:27702-27708.
13. Hirakawa K, Ouyang D, Ibuki Y, Hirohara S, Okazaki S, Kono E, Kanayama N, Nakazaki J, Segawa H. Photosensitized protein-damaging activity, cytotoxicity, and antitumor effects of P(V)porphyrins using long-wavelength visible light through electron transfer. Chem Res Toxicol, 2018;31:371-379.
14. Hirakawa K, Yoshida M, Hirano T, Nakazaki J, Segawa H. Photosensitized protein damage by diethyleneglycoxyP(V)tetrakis(*p*-*n*-butoxyphenyl) porphyrin through electron transfer: activity control through self-aggregation and dissociation. Photochem Photobiol, 2022;98:434-441.
15. Adler AD, Longo FR, Finarelli JD, Goldmacher J, Assour J, Korsakoff L. A simplified synthesis for meso-Tetraphenylporphine. J Org Chem, 1967;32:476.
16. Hirakawa K, Nishimura Y, Arai T, Okazaki S. Singlet oxygen generating activity of an electron donor connecting porphyrin photosensitizer can be controlled by DNA. J Phys Chem B, 2013;117:13490-13496.
17. Samperi M, Vittorio S, De Luca L, Romeo A, Monsù Scolaro L. Interaction of aggregated cationic porphyrins with human serum albumin. Int J Mol Sci, 2023;24:2099.
18. Marconi A, Mattioli EJ, Ingargiola F, Giugliano G, Marforio TD, Prodi L, Di Giosia M, Calvaresi M. Dissecting the interactions between chlorin e6 and human serum albumin. Molecules, 2023;28:2348.
19. Arnulphi C, Jin L, Tricerri MA, Jonas A. Enthalpy-driven apolipoprotein A-I and lipid bilayer interaction indicating protein penetration upon lipid binding. Biochemistry, 2004;43:12258-12264.
20. Wang X, Zheng K, Si Y, Guo X, Xu Y. Protein-polyelectrolyte interaction: thermodynamic analysis based on the titration method. Polymers, 2019;11:82.
21. Costa-Tuna A, Chaves OA, Loureiro RJS, Pinto S, Pina J, Serpa C. Interaction between a water-soluble anionic porphyrin and human serum albumin unexpectedly stimulates the aggregation of the photosensitizer at the surface of the albumin. Int. J. Boil. Macromol, 2024;255:128210.
22. Förster Th. Zwischenmolekulare energiewanderung und fluoreszenz. Ann Physik, 1948;437:55-75.
23. Ferrer ML, Duchowicz R, Carrasco B, de la Torre JG, Acuña AU. The conformation of serum albumin in solution: a combined phosphorescence depolarization-hydrodynamic modeling study. Biophys J, 2001;80:2422-2430.
24. He XM, Carter DC. Atomic structure and chemistry of human serum albumin. Nature, 1992;358:209-215.
25. Usui Y, Kamogawa K. A standard system to determine the quantum yield of singlet oxygen formation in aqueous solution. Photochem Photobiol, 1974;19:245-247.
26. Kalyanasundaram K, Neumann-Spallart M. Photophysical and redox properties of water-soluble porphyrins in aqueous media. J Phys Chem, 1982;86:5163-5169.
27. Zhang Y, Xie Z, Lu C, Guo J, Chen Z, Li H, Song Y, Han Y, Hou Y. Study on the electron transfer capability of porphyrin ring and the mechanisms in the catalytic denitrification. Biochem Eng J, 2021;175:108010.
28. Hirakawa K, Matsui S, Okazaki S. Fluorination of tetraphenylporphyrin zinc complex enhances the protein photodamaging activity through electron transfer mechanism. Photomed Photobiol, 2023;43/44:45-50.
29. Ouyang D, Inoue S, Okazaki S, Hirakawa K. Tetrakis(*N*-methyl-p-pyridinio)porphyrin and its zinc complex can photosensitize damage of human serum albumin through electron transfer and singlet oxygen generation. J Porphyr Phthalocya, 2016;20:813-821.
30. Hirakawa K, Nakajima S. Effect of DNA microenvironment on photosensitized reaction of watersoluble cationic porphyrins. Recent Adv DNA Gene Seq, 2014;8:35-43.

# Identification of trace target molecules by multifunctional diazirine-based photocrosslinkers

Takenori Tomohiro[1]

[1] *Laboratory of Biorecognition Chemistry, Faculty of Pharmaceutical Sciences, Academic Assembly, University of Toyama, 2630 Sugitani, Toyama 930-0194, Japan*

***Corresponding author**

Takeneori Tomohiro, Laboratory of Biorecognition Chemistry, Faculty of Pharmaceutical Sciences, Academic Assembly, University of Toyama, 2630 Sugitani, Toyama 930-0194, Japan
TEL: +81-76-434-7515
FAX: +81-76-434-5063
E-mail: ttomo@pha.u-toyama.ac.jp

## ABSTRACT

Omics studies have made remarkable progress, and many bioactive molecules have been newly discovered. To elucidate the relationship between these molecules and biological functions and diseases, it is essential to identify the enzymes or receptors on which they act. Unfortunately, many of these target proteins are present only in trace amounts, making their analysis complex and identification difficult. In general, specific interactions between proteins and their substrates (ligands) are used to identify target proteins. This review outlines an efficient strategy for target identification based on photoaffinity labeling (PAL), especially using photoreactive crosslinkers with multiple functions such as photocrosslinking, photocleavage, fluorogenisity, and mass difference in compact structures. These multifunctional crosslinkers greatly facilitate the identification of ligand-target proteins and obtaining information about their binding structures even in the presence of large amounts of contaminants.

**Key words:** photoaffinity label, diazirine, target identification, chemical probe, cinnamate

## Introduction

Phenotypic screening using compound libraries is one of the important methodologies in drug discovery and has produced many first-in-class drugs to date. Biomolecules that are highly effective against diseases can have a significant effect on their signals directly or indirectly, and such key proteins can be useful targets for drug discovery. Early identification of interacting proteins, including unknown proteins, can accelerate structural optimization and biofunctional analysis of drug candidates. However, their identification and analysis are generally difficult because many of the target proteins exist in trace amounts and are greatly affected by coexisting impurities. Identification of proteins interacting with bioactive compounds can be achieved by labeling or non-labeling methods, the former of which is described here.

Selective labeling of interacting proteins has been generally achieved by the chemical probe consisting of their specific substrate or inhibitor with a reactive group unit and a tag. After crosslinking each other, the interacting proteins can be introduced a tag, such as a biotin group for purification and detection, with a covalent bond. Therefore, it can be applied to proteins with weak interactions that are difficult to handle with general affinity purification methods, proteins that are prone to degradation/aggregation, and proteins expressed in trace amounts. Since the specificity of the probe is crucial for the target identification, the appropriate probe design and selection of crosslinker are essential. To date, some chemoproteomic protein profiling technologies that utilizes small molecular probes, for example, known as activity-based probes to react with the active sites of proteins[1], and proximity-based probes to react with functional groups near the ligand binding site of proteins[2], selectively and covalently. In the latter method, chemoselective reactions proceed efficiently when amino or mercapto groups, etc. are present in proximity. In other words, the proximity effect (concentration effect) during binding state increases the specific labeling, and non-specific reactions to other proteins are suppressed by controlling the chemical reactivity of the crosslinker. In principle, this method can capture enzymes and transporters in dynamic processes, but conversely, it is necessary to consider consumption of probes by such as carrier proteins existing on the way to the target protein. This paper focuses on labeling methods for identifying trace interacting proteins, particularly photoaffinity labeling (PAL), which introduces a chemical tag to interacting molecules with a covalent bond, forming by activation with light irradiation[3-5].

## Photoaffinity labeling for identification of target protein

In addition to chemical crosslinking utilizing the chemo-selective reactions as described above, there are also

nonselective crosslinking. The photochemical crosslinking of diazirine group belongs to the latter category. Upon photolysis by UV irradiation, the diazirine group generates a carbene, an extremely electron-poor species, that instantly inserts into any chemical bond of spatially closed molecule within a nanosecond, before leaving the binding pocket. This photoreactive property that allows to crosslink to the contacting site is a crucial point when the purpose is to identify interacting proteins (Figure 1). If the reactive intermediate has a long lifetime or chemoselectivity, the probe will diffuse and nonspecifically crosslink other proteins that are relatively abundant. It is important to suppress such nonspecific labeling as much as possible, especially when the expression level of the target protein is extremely low.

There are three kinds of photoreactive groups have been used for PAL as crosslinkers, benzophenone, aryl azide, diazirine as shown in Figure 2. In the case of benzophenone, an excited carbonyl, the active species generated by UV irradiation, abstracts hydrogen from a nearby molecule, and the resulting radical pair couples to form a crosslink[6]. This active species does not react with water, and the unreacted excited carbonyl returns to the original ground state. Therefore, longer irradiation increases the labeling yield. However, because the excited carbonyl has a relatively long lifetime and exhibits chemoselectivity in favor of hydrogens of methionine and histidine, so prolonged irradiation increases the risk of nonspecific labeling. Furthermore, long-term UV irradiation damages cells. On the other hand, aryl azides, which generate nitrenes as the active species by photolysis (denitrogenation), are also widely used as photocrosslinkers[7]. The azide group can be directly and easily introduced to the aromatic ring of the ligand. However, aryl azides require relatively short wavelength

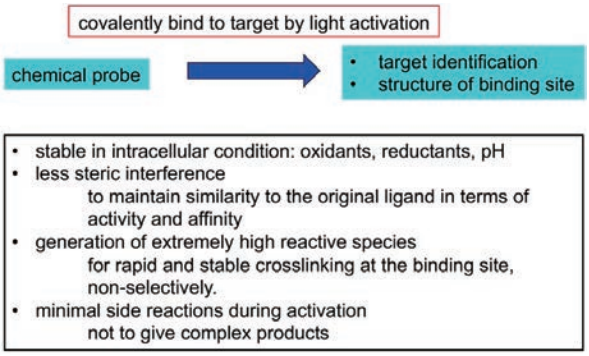


**Figure 1.** Ideal properties of photoprobe for identification of target proteins and the binding sites.

of light (<300 nm), and are easily degraded by biological reducing agents. Additionally, arylnitrenes undergo ring expansion reactions and potentially form unstable crosslinks, complicating the analysis.

Diazirine, another photoreactive group, undergoes n-π* transition when irradiated with UV-A light (around 355 nm) to generate carbene via denitrogenation (Figure 2). Lifetime of singlet carbene is very short, in the subnanosecond range[8], and this electrophilic species inserts into a chemical bond existing in close proximity to form a stable covalent bond. Carbenes react with both polar groups such as O-H and N-H and nonpolar groups such as C-H and C=C[9]. Therefore, carbenes are thought to instantly form a covalent bond at the site where they are generated. Theoretically, diazirine-based PAL has the potential to capture transition states during dynamic structural changes in proteins, but such highly sensitive snapshot analysis of labeled sites has not been realized so far. In general, it is difficult to chase dynamic processes such as enzymes using PAL. When labeling enzymes or transporters, it is often necessary to prepare probes of

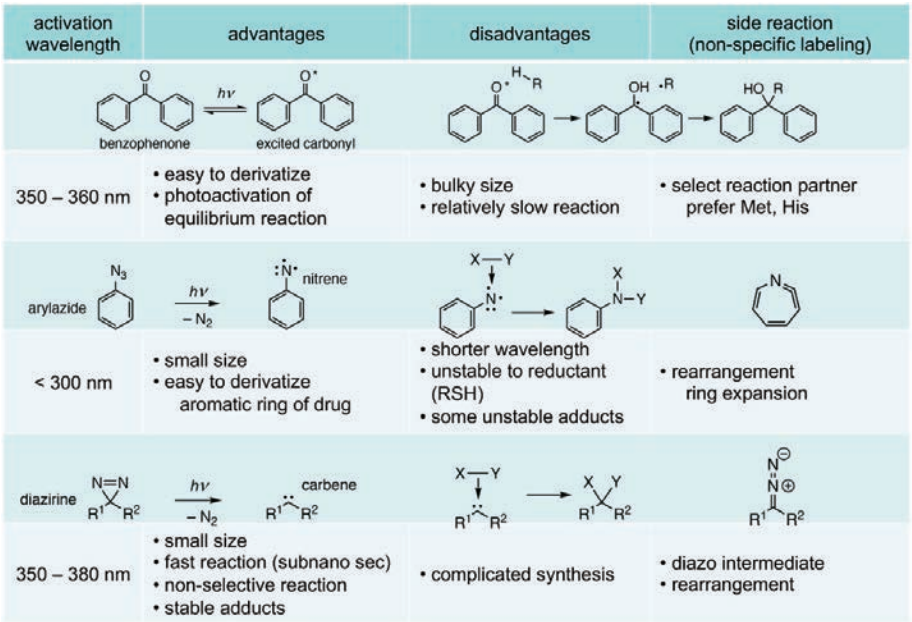


**Figure 2.** Properties of commonly used photophores.

their inhibitors to maintain its stable binding state for a certain period. Generally, after the probe reaches the target protein, it can be irradiated with light, an external stimulus, to initiate crosslinking reaction and capture the protein. Carbenes react with surrounding water and become deactivated. This property reduces the label yield, but gives the advantage of suppressing nonspecific labeling of other proteins with the free probes. In addition to these excellent reaction properties, the diazirine group is small in size, stable in the presence of nucleophiles or under acidic/basic conditions at room temperature and activated in a short irradiation time. It has become widely used since improved synthetic methods[10-12] have led to the development of many functionalized derivatives, including amino acid analogues. A serious problem is that diazirine photolysis also generates the diazo intermediate. The diazo intermediate is easily protonated to produce the diazonium ion which reacts with a nucleophilic group to form crosslink. Diazonium ions are positively charged and have a relatively long lifetime, so they are often reported to give products crosslinked with acidic groups in proteins[13]. In addition, aliphatic diazirines also undergo 1,2-rearrangement reactions of carbene to generate olefins. These long-lived reactive species may generate non-specific labels. Therefore, trifluoromethylphenyldiazirine, which suppresses the protonation of diazo intermediate and the rearrangement reactions of carbene species, appeared in the early stages of development of diazirine crosslinkers[14].

## Identification of trace interacting proteins using PAL

In affinity labeling methods, not all proteins are cross-linked even if the probe binds correctly to the protein (even if it shows biological activity). Trifluoromethylphenyldiazirine, a common cross-linking agent, is usually introduced at positions that do not reduce the affinity of the ligand molecule because of its bulky size. Therefore, the diazirine group of the probe is often located outside of the binding pocket and competes with inactivation by water, resulting in labeling yields of only a few percent to 10 percent. After purification, the crosslinked proteins are usually digested and identified based on peptide mass fingerprinting (PMF) of the peptide fragments and their amino acid sequence by MS/MS. Since labeled proteins are generally in trace amounts, especially in cases of target proteins with low expression or weak interactions, their enrichment/purification is necessary. For this purpose, biotin-avidin purification system with an extremely small dissociation constant ($K_d$ ~$10^{-15}$ M) is often used. Nonspecific adsorbates on the purification support can be washed away under strong conditions, which is very effective, but some impurities still remain on the surface. They are eluted under denaturing conditions, and in many cases their amount is considerably greater than that of the labeled protein, often making identification very cumbersome.

Typically, PAL experiments are performed both in the presence and absence of inhibitors. In the presence of the inhibitor, the label amount of the interacting protein is reduced, so the protein with reduced elution is considered the target protein. Currently, PAL strategy combined with quantitative proteomics methods such as stable isotope labeling by amino acids in cell culture (SILAC) is being promoted as a promising method (Figure 3)[15]. In this method, cells are cultured in both normal medium (Light) and medium containing stable isotope-labeled amino acids such as deuterium (Heavy). Incubation of cells with both the probe and free ligand/inhibitor reduces the amount of labeled target protein compared to other cells incubated with only the probe. Subsequently, these cells are mixed, and the PAL products are enriched by using avidin-immobilized support, and then the protein digestion product is analyzed by LC-MS/MS. The resulting MS signal intensity ratio (L/H ratio) of the target protein-derived peptide is greater. The advantage of this method is that the L/H ratio of nonspecific labels and adsorbates will be 1, thus eliminating all signals derived from them. This method has greatly improved the success rate of PAL target identification. A biotin tag is often introduced into cross-linked proteins by post-labeling method because of its large size, low solubility and low membrane permeability. For this purpose, the Huisgen reaction (click reaction, bioorthogonal) between the azido and alkynyl groups, which is not present in natural products, is often used[16,17]. Both groups are widely used as chemical reporters because they are small, stable, and have low antigenicity. Interacting proteins are firstly crosslinked with the probe bearing an azido or an alkynyl group, and then biotin tag is then introduced after cell lysis [18-20]. As an alternative

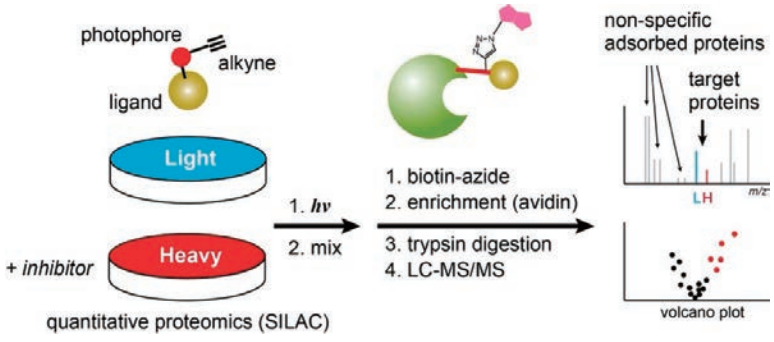


**Figure 3.** PAL-based target identification combined with quantitative proteomics.

to the biotin-avidin system, a purification method based on differences in hydrophobicity has been developed. PAL using diazirine crosslinkers with a perfluoroalkyl group dramatically changes the physical properties of the crosslinked products, which can be highly purified using fluorous solid-phase extraction (FSPE)[21].

## Photoreactive crosslinkers with integrated multiple functions

The MS-based protein identification has been generally accomplished by amino acid sequencing of peptides with high signal intensities. However, these are not labeled peptides. When these signal intensities are small, the difference between the L and H signals will be unclear, i.e., it will be unclear whether these signals are derived from the target protein or not. If labeled peptides can be identified along with unlabeled peptides, it will provide confidence that they are due to the target protein, and the determination of the labeled amino acid will also provide information on the ligand binding site. However, PAL using trifluoromethylphenyldiazirine gave a low label yield. Conversely, PAL using aliphatic diazirines, which have smaller and more flexible, gives higher yields but more complex labeling, making identification of the labeled amino acid more difficult.

On the other hand, repeated purification/concentration of trace labeled peptides will result in the loss of a significant amount of the peptide, depending on its physical properties, even with the use of highly sensitive detection using RI label[22]. An alternative approach is multifaceted identification through multifunctionalization of probes. However, attachment of multiple functions into probes generally leads enlargement of the structure, alter physical properties, and complicates probe synthesis and MS analysis. Therefore, multifunctional integration of crosslinker unit has been promoted, and small diazirines containing alkynyl groups/azide groups for post-labeling have been developed.

## Identification of labeled peptides using cinnamate-type crosslinkers

By partially modifying the conventional phenyldiazirine structure, we developed a photocrosslinker that has cleavability, fluorogenicity, and isotopic functions in addition to photocrosslinking ability[23]. The multiple properties allow the target peptide to be identified among many contaminants through a step-by-step identification process: capture by light (photocrosslinking), purification of crosslinked proteins (cleavage) and labeled peptide fragments (LC, fluorescence), followed by their identification (MS, mass difference) as shown in Figure 4[24]. Repeating the enrichment procedure using common biotin-avidin interaction is tedious and often leads to large losses, but this method does not need to repeat the procedure. As a result, it leads to clear and multifaceted identification of the labeled peptides, and we have succeeded in significantly reducing the amount and time required for analysis.

This photocrosslinker has a relatively simple structure, with a cinnamate backbone consisting of conventional phenyldiazirine crosslinker with one additional double bond (Figure 5). A hydroxyl group was introduced at the ortho position and an ethyl group at the α position of the carbonyl group. When this compound was irradiated with 355 nm light, two photoreactions occurred: diazirine photolysis and *E-Z* isomerization of the double bond. In the latter reaction, the carbonyl group is located close to the ortho hydroxyl group in the Z-form, inducing an

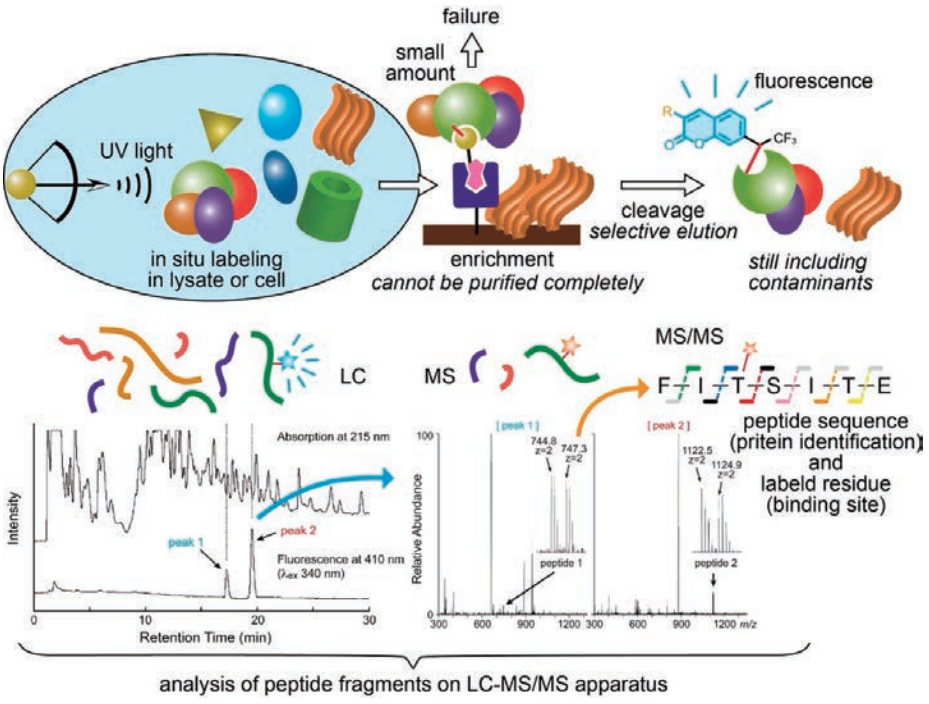


**Figure 4.** Outline of PAL-based identification of labeled peptides with cinnamate-type photocrosslinker.

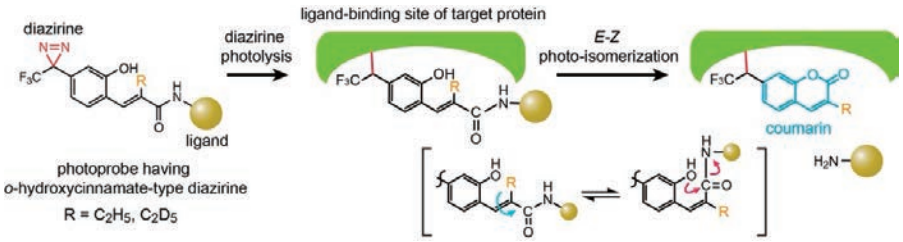


**Figure 5.** Structure and two photoreactions of o-hydroxycinnamate-type crosslinker.

intramolecular nucleophilic substitution reaction to form a corresponding coumarin ring (coumarinization). In synthetic chemistry, the *o*-hydroxycinnamic acid has been used as a photoreactive protecting group for hydroxyl groups and used to regulate activity of serine protease[25]. Since a ligand molecule is introduced to a carboxy group, the latter photoreaction removes the ligand via cleavage, leaving only the fluorescent coumarin derivative on the protein. In general, a fluorescent group is either directly introduced into the probe molecule or post-labeled using a click reaction. In this system, the crosslinker itself can be converted into a fluorescent group, meaning that there is little effect on the physical properties of the probe and the affinity to the protein. This cleavage function is particularly important for purification of trace proteins[26]. To utilize the coumarinization reaction to selective elution from the purification support, it is necessary to regulate two photoreactions, diazirine photolysis (crosslinking) and *E-Z* isomerization. However, these two photoreactions proceeded simultaneously at 0 °C to produce coumarin derivatives. Therefore, the cinnamate ester was then changed to an amide bond. The intramolecular nucleophilic substitution hardly occurred at 0 °C but proceeded efficiently at room temperature or higher (37 °C) to give the coumarin product[27].

To evaluate the analytical efficiency, a simple probe was prepared by coupling the crosslinker and biotin moiety via an amide bond. The probe was incubated with four proteins including avidin in a PBS solution. Then, the sample solution was irradiated with 365 nm light for 30 seconds at 0 °C and was then irradiated for 15 minutes at 37 °C after removal of non-crosslinked probes by ultrafiltration. The tryptic digestion products were analyzed by LC-MS/MS. Although the HPLC profile of the digests showed many peptide peaks, only two major peaks corresponding to the coumarin-labeled products were selectively detected by fluorescence emission at 410 nm ($\lambda_{ex}$ 340 nm). However, those peaks still contained many contaminants, which was expected to make it difficult to distinguish the labeled peptides in analysis using proteome. Therefore, we decided to apply a quantitative proteomics method using stable isotopes. In fact, we prepared a probe in which the ethyl group of the cinnamic acid unit was deuterated. This enabled us to detect the labeled peptide as a doublet with $\Delta m = 5$ units. The coumarin tag has a relatively small molecular weight of approximately 260, so the mass range of the analytes does not become large. In addition, MS/MS data does not become complicated since the coumarin unit is hardly decomposed by collision-induced dissociation (CDI). Even in MS/MS signals, the fragments with this tag appear as doublets, so even tiny peaks at the noise level can be distinguished as a part of labeled fragment, facilitating identification of the amino acid sequence and the labeled amino acids. As a result, two labeled amino acids of avidin were determined and shown to be in reasonable sites on the biotin-binding pocket surface. Conventional methods were limited to the identification of the main labeled sites, but this multifaceted data evaluation made it possible to analyze minor labeled peptides as well. Based on the information on multiple labeled sites, not only detailed information on the ligand binding structure could be obtained[28,29], but also the reliability of the target protein identification was improved.

## Identification of interacting proteins and the binding sites using cinnamate-type crosslinkers

This method was evaluated using cell extracts and the biotin probe was employed for targeting biotin-dependent carboxylases. Using approximately 1-2 mL of cell extract per run, some interacting proteins were able to be identified from the amino acid sequences of the labeled peptides in several weeks, including experiments for optimization of the PAL conditions. After photocrosslinking, crooslinked/biotinylated proteins can be enriched on an avidin-immobilized support. Elution of biotinylated proteins from an avidin support typically requires high temperature under denaturing conditions. In this system, after thorough washing of the avidin support, the coumarin-labeled proteins were selectively eluted under mild conditions of light irradiation at 37 °C. Moreover, this step did not elute biotinylated proteins present in the cells, allowing them to be excluded. Four proteins were identified including pyruvate carboxylase (PC) and acetyl-CoA carboxylase (ACC). Pyruvate carboxylase (PC), a protein with a molecular weight of 200 kDa, is an enzyme that catalyzes the biotin-dependent formation of oxaloacetate, and its X-ray crystal structure has been reported[30]. The labeled peptide identified as DT*QAMK (Thr1092 indicated by an asterisk was the labeled site), a part of C-terminal biotin carboxyl carrier protein (BCCP) domain. Thr1092 is located in the central area of the tetrameric structure, away from the enzyme active center to where biotin binds. The carbene, a product of diazirine photolysis, instantly crosslinks to a chemical bond of protein that is in direct contact with the diazirine group, including surrounding water molecule before diffusion. Therefore, this result

clearly demonstrated the dynamic conformational change of BCCP domain, an allosteric migration to the enzyme active center during the enzymatic reaction[31]. Another fluorescent peak has been identified as IT*IGNK fragment peptide of ACCs, and the labeled amino acid residue is located in the similar position to that of PC. The diazirine-based crosslinking makes it possible to prove the positional relationship with interacting molecules and dynamic changes in protein substructures based on the protein crystal structure.

This method was applied for identification of chloride ion channel. Chloride ion channels are known as volume-regulated anion channels (VRACs) and are necessary to maintain a constant cell volume in response to changes in extracellular or intracellular osmotic pressure. LRRC8A, leucine-rich repeat containing 8A, was first reported as an essential component of VRAC[32]. In vivo activity requires at least one other family member. We attempted identification by PAL using DCPIB (4-[(2-butyl-6,7-dichloro-2-cyclopentyl-2,3-dihydro-1-oxo-1*H*-inden-5-yl)oxy]butanoic acid), a VRAC-selective inhibitor. The affinity of the probe was confirmed by membrane potential analysis using patch clamp. After incubation with KB cells, the cells were exposed to light, and the concentrated and purified proteins was digested followed by analysis by LC-MS/MS. LRRC8B was identified from the labeled peptide sequence (SKL*VKNAQDK). Based on the LRRC8A crystal structure[33] and labeled amino acid (Leu414), it was clearly shown that DCPIB binds to the hinge region at around the terminal of leucine-rich repeats.

## Conclusion

Here, a PAL-based target-protein identification was introduced, especially using a small, multifunctional diazirine crosslinker based on hydroxycinnamic acid. Recently, we have developed new alkyldiazirines bearing cinnamate groups that have improved fluorescence properties and enable close-proximity labeling at the ligand-binding site[34] and a coumarin-type crosslinker utilizing photoinduced electron transfer (PeT) to regulate two photoreactions[35]. Our methodology using multifunctional crosslinker enabled target protein identification in a short time with a small sample amount without the need for repeated enrichment of labeled proteins, and also successfully identifies ligand-binding sites efficiently even in membrane proteins. The success rate of target protein identification has improved due to the development of combined use with quantitative proteomics methods, multifunctionalization of photoreactive groups, and improved instrument performance. Easy identification of multiple interacting proteins, including off-targets, will accelerate the optimization of effective bioactive compounds and contribute to the creation of innovative medicines such as the antibiotic teixobactin that exhibits a dual targeting mechanism.

## References


1. Cravatt B. F., Wright A. T., Kozarich J. W. Activity-based protein profiling: from enzyme chemistry to proteomic chemistry. Annu Rev Biochem, 2008:77:383-414.
2. Shiraiwa K., Cheng R., Nonaka H., Tamura T., Hamachi I. Chemical tools for endogenous protein labeling and profiling. Cell Chem Biol, 2020:27: 970-985.
3. Kozoriz K., Shkel O., Hong K. T., Kim D. H., Kim Y. K., Lee J.-S. Multifunctional photo-cross-linking probes: from target protein searching to imaging applications. Acc Chem Res, 2023:56:25–36.
4. Ge S.-S., Chen B., Wu Y.-Y., et al. Current advances of carbene-mediated photoaffinity labeling in medicinal chemistry. RSC Adv, 2018:8:29428–29454.
5. Hill J. R., Robertson A. A. B. Fishing for drug targets: a focus on diazirine photoaffinity probe synthesis. J Med Chem, 2018:61:6945–6963.
6. Dormán G., Nakamura H., Pulsipher A., Prestwich G. D. The life of pi star: exploring the exciting and forbidden worlds of the benzophenone photophore. *Chem Rev*, 2016:116:15284–15398, and references therein.
7. Zhang Y., Tan J., Chen Y. Visible-light-induced protein labeling in live cells with aryl azides. Chem Commun, 2023:59: 2413–2420, and references therein.
8. Zhang Y., Burdzinski G., Kubicki J., Platz M. S. Direct observation of carbene and diazo formation from aryldiazirines by ultrafast infrared spectroscopy. J Am Chem Soc, 2008: 130, 16134–16135.
9. Suzuki T., Okamura T., Tomohiro T., Iwabuchi Y., Kanoh N. Third generation photo-cross-linked small-molecule affinity matrix: a photoreactive and photocleavable system enabling quantitative analysis of the photo-cross-linked small molecules and their target purification. Bioconjugate Chem, 2015:26:389–395.
10. Church R. F. R., Kende A. S., Weiss M. J. Diazirines. I. Some observations on the scope of the ammonia-hydroxylamine-*O*-sulfonic acid diaziridine synthesis. The preparation of certain steroid diaziridines and diazirines. J. Am. Chem. Soc. 1965:87:2665–2671.
11. Nakashima H., Hashimoto M., Sadakane Y., Tomohiro T., Hatanaka Y. Simple and versatile method for tagging phenyldiazirine photophores. *J. Am. Chem. Soc*. 2006, 128, 47, 15092–15093.
12. Murai Y., Hashimoto M. Heteroaromatic diazirines are essential building blocks for material and medicinal chemistry. Molecules, 2023:28:1408–1431.
13. West A. V., Muncipinto G., Wu H.-Y., et al. Labeling preferences of diazirines with protein biomolecules. J Am Chem Soc, 2021:143:6691–6700.
14. Brunner J., Senn H., Richards F. M. 3-Trifluoromethyl-

3-phenyldiazirine. A new carbene generating group for photolabeling reagents. J Biol Chem, 1980:255:3313–3318.
15. Hulce J. J., Cognetta A. B., Niphakis M. J., Tully, S. E., Cravatt B. F. Proteome-wide mapping of cholesterol-interacting proteins in mammalian cells. Nat Methods, 2013:10:259–264.
16. Tornøe C. W., Christensen C., Meldal M. Peptidotriazoles on solid phase: [1,2,3]-triazoles by regiospecific copper(I)-catalyzed 1,3-dipolar cycloadditions of terminal alkynes to azides. J Org Chem, 2002:67:3057–3064.
17. Rostovtsev V. V., Green L. G., Fokin V. V., Sharpless K. B. A stepwise Huisgen cycloaddition process: copper(I)-catalyzed regioselective "ligation" of azides and terminal alkynes. Angew Chem Int Ed, 2002:41:2596–2599.
18. Li Z., Hao P., Li L., et al. Design and synthesis of minimalist terminal alkyne-containing diazirine photo-crosslinkers and their incorporation into kinase inhibitors for cell- and tissue-based proteome profiling. Angew Chem Int Ed, 2013:52:8551–8556.
19. Hosoya T., Hiramatsu T., Ikemoto T., et al. Novel bifunctional probe for radioisotope-free photoaffinity labeling: compact structure comprised of photospecific ligand ligation and detectable tag anchoring units. Org Biomol Chem, 2004:2:637–641.
20. Kumar N. S., Young R. N. Design and synthesis of an all-in-one 3-(1,1-difluoroprop-2-ynyl)-*3H*-diazirin-3-yl functional group for photo-affinity labeling. Bioorg Med Chem, 2009:17:5388–5395.
21. Song Z., Zhang Q. Fluorous aryldiazirine photoaffinity labeling reagents. Org Lett, 2009:11:4882–4885.
22. Nakayama H., Hatanaka Y., Yoshida E., et al. Photolabeled sites with a tetrodotoxin derivative in the domain III and IV of the electroplax sodium channel. Biochem Biophys Res Commun, 1992:184, 900–907.
23. Tomohiro T., Kato K., Masuda S., Kishi H., Hatanaka Y. Photochemical construction of coumarin Fluorophore on affinity-anchored protein. Bioconjugate Chem, 2011:22:315–318.
24. Tomohiro T., Morimoto, S., Shima, T., Chiba, J., Hatanaka, Y. An isotope-coded fluorogenic cross-linker for high-performance target identification based on photoaffinity labeling. Angew Chem Int Ed, 2014:53:13502–13505.
25. Turner A. D., Pizzo S. V., Rozakis G., Porter N. A. Photoreactivation of irreversibly inhibited serine proteinases. J Am Chem Soc, 1988:110:244–250.
26. Y. Kawaguchi, Takeuchi T., Kuwata K., et al. Syndecan-4 is a receptor for clathrin-mediated endocytosis of arginine-rich cell-penetrating peptides. Bioconjugate Chem, 2016, 27, 1119.
27. Tomohiro T., Inoguchi H., Masuda S., Hatanaka Y. Affinity-based fluorogenic labeling of ATP-binding proteins with sequential photoreactive cross-linkers. Bioorg Med Chem Lett, 2013:23:5605–5608.
28. Hayashi R., Morimoto S., Tomohiro T. Tag-convertible photocrosslinker with click-on/off N-acylsulfonamide linkage for protein identification. Chem Asian J, 2019:14:3145–3148.
29. Morimoto S., Tomohiro T., Maruyama N., Hatanaka Y. Photoaffinity casting of a coumarin flag for rapid identification of ligand-binding sites within protein. Chem Commun 2013:49:1811–1813.
30. Xiang S., Tong L. Crystal structures of human and staphylococcus aureus pyruvate carboxylase and molecular insights into the carboxyltransfer reaction. Nat Struct Mol Biol, 2008:15:295–302.
31. Lietzan A. D., Maurice M. St, A substrate-induced biotin binding pocket in the carboxyltransferase domain of pyruvate carboxylase. J Biol Chem, 2013:288:19915–19925.
32. Voss F. K., Ullrich F., Münch J., et al. Identification of LRRC8 heteromers as an essential component of the volume-regulated anion channel VRAC. Science 2014:344:634–638
33. Deneka, D., Sawicka, M., Lam, A. K. M., Paulino, C., Dutzler, R. Structure of a volume-regulated anion channel of the LRRC8 family. Nature 2018:558:254–259.
34. Nakashima T., Iwanabe T., Tanimoto H., Tomohiro T. Fluorescent labeling of a target protein with an alkyl diazirine photocrosslinker bearing a cinnamate moiety. Chem Asian J, 2024:e202400288.
35. Hotta Y., Kaneko T., Hayashi R., et al. Photoinduced electron transfer-regulated protein labeling with a coumarin-based multifunctional photocrosslinker. Chem Asian J, 2019:14:398–402.

# Author Guidelines

## Submission of manuscripts

Editor-in-Chief requests authors to submit manuscripts via e-mail <dts211@gmail.com>. Manuscripts must be submitted as Microsoft Word or compatible software (doc or docx files). Figures should be prepared as high resolution (>300 dpi) JPEG files. Word limit for summary must be 250 words. Authors for whom English is not a mother tongue may submit their manuscript to professional English Editing Service. The work to be submitted has not been published before, is not considered for publication elsewhere. The manuscript for submission must be carefully written and approved fully by all authors. Color artwork is free for submission.

## Editor-in-Chief

Daisuke Tsuruta, MD, PhD
Department of Dermatology
Osaka Metropolitan University Graduate School of Medicine
1-4-3 Asahimachi, Abeno-ku,
Osaka 545-8585, Japan

## Manuscript types

Photomedicine and Photobiology accepts original articles, review articles, and letters to the editor. Figures are acceptable in either black and white or color, according to the authors' preference. The use of color is encouraged when it enhances clarity or data interpretation.

Original articles are investigative studies in fields such as photomedicine, photobiology, and photochemistry. It should not exceed 3500 words (10,000 characters in Japanese), including 250 words (750 characters in Japanese) abstract, Figure legends (excluding references), and a maximum of 4 figures/ tables.

Review articles are for authors essentially invited by Editors. However, suggestions from readers are welcome. It should not exceed 5000 words (15,000 characters in Japanese), including 250 words (750 characters in Japanese) abstracts, figure legends (excluding references), and maximum of 5 figures/tables

Letters to the Editor are for brief reports. Word count limits for this category are 1500 words (4,000 characters in Japanese), including legends (excluding references) with 2 figures or tables. Reference should not exceed 10 in number. Abstract is not required for this category.

## Manuscript arrangement

The manuscript should be written in either English or Japanese. Double spaced typing and minimal margin of 25 mm are required. Each manuscript requires following: 1) Title page, 2) Abstract and 3-5 key words, 3) Text, 4) acknowledgements, 5) References, 6) Tables/Figures with separate legends. Please number each page. Structured abstract, including Background, Methods, Results and Conclusions, is requested. The abstract should be written in English even if the manuscript was written in Japanese.

## References

Number references consecutively in the order appeared in the text. Identify references by Arabic numerals in parentheses. Ex) (1). List all authors when 6 or less. When 7 or more authors exist, list only the first 3 and add "et al." Journal titles should be properly abbreviated according to Index Medicus style. Examples of references are as follows:

1. Rahmani F, Razaei N. Therapeutic targeting of Toll-like receptors: a review of Toll-like receptors and their signaling pathways in psoriasis. Expert Rev Clin Immunol, 2016;12:1289-1298.
2. Frain-Bell W. The photodermatoses. In: Rook A, ed. Recent advances in dermatology. Edinburgh: Churchill Livingstone, 1973: 101-133.

## Conflict of Interest

Please disclose all conflict of interests. These include financial, personal, political, intellectual or religious interests.

## Offprints

PDF offprint will be provided for authors. If additional printed offprints are required, the authors can order them via e-mail <dts211@gmail.com>.

# 「Photomedicine and Photobiology」投稿規定

1．筆頭著者は日本光医学光生物学会員とし，共著者は原則として日本光医学光生物学会員に限る．

2．投稿内容は original article（原著），review article（総説），letter to the editor（短報）を主とし，和文または英文で他誌に掲載されていないものとする．投稿原稿は和文と英文のいずれも可とする．

3．投稿原稿の執筆要綱は下記のとおりとする．
原著（英文 3,500 語，和文 10,000 字）：
医学，薬学，生物学，化学，物理学などの分野における光に関連した研究論文．
本文，要約，図の説明を含む（参考文献は除く）．図・表は 4 点以内．
総説（英文 5,000 語，和文 15,000 字）：
原則，編集者からの依頼原稿であるが購読者からの推薦も歓迎する．
本文，要約，図の説明を含む（参考文献は除く）．図・表は 5 点以内．
短報（英文 1,500 語，和文 4,000 字）：
臨床症例報告や速報的研究．
本文，図の説明を含む．参考文献は 10 編以内．要約は不要．図・表は 2 点以内．
要約は英語で 250 字以内とする．
図・表が制限を超える場合については，編集委員会で調整する．

4．原稿は英文あるいは和文で Microsoft Word かそれと互換性のあるソフトウェア（doc or docx file）で作成し，メールで dts211@gmail.com へ提出する．

5．原稿には 1）タイトルページ，2）要約と key words（3－5 個），3）本文，4）謝辞，5）参考文献，6）図・表の説明を記載し，頁番号をつける．

6．要約は和文，英文に関わらず英語（250 語）で，背景，方法，結果，結論と構造化して記載する．

7．図は高解像度（300dpi 以上）で JPEG ファイルで作成し必ず説明を付ける．図は，著者の選択に応じて白黒またはカラーのいずれでも可とする．カラーの使用は，明瞭性やデータ解釈を向上させる場合に推奨される．

8．文献は本文に用いられたもののみをあげる．引用番号は本文の引用順とし，本文中の引用箇所にアラビア数字を入れた括弧を記載する．例（1）．

9．文献は，下記の形式に従って記載する．著者は 6 名以下の場合は全員を，7 名以上の場合は最初の 3 名を記載し，「他」または et al. を付ける．雑誌名は Index Medicus に従い適切に略記する．
（例）Rahmani F, Razaei N. Therapeutic targeting of Toll-like receptors: a review of Toll-like receptors and their signaling pathways in psoriasis. Expert Rev Clin Immunol, 2016;12:1289-1298.
Frain-Bell W. The photodermatoses. In: Rook A, ed. Recent advances in dermatology. Edinburgh: Churchill Livingstone, 1973: 101-133.

10．利益相反に関してはすべて記載する．

11．著者には PDF のオフプリントを提供します．印刷版が必要な場合はメールでご注文ください．

Photomedicine and Photobiology
編集長　鶴田 大輔
〒 545-8585　大阪府阿倍野区旭町 1-4-3
大阪公立大学院医学研究科皮膚病態学
E-mail：dts211@gmail.com


# We help people achieve healthy skin

## 私たちは、世界中の人々が健康な肌を手に入れるための手助けをします

LEO Pharmaは、豊富な臨床開発パイプラインや幅広い治療薬とともに、開拓者精神を併せ持つ皮膚科医療のリーダー企業です。創立は 1908年であり、LEO財団が会社を保有しています。LEO Pharmaは、皮膚科学の進歩のため、長年にわたり臨床開発に専念し、皮膚疾患を有する患者さんを対象とした新たな標準治療を提供してきました。
本社はデンマークにあり、グローバルで5,800人の従業員が、130カ国の何百万人にものぼる患者さんのために従事しています。

レオ ファーマ株式会社は、デンマークにあるLEO Pharma A/Sの100%出資の日本法人として2010年6月に設立されました。皮膚科領域に特化した、スペシャリティファーマとして日本での確固たる地位を築くべく、事業活動を展開しています。

L E O

**レオ ファーマ株式会社**
〒101-0051東京都千代田区神田神保町1-105
神保町三井ビルディング9F
http://www.leo-pharma.jp/

MAT-65216
2023年4月作成

# 私たちは医療の未来を切り拓き
# 革新的な医薬品をお届けします

未だ満たされない医療上のニーズを解消する
イノベーションは、患者さんの人生に変革をもたらします。
その信念のもと、私たちは、患者さんから学び、
科学の力をもって、未来の医薬品の可能性を切り拓いていきます。

ヤンセンファーマ株式会社
innovativemedicine.jnj.com/japan/

Johnson&Johnson

# 笑顔につながる
# 明日を、共に。

この社会の誰もが

その人らしく

笑顔ある日々を

過ごせることを目指して。

**アッヴィ合同会社**
〒108-0023 東京都港区芝浦三丁目1番21号
msb Tamachi 田町ステーションタワーS
https://www.abbvie.co.jp/

abbvie


Kracie

twice or three times a day 選べるやさしさ

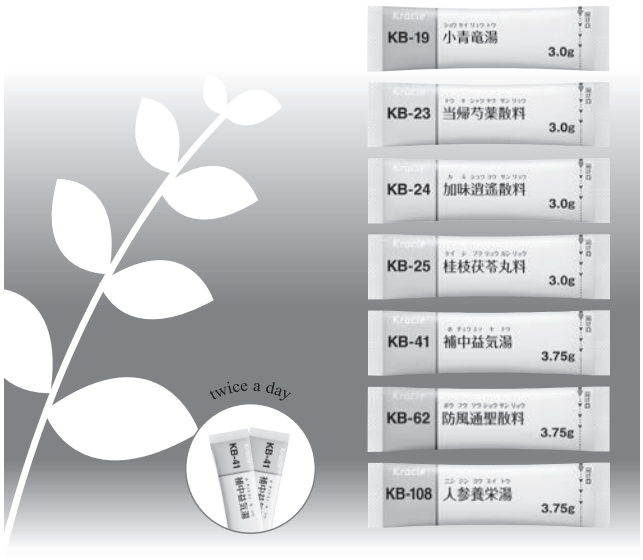



スティックで、健やかな暮らしへ

クラシエ 薬品株式会社

［資料請求先］〒108-8080 東京都港区海岸3-20-20

医療用医薬品ウェブサイト 「漢・方・優・美」 www.kampoyubi.jp

■各製品の効能又は効果、用法及び用量、警告・禁忌を含む注意事項等情報等については電子添文をご参照ください。

# We chase the *miracles* of science to improve people's lives

私たちは人々の暮らしをより良くするため、科学のもたらす奇跡を追求します。

**サノフィ株式会社**
〒163-1488 東京都新宿区西新宿三丁目20番2号 東京オペラシティタワー
www.sanofi.co.jp

sanofi

ヒト化抗ヒトIL-23p19モノクローナル抗体製剤

# イルミア®
薬価基準収載

皮下注
100mgシリンジ

ILUMYA®　チルドラキズマブ(遺伝子組換え)注射液

生物由来製品　劇薬　処方箋医薬品*

*注意－医師等の処方箋により使用すること

効能又は効果、用法及び用量、警告・禁忌を含む注意事項等の詳細については電子添文をご参照ください。

製造販売元［文献請求先］
**サンファーマ株式会社**
東京都港区芝公園　1－7－6

お問い合わせ先
くすり相談センター
TEL:0120-22-6880

2024年11月作成

maruho　NOVARTIS

ヒト型抗ヒトIL-17Aモノクローナル抗体製剤

薬価基準収載

生物由来製品　劇薬　処方箋医薬品注）

# コセンティクス®

皮下注150mgペン
皮下注300mgペン
皮下注75mgシリンジ

Cosentyx®
secukinumab

セクキヌマブ（遺伝子組換え）注射剤

注）注意－医師等の処方箋により使用すること

●効能又は効果、用法及び用量、警告・禁忌を含む注意事項等情報等については電子添文をご参照ください。


販売
maruho
〔文献請求先及び問い合わせ先〕
マルホ株式会社
大阪市北区中津1-5-22 〒531-0071
（ホームページアドレス）
https://www.maruho.co.jp/

本製品に関するお問い合わせ
TEL：0120-12-2834
販売情報提供活動に関するご意見
TEL：0120-12-3821
受付時間:9:30～17:30
（土･日･休日および当社休業日を除く）

製造販売（輸入）
〔文献請求先及び問い合わせ先〕
ノバルティス ファーマ株式会社
東京都港区虎ノ門1-23-1　〒105-6333

ノバルティス ダイレクト
TEL：0120-003-293
販売情報提供活動に関するご意見
TEL：0120-907-026
受付時間:月～金 9:00～17:30
（祝日および当社休日を除く）


（2022.08作成）

Inspired by patients.
Driven by science.

ヒト化抗ヒトIL-17A / IL-17F
モノクローナル抗体製剤
（ビメキズマブ（遺伝子組換え）製剤）

薬価基準収載

# ビンゼレックス®
## 皮下注160mg オートインジェクター・シリンジ

生物由来製品、劇薬、処方箋医薬品
（注意ー医師等の処方箋により使用すること） **Bimzelx®**

「効能又は効果」「用法及び用量」「警告・禁忌を含む使用上の注意」等につきましては、電子化された添付文書をご参照ください。

製造販売元
**ユーシービージャパン株式会社**
東京都新宿区西新宿8丁目17番1号

2022年3月作成
JP-P-BK-PSO-2300199-4


ヒト化抗ヒトIL-36レセプターモノクローナル抗体製剤

薬価基準収載

# スペビゴ®点滴静注450mg

スペソリマブ（遺伝子組換え）製剤 **Spevigo®450mg for I.V. Infusion**

**生物由来製品、劇薬、処方箋医薬品**（注意ー医師等の処方箋により使用すること）

効能又は効果、用法及び用量、警告・禁忌を含む注意事項等情報等については電子添文を参照ください。

製造販売元（文献請求先及び問い合わせ先）
日本ベーリンガーインゲルハイム株式会社

DI センター
〒141-6017 東京都品川区大崎2丁目1番1号ThinkPark Tower
Tel：0120-189-779【受付時間】9:00～18:00（土・日・祝日・弊社休業日を除く）

PC
2023年11月作成


日本イーライリリーは製薬会社として
人々が健康で、より豊かな生活を送れるよう
がん、糖尿病、自己免疫疾患、
アルツハイマー病などの中枢神経系疾患を含む
幅広い領域で革新的な医薬品を提供し
日本の医療に貢献しています。

日本イーライリリー株式会社
〒651-0086 神戸市中央区磯上通 5-1-28
https://www.lilly.com/jp/

協和キリン株式会社

たった一度の、いのちと歩く。


KYOWA KIRIN

私たちの志 検索

2019年7月作成

選択肢をつくる。
希望をつくる。

なんでも選べるこの時代に、
まだ選択肢が足りない世界があります。
そこでは、たったひとつの選択肢が生まれることが、
たくさんの希望につながります。
だから、田辺三菱製薬はつくります。

病と向き合うすべての人に、希望ある選択肢を。

この国でいちばん長く培ってきた
薬づくりの力を生かして、
さまざまな分野で、挑みつづけていきます。
そこに待っている人がいるかぎり。

田辺三菱製薬
https://www.mt-pharma.co.jp/

MITSUBISHI CHEMICAL GROUP